THE UNIVERSITY OF QUEENSLAND

Development of Finite Element Tool for Study of Interaction between Air-Coupled Ultrasonic Wave and Solid Plate

Student Name: Muhammad Zulfadhli, BAKHTIAR

Course Code: MECH4501

Supervisor: Associate Professor Dr Martin Veidt

Submission date: 30 May 2019

Abstract

Air-coupled ultrasonic testing has become one of the most used methods for non-destructive testing of material. It's characteristic of not having to be in contact with test specimen has become a key role in preserving the integrity of a test specimen and transducer. However, air-coupled ultrasonic transducer suffered from high impedance mismatch between transducer surface and air medium which makes it inefficient for analyzing defect at high frequency. This means that it is hard to analyze small defects which is only possible at high frequency of analysis.

In this study, ANSYS software is used to develop a finite element tool to study the interaction between ultrasonic wave and solid plate. The reliability of this tool is validated through a series of validation tests. Important aspects of finite element modelling such as element type and size used, fluid-structure interaction and absorbing boundary condition are tested. From this, it was decided that the use of quadratic hexahedral element with six and 20 elements per wavelength for fluid and structural body respectively is the best choice for this model. Furthermore, PML is chosen for absorbing boundary condition with three element per thickness layer for best accuracy and computational efficiency. 2.5D model has also been developed with reliability for use in validation tests to replace the 3D model and proved to be more computational efficient.

Interaction between air-coupled ultrasonic wave and solid plate is also studied. The effect of varying the frequency of wave propagation, wave incident angle and plate material on plate deformation is examined. For all these three aspects, the deformation of the plate becomes larger when 1) frequency is lower, 2) wave incident is larger and 3) plate material with high impedance mismatch with air is used.

Acknowledgement

First and foremost, I would like to thank my supervisor, Dr Martin Veidt for his continuous support throughout my thesis. Thank you for always giving me words of encouragement as it helps to push me forward at times when I thought I will never be able to complete my thesis. And thank you, for all the guidance and knowledge you've assisted me with to ensure I keep on progressing.

Next, I would like to express my deepest gratitude to my parents for the unconditional love they have given me and for all the prayers that they never miss for me. Thank you for always supporting me and become my motivation to always be a better person. I owe you two everything in my life <3.

My thanks also go to my thesis mate, Aliff Azizi aka Empengu who together with me has pushed through the obstacles we faced. Also, to my other friends who have given me advices for my thesis especially Syariqul aka Cikoirita and Ikhwan Deni.

I would also like to thank Alan from helpdesk EAIT for helping me through the series of problems I had with UQ ANSYS license. Without your help, I don't know how I'm going to complete my tons of simulations.

Finally, to Natasha Farina, thanks for always be there for me during the tough times, for proofreading my thesis even though you don't understand a thing and for all the calls you made to wake me up during the last few days of my thesis. Thank you everyone.

Table of Contents

Abstract I

Acknowledgement II

Table of Contents III

List of Figures VI

List of Tables IX

Chapter 1: Introduction 1

1.1 Background 1

1.2 Aim 4

1.3 Scope 4

1.4 Thesis Outline 5

Chapter 2: Literature Review 6

2.1 Overview of Ultrasonic Testing 6

2.1.1 Properties of Ultrasonic Wave 6

2.1.2 Generation of Ultrasonic Wave 7

2.1.3 Piezoelectric Transducer 8

2.1.4 Wave Radiation 12

2.2 Finite Element Method 14

2.2.1 Introduction to Finite Element Method 14

2.2.2 Element 14

2.2.3 Absorbing Boundary Condition 18

2.2.4 Fluid-Structure Interaction 23

Chapter 3: Model Description 27

3.1 Model Configuration 28

3.1.1 Excitation Source 29
3.1.2 Solid Plate 31
3.1.3 Fluid Domain 31
3.2 Material Properties 32
3.2.1 Transducer 32
3.2.1 Solid Plate and Fluid Domain 33
3.3 Mesh 34
3.3.1 Element Type 34
3.3.2 Element Size 34
3.4 Boundary Condition 36
3.4.1 Transducer 36
3.4.2 Solid Plate 36
3.4.3 Fluid Domain 37
3.4.4 Fluid-Structure Interaction (FSI) 38
3.4.5 Symmetry 38
3.5 Excitation Load 40
3.6 2.5D Model 40
Chapter 4: Validation Test 42
4.1 3D and 2.5D 43
4.1.1 Surface deformation and velocity 44
4.1.2 Pressure Field 47
4.1.3 Computational Cost 58
4.1.5 Validity of the model 63
4.2 Mesh 64
4.2.1 Element type 64

4.2.2 Element size 66
4.3 Boundary Condition 70
4.3.1 Transducer 70
4.3.2 Fluid Domain 75
4.3.3 Symmetry 81
Chapter 5: Interaction between Ultrasonic Wave and Solid Plate 84
5.1 Flexible vs Rigid plate 84
5.2 Effect of frequency on plate deformation 87
5.3 Effect of incident angle on plate deformation 90
5.4 Effect of material change on plate deformation 93
5.5 Chapter Summary 94
Chapter 6: Conclusion and Recommendation 95
6.1 Conclusion 95
6.2 Recommendations for Future Work 96
References 97

List of Figures

Figure 1 Types of coupling for transducer 2
Figure 2 Illustration of wave signals 6
Figure 3 Overview of conventional piezoelectric transducer 8
Figure 4 Signal resolution 9
Figure 5 Effect of no of matching layer on fractional bandwidth 11
Figure 6 Example of horn structure in matching layer 11
Figure 7 Pressure gains by different types of matching layer 12
Figure 8 Example of elements [18] 15
Figure 9 Linear and quadratic element comparison 15
Figure 10 Comparison of computational time of different types of elements [19] 17
Figure 11 Boundary reflection results by A. Rahimi Dalkhani et al on the comparison between PML and CE-ABC. L = thickness, R = radius of excitation source 19
Figure 12 Wave reflection for (a) PML and (b) CE-ABC as studied by A Rahimi Dalkhani et al 20
Figure 13 Configuration of model with PML [20] 21
Figure 14 Mechanism of FSI coupling 23
Figure 15 Coupling region at the fluid-structure interface 25
Figure 16 Comparison of coupling matrix from [20] 26
Figure 17 Model development process 27
Figure 18 Configuration of full model 28
Figure 19 Coupling matrix for piezoelectric material 33
Figure 20 Mesh structure near structural body 35
Figure 21 Boundary condition of active element 36
Figure 22 Boundary condition of solid plate 37
Figure 23 PML dimensions 37
Figure 24 FSI boundary condition 38
Figure 25 Symmetrical model 39
Figure 26 Wave emission direction 40
Figure 27 2.5D model 41
Figure 28 Measurement point for surface deformation and velocity 44

Figure 29 Comparison of surface (a) deformation and (b) velocity for 3D and 2.5D model 44
Figure 30 Percentage error of surface deformation and velocity in 2.5D model 45
Figure 31 Surface velocity of (a) 2.5D and (b) referred model 46
Figure 32 FRF plot of curved ultrasonic transducer in [38] 47
Figure 33 Comparison of pressure field of (i)3D and (ii)2.5D at (a)16 and (b)20kHz 48
Figure 34 Pressure field of 2.5D model at 50 and 60kHz 49
Figure 35 Pressure field of referred model at 60kHz 49
Figure 36 Measurement points of acoustic pressure 51
Figure 37 Plot of acoustic pressure vs frequency for (a)3D and (b)2.5D in near and far-field zone 52
Figure 38 Acoustic pressure comparison between 3D and 2.5D 53
Figure 39 Acoustic pressure of referred model at 140mm 54
Figure 40 Acoustic pressure percentage error of 2.5D model 56
Figure 41 Nodes/elements vs frequency of 3D model 60
Figure 42 Plot of no of elements vs frequency 60
Figure 43 Plot of simulation time vs no of elements 61
Figure 44 Error due to lack of physical memory 62
Figure 45 Elapsed time exceeded CPU time warning 62
Figure 46 Example of difference in elapsed and CPU time 62
Figure 47 Mesh structure of hexahedral and tetrahedral element 64
Figure 48 Acoustic pressure comparison between Hexahedral and Tetrahedral element 65
Figure 49 Convergence test for fluid domain element size 67
Figure 50 Pressure field when not enough elements per wavelength are used 68
Figure 51 Convergence test for structural body element size 69
Figure 52 Graph of transducer's surface deformation in y-axis for (a) fixed support, (b) free support, (c) both support 71
Figure 53 Comparison of pressure field at 20 and 40kHz for both (a) fixed and (b) free support 72
Figure 54 Comparison of acoustic pressure at measurement point marked X 73
Figure 55 Acoustic pressure/surface deformation vs frequency 73
Figure 56 Pressure field using different ABC 75

Figure 57 Comparison of pressure field between (a)PML and (b)Radiation BC 76
Figure 58 Measurement points for pressure to compare RBC and PML 77
Figure 59 Percentage error of RBC in relative to PML 77
Figure 60 PML thickness convergence test measurement points 79
Figure 61 PML thickness convergence test 80
Figure 62 Pressure field using of (a) full model, (b) half model, (c) quarter model 82
Figure 63 Setup for plate study 85
Figure 64 Deformation of flexible and rigid body 85
Figure 65 Pressure field on flexible and rigid plate at 40kHz 86
Figure 66 acoustic pressure at the center of flexible and rigid plate's surface 87
Figure 67 Average plate deformation vs frequency 87
Figure 68 Plate deformation at 40, 60 and 80kHz 88
Figure 69 pressure field at 40, 60 and 80kHz 89
Figure 70 Incident angle vs plate deformation 90
Figure 71 Pressure field produced at 30^0, 60^0 and 90^0 incident angle 92
Figure 72 Average plate deformation vs acoustic impedance 93

List of Tables

Table 1 Specific acoustic impedance of different material 2
Table 2 Thesis Outline 5
Table 3 Reflection and transmission coefficient of air and water interface with steel 10
Table 4 Element types for acoustic analysis [21] 18
Table 5 Types of analysis available for each ABC [13] 21
Table 6 Limitation on the comparison between 2.5D and 3D model with referred model 43
Table 7 Results of near to far-field transitional point for 3D and 2.5D compared with theory 50
Table 8 Acoustic pressure in far-field of referred model 54
Table 9 Trendline equation of acoustic pressure percentage error 56
Table 10 Prediction of percentage error of acoustic pressure at high frequency using trendline . 56
Table 11 No of nodes and elements based on element size 58
Table 12 Computational cost of 3D and 2.5D models 59
Table 13 Simulation time prediction for 3D 61
Table 14 3D and 2.5D simulation time comparison 61
Table 15 Hexahedral and Tetrahedral comparison 65
Table 16 Max mesh size allowed at 20 and 40kHz 66
Table 17 Computational cost of different far-field boundary conditions 78
Table 18 Computational time of model with different symmetry BC 83
Table 19 Parameter used for flexible vs rigid plate study 84

Chapter 1: Introduction

1.1 Background

Defects in structure are common whether in manufacturing stage or industrial application stage. Early detection of defects is crucial in preventing the failure of structure during application. However, some defects such as internal cracks, porosities and fiber misalignment in composite materials are frequently not visible to the naked eye. Hence, various studies have been done to explore the different ways to detect internal flaws using a system called non-destructive test (NDT). The most common methods are the use of ultrasonic testing (UT), acoustic emission, eddy current and radiographic as techniques to evaluate the mechanical properties of a component and detect its internal flaws without causing damage to it.

This paper will focus on the use of ultrasonic testing. Ultrasonic is the spectrum of sound with frequency more than 20kHz. This sound is produced by ultrasonic transducer device which converts electrical energy to mechanical energy in a form of vibrations in the ultrasonic frequency range which consequently produces sound waves. Ultrasonic testing usually requires two transducers to operate which are transmitter and receiver transducer. This energy conversion is applied for transmitter transducer whose function is to produce the ultrasonic waves. At receiver transducer, the opposite energy conversion occurred where ultrasonic waves are converted to electrical signal for result analysis. This is called a direct technique of sound wave generation.

Indirect technique on the other hand, generate an ultrasonic wave at the test piece instead of the transmitter such as the use of laser to heat up an area on the test piece which in turn will generate ultrasonic wave [1]. One of the direct techniques of ultrasonic testing is the use of air-coupled ultrasonic transducer. Air-coupled means that the coupling between the transducer and test specimen is air. An illustration of different types of coupling used in ultrasonic testing are shown in figure 1.

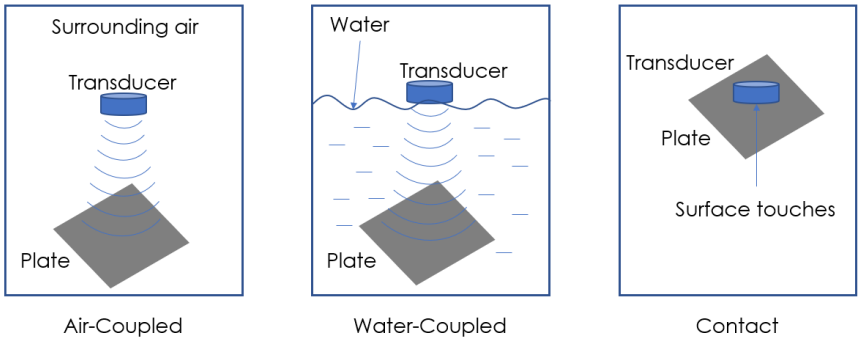

Figure 1 Types of coupling for transducer

In water-coupled, the medium between transducer and test plate is water. On the other hand, for contact transducer, surface of the transducer touches the test plate causing direct vibration to the plate. Air-coupled transducer has advantages over water and contact transducer such as:

1) Suitable for testing materials that are highly reactive to water such as foams, composites and paper
2) Transducer design doesn't have to consider interaction with water such as water-resistant properties or corrosion due to water.
3) No damage to the surface of transducer and tested material since there is no vibration contact between the two surfaces as in contact transducer.

However, non-contact transducer often faces a problem of impedance mismatch since the coupling used between the transducer and test plate is air. Air has very low acoustic impedance in relative to other solid materials. Table 1 shows examples of acoustic impedance of different materials and air.

Material	Specific acoustic impedance, MRayls
Air	0.0004
Magnesium	10.98
Aluminium	17
Stainless steel	45.45

Table 1 Specific acoustic impedance of different material

In theory, when the higher the impedance mismatch between two mediums, more waves are reflected at the interface. In air-coupled transducer, most of the waves are reflected at the interface thus reducing the wave signals received by the receiver transducer. This subsequently decreases its efficiency. For example, a book by Bhardwaj, M.C [2] shows that the amount of energy loss at the interface using air-coupled ultrasound is about 160 dB while transmission through water only has a loss of 20 dB. Many researches have been done to overcome this problem such as the

use of piezoelectric crystals that contain high piezoelectric properties to increase its efficiency [3] and using thin polymer film as the matching layer [4].

However, studying the efficiency of air-coupled transducer through experimental work alone may require a lot of time due to various factors that need to be considered. Using numerical simulation to model the testing system will decrease the amount of time and cost required to choose the best experimental set-up for further research. And this is the motivation for this thesis. It focuses on building a simulation model so that studies on the interaction between air-coupled ultrasonic wave and solid plate can be accomplished. This thesis focuses on using ANSYS software for developing the model. ANSYS is a finite element method (FEM) software which is a numerical problem-solving tool for engineering simulation. It covers various areas such as structural analysis, heat transfer and fluid mechanics.

The reason this software is chosen is because it has the capability to perform acoustic analysis which is the main part of this thesis. This means modelling of ultrasonic waves is possible and studies on the interaction between ultrasonic waves and solid plate can be done. Besides, this research will be the foundation for future research regarding air-coupled ultrasonic testing for University of Queensland (UQ). As a foundation for future research, it is important that the software used is easily accessible by researchers and students in UQ hence the other reason why this software is chosen.

The motivations of this thesis can be summarized into two:

1) To study the interaction between air-coupled ultrasonic waves and solid plate. This is motivated by the fact that the interface between transducer's surface and its coupling medium, air has very high impedance mismatch which could lead to inefficiency of ultrasonic testing. With this study, it could open up possibilities for future research on ways to reduce the effect of impedance mismatch.
2) Using simulation tool to model the interaction between air-coupled ultrasonic waves and solid plate provides a lot of practicability since using the simulation tool, various testing condition can be done that otherwise would be expensive and time consuming if done experimentally.

1.2 Aim

The primary aim of this thesis is to develop a reliable finite element tool capable of studying the interaction between air-coupled ultrasonic wave and solid plate. This tool needs to be computationally cost efficient and accurate. This can be achieved through:

1) Literature review on the characteristic of air-coupled ultrasonic wave such as wave generation and propagation and it's interaction with solid
2) Literature review on the important aspect of finite element modelling such as element type, fluid-structure interaction and absorbing boundary conditions to gain better understanding on finite element method and to determine the best way to develop the model
3) Performing validation tests on each aspect of the developed model to determine the best condition for it
4) Simplification of model through symmetry boundary condition and development of 2.5D model to achieve computational efficiency.

The secondary aim of this thesis is to study the interaction between air-coupled ultrasonic wave and solid plate using the developed finite element tool. This is done by varying various parameters of the model configuration such as frequency, wave incident angle and plate material. The effect of changing these parameters is studied.

1.3 Scope

This section presents the scope of this thesis.

In scope

- Studies on the generation of ultrasonic wave and analysis on the vibrational behavior of the transducer and pressure field produced
- Studies on different element types and effect of not using required size on the accuracy of the model
- Defining the fluid-structure interaction to allow the interaction between ultrasonic wave in air and structural body to be analyzed

- Studies on different absorbing boundary conditions to investigate their suitability for the model
- Studying the validity of using 2.5D model to replace 3D model to reduce computational cost
- Investigation on the effect of changing testing parameters of the studies on interaction between air-coupled ultrasonic waves and solid plate.

Out of scope

- Modelling the wave propagation through the plate and from the plate to the receiver transducer
- Analysis in time domain

1.4 Thesis Outline

Table 2 shows the structure of this thesis:

Chapter	Description
2	This chapter provide literature review on the concept of ultrasonic testing and finite element method.
3	This chapter describes the simulation model developed based on knowledge from literature review.
4	This chapter presents all validation tests that has been done to provide confidence on the reliability of the described model in Chapter 3.
5	This chapter shows studies on the interaction between air-coupled ultrasonic waves and solid plate.
6	This chapter provides conclusion of the completed work along with recommendations for future work

Table 2 Thesis Outline

Chapter 2: Literature Review

In this chapter discussions on the concept of ultrasonic testing and finite element method are made. These concepts are further analyzed by reviewing past researches made regarding this topic. With this discussion of the concept and literature reviews, it aims to provide understanding and justifications to readers on the design of finite element model described in Chapter 3.

2.1 Overview of Ultrasonic Testing

2.1.1 Properties of Ultrasonic Wave

Sound is a mechanical vibration of particles that propagate as a wave of pressure in medium such as air and solid. Ultrasonic transducer utilizes the use of ultrasonic waves in the sound spectrum. Generally, the spectrum is divided into three which are infrasonic, audio and ultrasonic identified based on the vibration oscillation of their sound pressure known as frequency. Human ear can only detect sound in the audio spectrum which has a range of frequency between 20 and 20000Hz. Infrasonic on the other hand has frequency less than 20Hz whereas ultrasonic is more than 20000Hz [5].

What makes ultrasonic waves applicable for non-destructive test is that it can be reflected and refracted, properties very similar to light wave. In ultrasonic testing, ultrasonic waves are propagated along the test subject and if the wave coincide with any anomaly in the subject, some of the wave will be reflected thus giving information of the defect location. Figure 2 obtained from [6] shows an illustration of how it works.

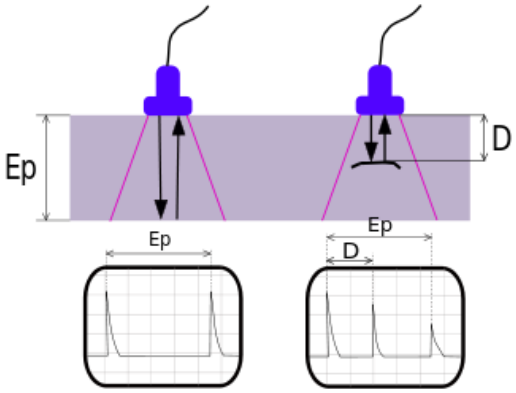

Figure 2 Illustration of wave signals

The probes are used to generate ultrasonic waves where it is transmitted into a test plate. For the probe on the left, two peaks can be observed. The first peak indicates the initial pulse of the probe while the second peak is due to reflection at the bottom of the plate. When tested at area with defect, three peaks are observed. The additional peak at the middle is due to waves reflected at the defect. Waves that are not reflected travel through the defect but with less amplitude compared to the initial pulse as seen on the third peak. Using this information, the location of the defect can be determined by evaluating the time taken for the wave to reach the defect.

2.1.2 Generation of Ultrasonic Wave

Ultrasonic wave can be generated by utilizing a piezoelectric effect. It was discovered in 1880 by Curie brothers where when a piezo-electric material is deformed by a mechanical vibration or pressure, electrical charges are produced on its surface. In 1881, the reverse phenomenon is discovered where when an electric current is applied to the said material, the electrical energy is converted into mechanical vibrations [7]. This is the phenomenon used in ultrasonic testing to generate an ultrasonic wave.

As mentioned in previous section, the frequency of sound wave is measured from the vibration oscillation of the sound pressure. Hence, by applying an alternating voltage across the piezo-electric material, the material will oscillate at the same frequency of the alternating voltage. Knowing that sound spectrum is really huge, generating a desired wave frequency is important to produce high quality result. This is because the size of defect that can be detected depends on the wave frequency. As the frequency of the wave increases, the smaller the defect that can be detected [8]. However, higher frequency also means that the waves are more prone to dispersion causing signal to noise ratio detected at receiver to be fairly low. On the other hand, the lower the wave frequency, the less prone it is to dispersion in exchange of its ability to detect small defect. Thus, the correct frequency for the application need to be chosen so that the frequency used is enough to detect defect in structure while still allowing high signal to noise ratio to be measured [8].

Another important factor to consider in generating an ultrasonic wave is its amplitude. Most common problem faced by an air-coupled ultrasonic transducer, is low wave amplitude

measured at receiver probe. This is because lots of the wave transmitted from transmitter probe to solid are reflected due to impedance mismatch. This will reduce the wave amplitude measured at receiver probe, making the results hard to be analysed due to low signal to noise ratio. To address this problem, the desired wave amplitude can be determined by adjusting the voltage applied to the transmitter probe since the two variables are linearly proportional to each other.

2.1.3 Piezoelectric Transducer

In a conventional piezoelectric transducer, there are four main components that made the transducer which are the active element, backing material, matching layer and casing as shown in figure 3. Each of these components has its own purpose.

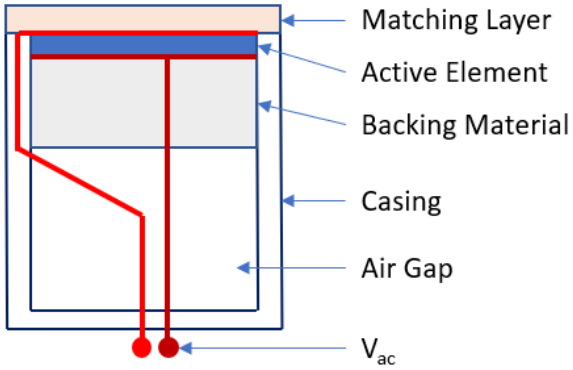

Figure 3 Overview of conventional piezoelectric transducer

Active Element and Casing

Active element is the source of vibration in the transducer. It is made from piezoelectric material and as explained previously, will vibrates when voltage is applied to it and vice versa. As shown in the figure, voltages are applied at the top and bottom surface of the active element to produce a voltage difference across the its thickness. This way, it will cause the active element to vibrate the most in the direction of the thickness. The purpose of the casing is to provide an enclosure to the whole system of the transducer.

Backing Material

In non-destructive testing, having a good axial resolution is one of the parameters that indicates the efficiency of a transducer. Axial resolution is based on the duration of received signal. Shorter signal duration means higher axial resolution. In high axial resolution, results can be interpreted much easier due to the low disturbance in signal produced by damped waves [9].

Figure 4 shows the difference between high and low signal resolution. Less disturbance in signal is observed on high resolution compared to low-resolution signal. To obtain a high-resolution signal, the backing material is required as it will acts as a damper on the active element to damped out the oscillation.

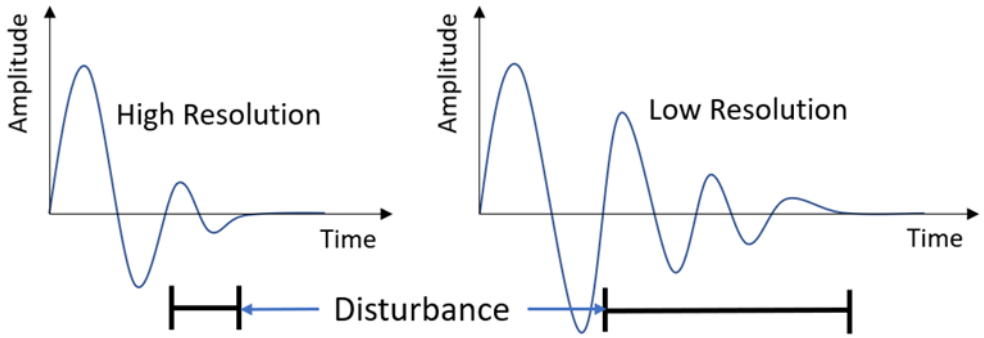

Figure 4 Signal resolution

Many studies have been done to incorporate an efficient backing material to the transducer. Most of these studies focus on trying to achieve transducers with wide bandwidth so that the receiving sensitivity is high for larger range of frequency. One of the studies suggests manufacturing a really thin backplate. However, the problem with this is, it is almost impossible to manufacture the plate to less than 50µm without damaging it due to its fragility. An example of backplate technology can be seen in [10] where Zhihong Wang et al have studied on the use of PZT/silicon wafer bonding technique to integrate a perforated damping backplate onto the transducers. Using the technique developed, PZT wafer with thickness less than 20µm can be manufactured and attaching the silicon backplate to the transducer, the damping factor of the transducer is increased thus producing a wider bandwidth and higher resolution.

Matching Layer

The function of matching layer is to assist with the transfer of energy from the active element to the coupling medium. It aims to reduce the effect of impedance mismatch between the transducer's surface and coupling medium to avoid disturbance in the transfer of energy between the two mediums. When sound wave propagating in a medium meets an interface of other medium, it will either gets partially reflected, totally reflected or totally propagated through the medium. This depends on the characteristic acoustic impedance, Z of the two mediums given by equation 1:

Equation 1 Acoustic Impedance

$$Z = \rho c$$

Where ρ = density of medium and c = speed of sound in the medium. The relationship of acoustic impedance between the two mediums can be described in terms of pressure, $p_{R/T}$ and power, $W_{R/T}$ coefficient as follows:

Equation 2 Power and Pressure coefficient

$$p_R = \frac{Z_2 - Z_1}{Z_2 + Z_1}$$

$$p_T = 1 + p_R = \frac{2Z_2}{Z_2 + Z_1}$$

$$W_R = \left|\frac{Z_2 - Z_1}{Z_2 + Z_1}\right|^2$$

$$W_T = 1 - W_R = 1 - \left|\frac{Z_2 - Z_1}{Z_2 + Z_1}\right|^2$$

Where Z_1 and Z_2 = acoustic impedance of 1st and 2nd medium respectively and subscript R and T stands for reflection and transmission respectively. Table 2 shows the comparison between air-steel and water-steel mediums, pressure and power coefficient obtained from [11]. From the table, it is evident that the coefficient of power transmission from water to steel is higher than air to steel with a ratio of 3525. This shows how low the amount of wave energy is transmitted from air to steel compared to from water to steel due to huge impedance mismatch.

Medium	p_R	p_T	W_R	W_T
Air-Steel	0.9998	1.9998	0.9996	0.0004
Water-Steel	0.927	1.927	0.859	0.141

Table 3 Reflection and transmission coefficient of air and water interface with steel

The most common way to reduce the effect of impedance mismatch is by matching the impedance of the matching layer to the mean of impedances of the active element and the coupling medium as shown in equation 3.

Equation 3 Mean acoustic impedance of matching layer

$$Z_{ml} = \sqrt{Z_1 Z_2}$$

Where Z_{ml} = Impedance of matching layer, Z_1 = Impedance of active element, Z_2 = Impedance of coupling medium. More than one matching layer can be used to greatly reduce the impedance mismatch. Studies by Thiagarajan et al [12] is an example of transducer with dual matching layer using Glass and Perylene. Figure 5 shows the effect of number of matching layers on fractional bandwidth [13]. Higher bandwidth is achieved with higher number of matching layers. Furthermore, thickness of the matching layer is typically cut to 1/4 of the desired wavelength. This thickness ensures that the waves reflected within the matching layer to be in phase with other waves when exiting the layer [14].

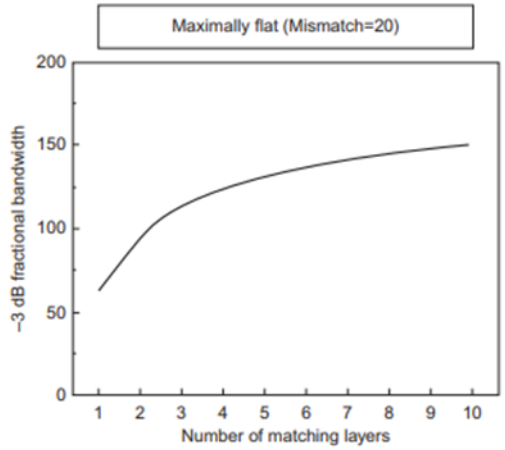

Figure 5 Effect of no of matching layer on fractional bandwidth

Apart from this, many techniques have been developed to reduce the effect of impedance mismatch in an air-coupled ultrasonic transducer. Most of these techniques focus on the structure of the matching layer. One example is the use of horn structure by Fletchers and Thweites [14]. Figure 6 shows an example of the horn structure as the matching layer. By optimizing the shape of horn and the spacing between the horn and transducer surface, a gain of sound pressure level about 10dB is achieved for a frequency range between 30 and 100kHz when compared to no matching layer.

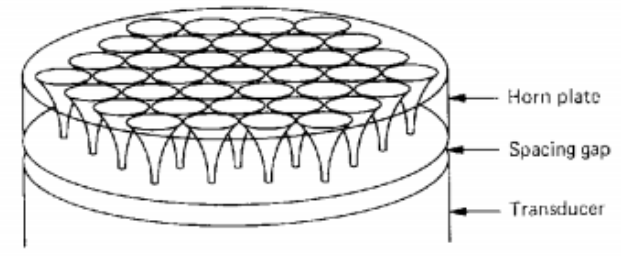

Figure 6 Example of horn structure in matching layer

Furthermore, Minoru Toda [4] has also proposed new methods to reduce the impedance mismatch. In his work, two types of matching layer have been proposed which are 1) thin polymer film 2) thick solid plate with many tiny through holes. By optimizing the hole size, hole area, thickness of the layer and other parameters, high sound pressure gain is achieved compared to when no matching layer is used. Based on figure 7 [4], a gain of 15Pa of sound pressure is achieved by both types of matching layer at 41Hz of frequency. This shows the importance of matching layer in reducing the impedance mismatch between the air and transducer's surface.

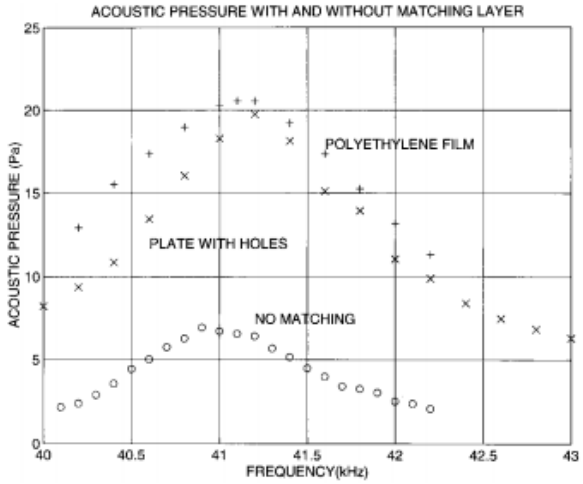

Figure 7 Pressure gains by different types of matching layer

2.1.4 Wave Radiation

When transducer vibrates, sound waves are not produced only at one point but across the whole transducer surface [15]. Since many waves are produced across the transducer's surface, constructive and destructive waves interferences occurred among the waves produced. This causes fluctuation in the acoustic pressure field produced near the surface. This zone is called near field. In this zone, the acoustic beam produced are hard to analyze due to the fluctuations. In ultrasonic testing, the test specimens are usually not positioned in this zone but in the far field zone to avoid the uncertainty of the acoustic pressure field produced.

The transition point from near to far-field is where the sound waves begin to merge and start forming a relatively uniform front. Near this point, maximum acoustic pressure produced by the transducer occurred. Past this transition point is the far field where the sound beam is unfluctuating compared to the beam in near field. For a circular transducer, the beam originates from the center of the transducer and uniformly spreads out as the waves moves further from the

transducer surface. This means that the further the measurement point from the transitional point is, the lower the pressure field would be due to the spreading. Hence, it is essential to determine the distance from transducer surface to the near to far field transitional point. This is to ensure that the point where maximum pressure occurred is used during ultrasonic testing for maximum effectiveness and also to avoid the use of acoustic beam in near field due to its uncertainty. Figure below shows the near and far field produced by an unfocused transducer [15].

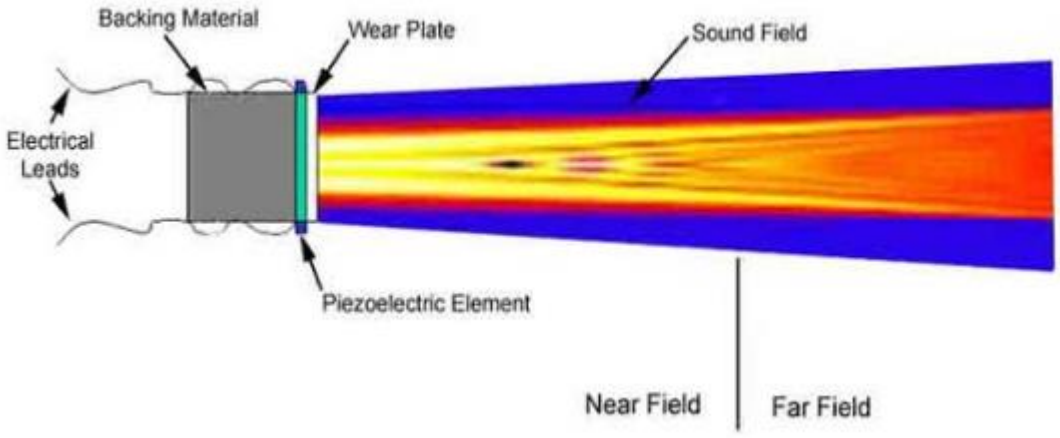

[15]

For an unfocused transducer generating sound pressure in air, the distance between transition point from near to far field to the transducer surface are given by equation 4 [15]:

Equation 4 Near to far-field transition point

$$N = \frac{D^2}{4\lambda}$$

Where N = distance between transducer and transition point, D = diameter of transducer, λ = wavelength.

2.2 Finite Element Method

In this section, the use of finite element method (FEM) is discussed. Starting with the introduction to finite element method and its concept, this section will explore in detail the important aspect of it such as the element used for the modelling. Furthermore, since this thesis focus on the interaction of ultrasonic waves and solid plate, the aspects of acoustic modelling such as fluid-structure interaction and absorbing boundary condition are analysed. In addition to literature sources, descriptions of these aspects with respect to ANSYS are given.

2.2.1 Introduction to Finite Element Method

Finite Element Method is a numerical method used to solve a wide range of differential equations for various engineering problems. It was first used in 1956 by Turner et al. for calculation on aircraft structures by using joint bars and triangular plates to discretize the structures into individual components. These individual components are later known as 'element' and the discretization of structures became the basis of FEM. The underlying concept of FEM is, any domain can be divided into smaller subdomains called the finite elements. In this subdomain consist a finite number of prescribed points called 'node' and each node has continuous quantities with unknown value referred as degree of freedom (DOF). The elements are connected numerically and are represented by polynomial that approximate each element's displacement field. The approximation is done by interpolating the unknown continuous quantity of the elements to determine its nodal values. By computing the nodal values for each element, approximation on the value at nodes and elements of the whole domain can be done to solve the problem [16] [17].

2.2.2 Element

Element types can be divided into four categories which are point, line, planar and solid element. Point element such as mass element usually contains only one node. Line element consists of 2(truss) or 3(beam) nodes connected by a line. Planar element on the other hand contains 3 or 4 nodes forming a triangular or quadrilateral shape which could be used for 2D or 3D model. Solid element could only be used for 3D model and has nodes ranging between 4-20 depending on its shape. These elements can then be categorized further based on the order of the interpolation polynomials which are linear first-order and quadratic second-order polynomials. Figure 8 shows some examples of element shapes available consisting of their irrespective nodes.

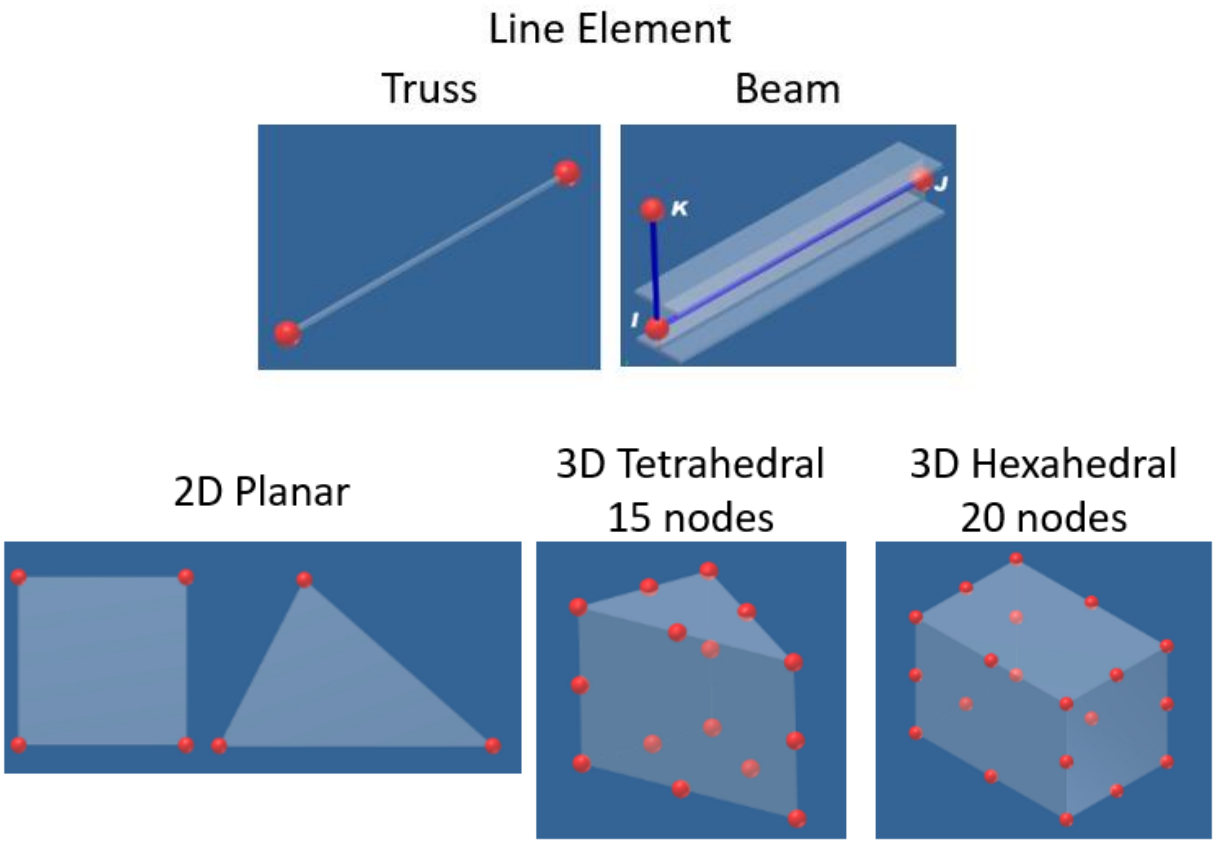

Figure 8 Example of elements [18]

The efficiency of each element varies based on their capabilities in solving the mathematical equation of the corresponding system. For example, first-order element won't be able to solve problems with higher order equation accurately. Figure 9 shows an illustration why that's the case. It shows that the linear plot can't approximate the quadratic plot of the pressure distribution correctly whereas the quadratic plot can produce almost similar approximation.

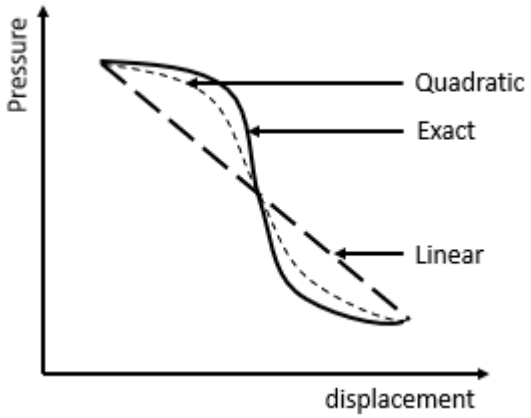

Figure 9 Linear and quadratic element comparison

Langer et al [19] has made a research on the efficiency of elements with different shapes and order. In one of his studies, two hexahedral elements with different polynomial order named C3D20 and C3D8 in ABAQUS are compared. C3D20 is a 3D hexahedral element with 20 nodes discretized using quadratic polynomial while C3D10 is also a 3D hexahedral element but with 8 nodes and discretized using linear polynomial.

A beam structure models are meshed using these two elements and the number of elements per wavelength required from the beam vibration at 10kHz are determined. For the quadratic element, 20 elements per wavelength is required to obtain accurate result with percentage error less than 1%. 400 DOF is enough to calculate the first natural frequency of the beam vibration. For the highest natural frequency, less than 0.1 seconds computational time is needed to solve the model. For the linear element, more than 500 elements per wavelength is needed to obtain accurate result with less than 1% percentage error. Using this minimum no of elements, the model consists of 4500 DOF with a simulation time of 0.6 seconds. If no. of elements used is less than the specified amount, the accuracy is reduced significantly.

A plot of simulation time against total DOF required is plotted for different elements as shown in figure 10. C3D10 is a quadratic 3D tetrahedral element with 10 nodes. From the figure, the trend for quadratic C3D20 and linear C3D8 is similar where as the DOF increases, the simulation time also increases. However, since quadratic elements requires less elements and DOF to obtain similar accuracy as linear elements, it will have a shorter simulation time to obtain accurate results. Furthermore, it was found that C3D10, the tetrahedral quadratic element was able to provide more accuracy but requires higher computational time to solve the same no degree of freedom compared to quadratic hexahedral element. Book by Howard et al [20] agrees with the accuracy of tetrahedral where for modelling of complex geometry, tetrahedral works better to model shapes that is hard to be modelled by hexahedral element.

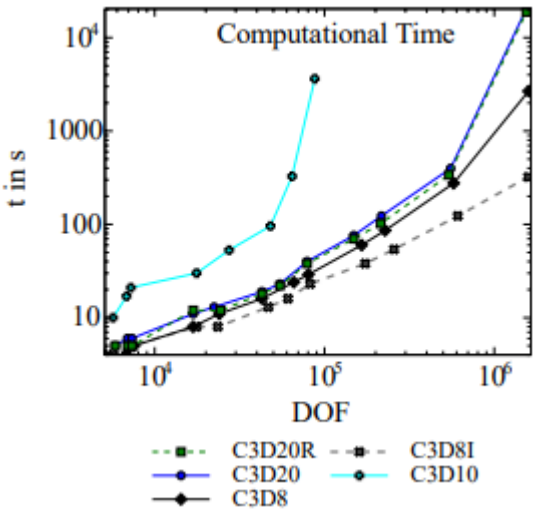

Figure 10 Comparison of computational time of different types of elements [19]

Test on a model of air-filled duct is also done by Langer et al [19] to determine the minimum required elements per wavelength for linear and quadratic elements in an acoustic region. This results in a conclusion that more than six elements per wavelength is required for quadratic elements and more than 10 for linear element to obtain accurate result. These requirements on the minimum elements per wavelength for acoustic region is also noted in a book by Howard & Cazzolato [20].

In addition to the minimum no of elements per wavelength required in a general structural and acoustic model, Langer et al [19] has also studied on the meshing requirements of a thin-walled structures. It is found that across the thickness of the thin-walled structures, a minimum of two layers of elements are required for quadratic element and three layers for linear element in order to obtain accurate results. Furthermore, the maximum aspect ratio allowed of the elements in a thin-walled structure is determined to be 1:10 for quadratic and 1:4 for linear element. Aspect ratio larger than this will cause the results to diverge.

ANSYS

ANSYS has separate elements for modelling of acoustic region and structural body. For modelling of acoustic region and structural body made from piezoelectric material, there are six elements that can be used for each. For homogenous structural solid, two examples of suitable elements are shown. Each has its own characteristics and applicability. Table 4 gives the list of elements available

and its characteristics. More information on these elements such as the DOFs at each node, shapes, analysis types available, FSI coupling options etc. can be found in [20] and [21].

Name	2D/3D	Nodes	Types	Orders
FLUID ELEMENT				
FLUID29	2D	4	Planar element	Linear
FLUID129	2D	2	Line element	Linear
FLUID30	3D	8	Brick element	Linear
FLUID130	3D	4, 8	Planar element	Linear
FLUID220	3D	20	Brick element	Quadratic
FLUID221	3D	10	Tetrahedral element	Quadratic
PIEZOELECTRIC ELEMENT				
PLANE13	2D	4	Planar element	Linear
PLANE223	2D	8	Planar element	Linear
SOLID5	3D	8	Brick element	Linear
SOLID98	3D	10	Tetrahedral element	Quadratic
SOLID226	3D	20	Brick element	Quadratic
SOLID227	3D	10	Tetrahedral element	Quadratic
STRUCTURAL ELEMENT				
SOLID186	3D	20	Brick element	Quadratic
SOLID187	3D	10	Tetrahedral element	Quadratic

Table 4 Element types for acoustic analysis [21]

2.2.3 Absorbing Boundary Condition

Modelling of an air-coupled ultrasonic wave consists of an infinitely large air domain. Modelling this infinite domain is computationally expensive and is not feasible. To overcome this, absorbing boundary condition (ABC) need to be used for simulation of an unbounded system. Using ABC, a finite size domain can be used. This boundary condition is applied at the outer boundary of the finite domain to absorb outgoing waves within the domain. This way the infinite air domain can be modelled as finite. Without this boundary condition, waves incidence on the outer boundary will be reflected back into the domain making it a closed system. The equations used to model the absorbing boundary condition can be referred to many literatures such as Gan et al [22], Jianguo et al [23] and Bielak et al [24].

Various types of ABC have been developed in the past few decades such as Radiation boundary condition (RBC) [23], Lysmer boundary condition [25], Clayton and Engquist absorbing boundary condition (CE-ABC) [26] and Perfectly-Matched Layer (PML) [27]. Each of the ABC has their own strengths and weaknesses. For example, CE-ABC cannot model the boundary condition at corner [28] and has low effectiveness at low frequency analysis [29]. RBC on the other hand, needs to comply to plane wave condition and are limited for waves propagating normal to the radiation surface for effective absorption [20]. PML, suffers from high computational cost due to requiring added layers of element to the model. PML also has issue on instability of absorption of tangential incident waves and has complex theoretical derivation [28]. Despite the disadvantages, PML excels at absorbing waves from a wider range of angle and frequency.

A. Rahimi Dalkhani et al [28] has made a comparison between PML and CE-ABC to study their efficiency as an ABC. In the study, wave reflections at the boundary of a 2D homogenous model with a dimension of 1000m in x and z-directions are measured. Ricker wavelet source with 20Hz frequency is used. PML and CE-ABC are applied to the model and different thickness of 100 and 200m are used for PML layer. The results obtained shown in figure 11 shows that the CE-ABC is much more efficient than PML with minimal reflection. Besides, comparing between the two thickness of PML, a lot of boundary reflections are detected for PML with 100m thickness compared to 200m. This shows that the effectiveness of PML depends on its layer thickness.

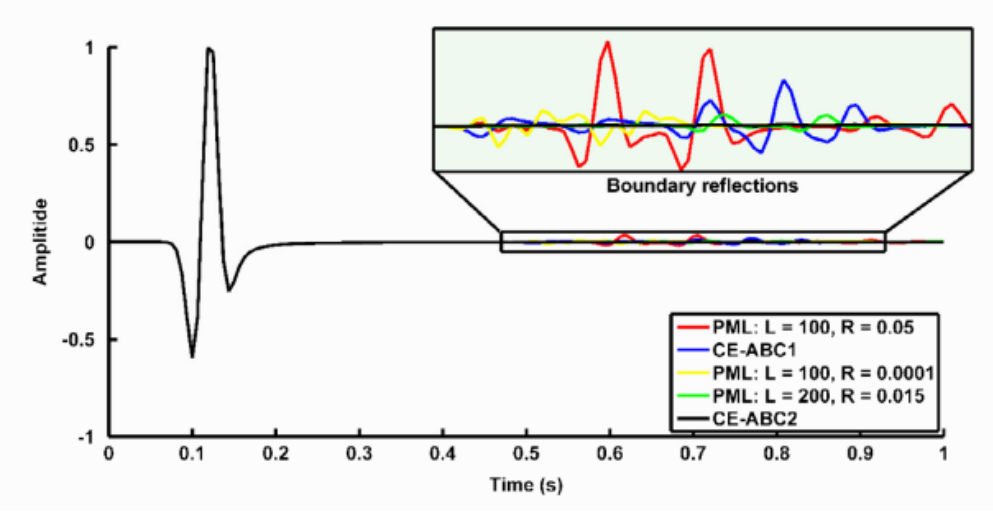

Figure 11 Boundary reflection results by A. Rahimi Dalkhani et al on the comparison between PML and CE-ABC. L = thickness, R = radius of excitation source

Furthermore, A. Rahimi Dalkhani et al [28] has also studied the effect of incident wave angle on the efficiency of PML and CE-ABC. Ricker wavelet with a peak frequency of 15Hz is used as the source. The study concludes that for high incident angle and when the source is near the boundaries, PML works better than CE-ABC. However, at low incident angle CE-ABC is better. Figure 12 shows examples of wave reflection observed for (a) PML and (b) CE-ABC. More dispersion in waves is observed in CE-ABC especially in the area circled at the bottom left of the figure. Apart from study on incident wave angle, computational cost associated with each ABC are studied. For model with PML, the computational cost is significantly higher than CE-ABC. This is due to the added layers of elements on the whole model required by PML whereas in CE-ABC no added elements are required. The time taken to complete the simulation with multi-source modelling for PML is 6.7 hours and three hours for CE-ABC. This shows the main weakness of PML boundary condition.

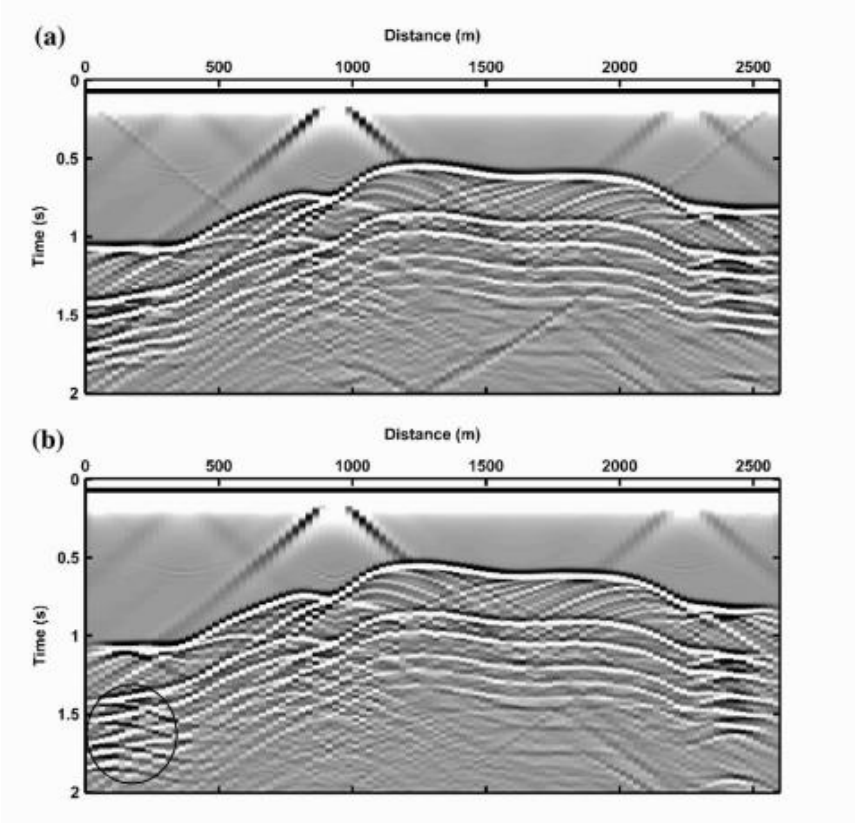

Figure 12 Wave reflection for (a) PML and (b) CE-ABC as studied by A Rahimi Dalkhani et al

ANSYS

In ANSYS, three ABCs are available and ready to use which are PML, RBC and infinite acoustic elements. Each of these ABCs have their own characteristics and are limited to certain types of analysis as shown in table 5. The characteristics and capabilities of each ABC are explored in this section and procedures to implement them in ANSYS are presented.

Boundary Conditions	Modal	Harmonic	Transient
PML	No	Yes	No
RBC	Yes	Yes	No
Infinite fluid elements	Yes	Yes	Yes

Table 5 Types of analysis available for each ABC [13]

Perfectly Matched Layer

According to Howard et al [20], the PML ABC in ANSYS is able to absorb all outgoing waves except for waves propagating tangential to the boundary layer. This is similar to the statement made by A. R. Dalkhani et al [28] regarding the disadvantages of PML. To use the PML in ANSYS, it requires certain requirements on the configuration of the model. Figure 13 shows the standard configuration of model with PML.

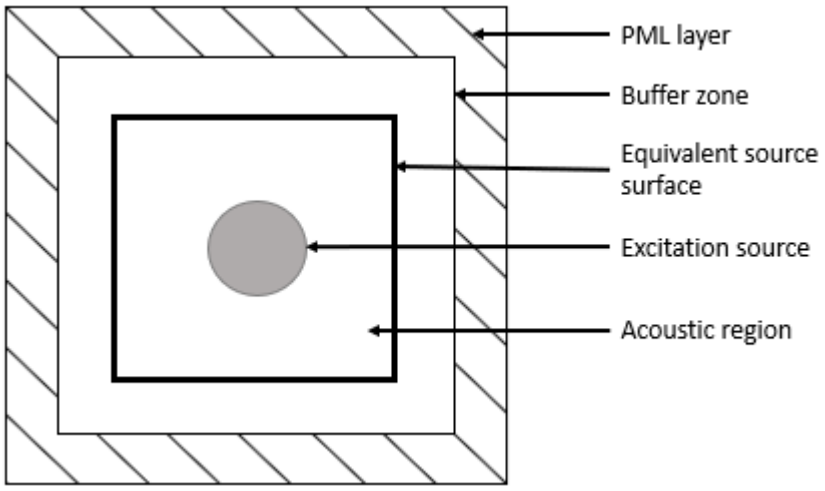

Figure 13 Configuration of model with PML [20]

As mentioned previously, PML ABC needed another added layer marked with dash line at the outer boundary of the acoustic region as shown in figure 13. This is the reason PML layer requires higher computational time compared to other ABCs. Besides, the PML layer also needs to have rectangular shape. If not, the boundary condition can't be defined. This layer can only be modelled using FLUID30, FLUID220 and FLUID221. The purpose of equivalent source surface is to

provide measurement of various acoustic results outside of the modelled region. Using this, the model doesn't have to be large to measure results at far-field thus the possibility to minimize the model size. Buffer zone is needed to separate the equivalent source surface and PML layer. All these layers and zones need to follow these conditions:

1. Distance between excitation source and equivalent source surface needs to be greater than half a wavelength of the acoustic wave
2. Thickness of buffer zone needs to be more than three layers of elements
3. Thickness of PML layer needs to have more than three elements and more than a quarter of the acoustic wave wavelength.

If these conditions are not met, some of the waves will be reflected back into the computational domain affecting result accuracy. However, if the PML is too thick, higher computational cost and simulation time is needed [20].

Radiation Boundary Condition

Different to PML, RBC doesn't require added layers of elements at the boundary of the acoustic region instead, the boundary condition is applied at the boundary's surface. This boundary condition uses "Robin boundary condition" which defines the surface to has an impedance of:

Equation 5 Impedance of Robin Boundary Condition

$$Z = \frac{p}{v_n} = \rho_0 c_0$$

Where p = pressure, v_n = acoustic particle velocity, ρ_0 = density of fluid and c_0 = sound speed of fluid. This boundary condition is effective only under these conditions:

1. Plane wave condition is complied
2. Outgoing wave propagates normal to the radiation surface

If these conditions aren't met, some of the waves will be reflected back into the computational domain thus reducing its accuracy.

Infinite Fluid Elements

For infinite fluid element ABC, the boundary condition can be applied only on a spherical surface. Hence, the air domain needs to be spherically-shaped. Sommerfeld radiation condition are used

for this ABC. To satisfy Sommerfeld radiation condition, the waves produced need to spread out spherically and if it's not, some of the waves will be reflected back into the acoustic domain. This is opposite to the RBC hence, planar waves are not suitable for this boundary condition. Otherwise, it would have excellent absorption similar to PML. The only drawback of this ABC is that since spherical-shaped is used, it will cause the acoustic domain to be larger than required hence increasing the nodes and elements of the model.

2.2.4 Fluid-Structure Interaction

Fluid-structure interaction (FSI) describes the coupled dynamics of a moving fluid and a movable or deformable solid structure. An illustration in figure 14 briefly describes the mechanism of the FSI coupling. In general, when a fluid with motion impact and compressed on a structural body, loading is applied to the body and cause it to deform. Subsequently, the deformation of the structure causes fluctuation in the pressure of the fluid and this continues. This coupling is governed by a set of partial differential equations with specified boundary conditions. It can be solved analytically or numerically. However, analytical solution is only effective for simple geometries. An example of this can be seen in study by Andre et al [30]. For most cases, numerical methods are more commonly used to approximate the FSI coupling equations.

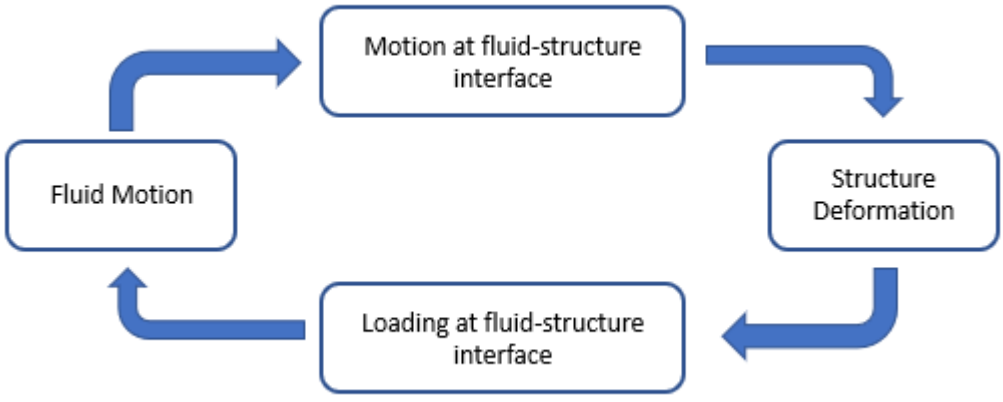

Figure 14 Mechanism of FSI coupling

There are many numerical methods that have been established to solve FSI problems. Some of them are immersed boundary method, proposed by Peskin [31], fictitious domain method (FictD) [32] Lagrangian Eulerian method (ALE) [33] and Immersed Finite Element Method [34]. Van Loon et al [35] has made a comparison between different FSI method in his study comparing between ALE, FictD and Combined fictitious domain/adaptive meshing method (FictD/adap). Based on the study, each method has its own advantages and disadvantages. For example, at a fixed mesh size, ALE is proved to have more accuracy than FictD method. However, FictD has the advantage that the fluid and structural body can be meshed separately, and that meshing is only required prior to simulation. Since, the meshing can be done separately, FictD has lower computational cost than ALE. When comparing the implementation practicality, ALE is the easiest to implement. This is followed by FictD and FictD/adap method where FictD/adap is the most labour intensive method. From this study, it can be concluded that it is important to choose the right method to model the FSI befitting the aim of the analysis. And this would be by analyzing their applicability on different type of situations.

ANSYS

In ANSYS, the FSI coupling has already been established within the software. Hence, no derivation is required to define the FSI coupling. Two types of coupling are available which are:

1) Matrix-coupled FSI solutions
2) One-way coupling FSI solutions

In matrix-coupled FSI solutions, the fluid interacts with the structural body via coupling boundary conditions. In this coupling, pressure and displacement DOF are solved at the same time. Figure 15 shows the coupling at the FSI interface.

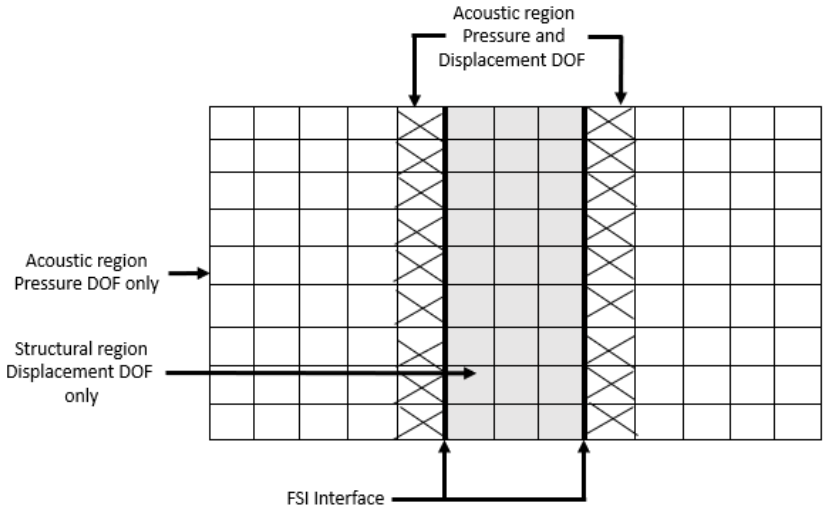

Figure 15 Coupling region at the fluid-structure interface

In the purely acoustic region, only pressure DOF is solved, in purely structural body region, displacement DOF is solved. However, at the interface between the two, both DOFs are solved. The governing equation of motions of the coupling are shown below. The reason these equations are shown is to show how the pressure and displacement interaction is connected. There are two governing equations, one for unsymmetric matrix coupling and the other is for symmetric matrix coupling.

Unsymmetric matrix: $$\begin{bmatrix} -\omega^2 M_s + j\omega C_s + K_s & -R \\ -\omega^2 \rho_0 R^T & -\omega^2 M_f + j\omega C_f + K_f \end{bmatrix} \begin{Bmatrix} U \\ p \end{Bmatrix} = \begin{Bmatrix} F_s \\ F_f \end{Bmatrix}$$

For Symmetric matrix, nodal pressure transformation variable defined as $\dot{q} = j\omega q = p$ is substituted to the unsymmetric matrix. This results in:

$$\begin{bmatrix} -\omega^2 M_s + j\omega C_s + K_s & -j\omega R \\ -j\omega R^T & \frac{\omega^2 M_f}{\rho_0} - \frac{j\omega C_f}{\rho_0} - \frac{K_f}{\rho_0} \end{bmatrix} \begin{Bmatrix} U \\ q \end{Bmatrix} = \begin{Bmatrix} F_s \\ \frac{j}{\omega \rho_0} F_f \end{Bmatrix}$$

Where ω = natural frequency, ρ_0 = density, j = imaginary parts, M_f = fluid mass, M_s = structural mass, K_f = fluid stiffness, M_s = structural stiffness, F_f = applied fluid load, F_s = applied structural load, C_f = fluid damping coefficient, C_s = structural damping coefficient, U = nodal displacement, p = nodal acoustic pressure, q = nodal pressure transformation variable, R = coupling coefficient for each node in the FSI surface. Derivation of these equations can be found in [20]. To solve the nodal displacements and pressures, the matrix needs to be inversed. This is problematic for the

unsymmetric matrix where the computational resource required to invert this matrix is highly expensive. Hence, the reason symmetric matrix coupling is developed. Inverting the coupled matrix to solve the nodal displacements and pressures is much easier thus lower computational resource is required. An example of the comparison between these two matrices coupling is provided in [20]. In the book, study of FSI interaction of a flexible plate in an acoustic cavity is made. Based on the study, the displacement of the plate and acoustic pressure measured is similar between the two coupling matrices as shown in figure 16. The only difference is in the computational time to solve the model. Using the symmetrical matrix coupling, the model is solved in 4.5 hours while for unsymmetrical coupling, it took 8.8 hours using the same computer resources. This shows the advantage of symmetric matrix coupling available in ANSYS.

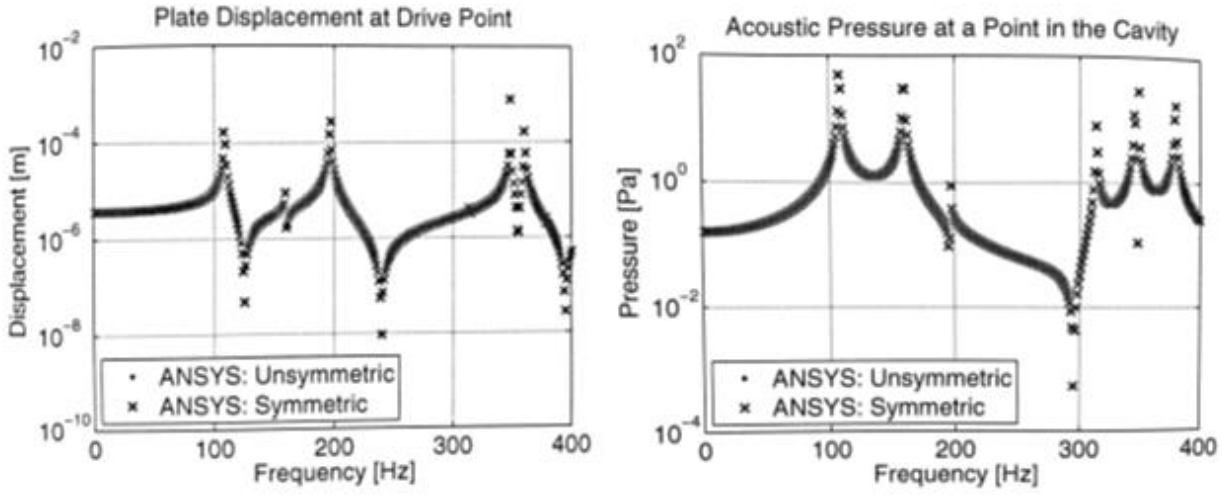

Figure 16 Comparison of coupling matrix from [20]

Chapter 3: Model Description

In this section, the model developed to study the interaction between ultrasonic sound and solid plate is described. The model is created using ANSYS version 19.1 on ANSYS Workbench using Harmonic Acoustic analysis tool. Harmonic Acoustic is an implicit analysis that simulates the generation and propagation of acoustic wave in an acoustic medium. It is also capable of simulating the coupled fluid and structural interaction (FSI). The general Acoustic Equations used in Harmonic Acoustic can be found in Acoustic Analysis Guide found in ANSYS HELP [36]. In Harmonic Acoustic, steady-state response caused by sinusoidal loads is calculated while excluding the transient behavior of the system. Harmonic Analysis operates in frequency domain while in Transient Analysis, time domain is used. In a typical transducer system, transient behavior is observed due to damping caused by the backing material. However, in this thesis, focus is given on the study in the frequency domain for study at various frequency.

Figure 17 shows the steps used to develop the model. First, a model is built, and material properties are defined for each component in the model. Next, the model is meshed with suitable element type and size. The boundary conditions, excitation source and fluid structure interaction (FSI) is then defined. Finally, the model is solved, and the results are validated. If the model doesn't adhere to the expected results, changes are made to the model and this is iterated until the final model is obtained. To supplement the model descriptions in this section, a step-by-step navigation through the DesignModeler and Workbench of the model development are included in Appendix A.

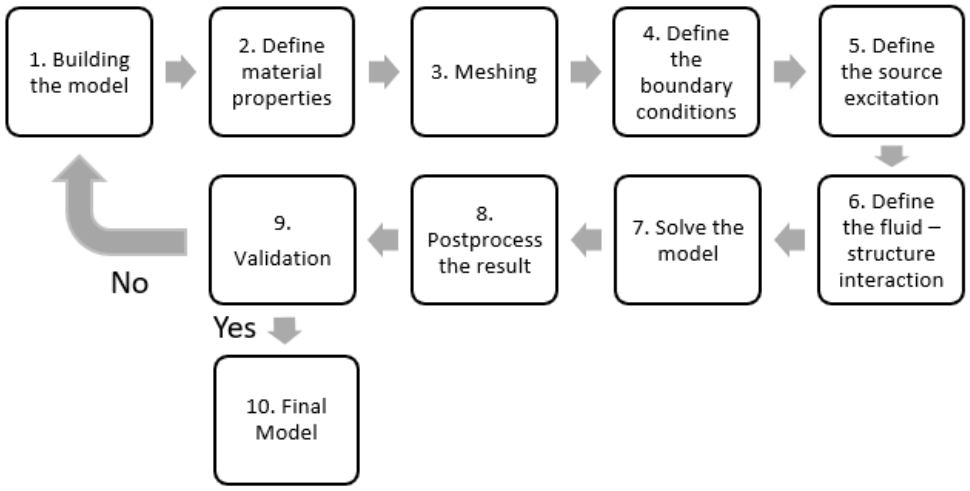

Figure 17 Model development process

3.1 Model Configuration

The model consists of 2 main parts which are the structural body and fluid domain. The solid plate and excitation source are categorized into the structural body. Fluid domain consists of the fluid that surrounds the structural parts and PML layer. The upcoming sections explain the purpose and modelling method of each components of the model. The model is build using ANSYS Design Modeler. Figure 18 shows the model configuration in (a) 3D, (b) Top (XZ plane) and (c) Side view (XY/YZ plane)

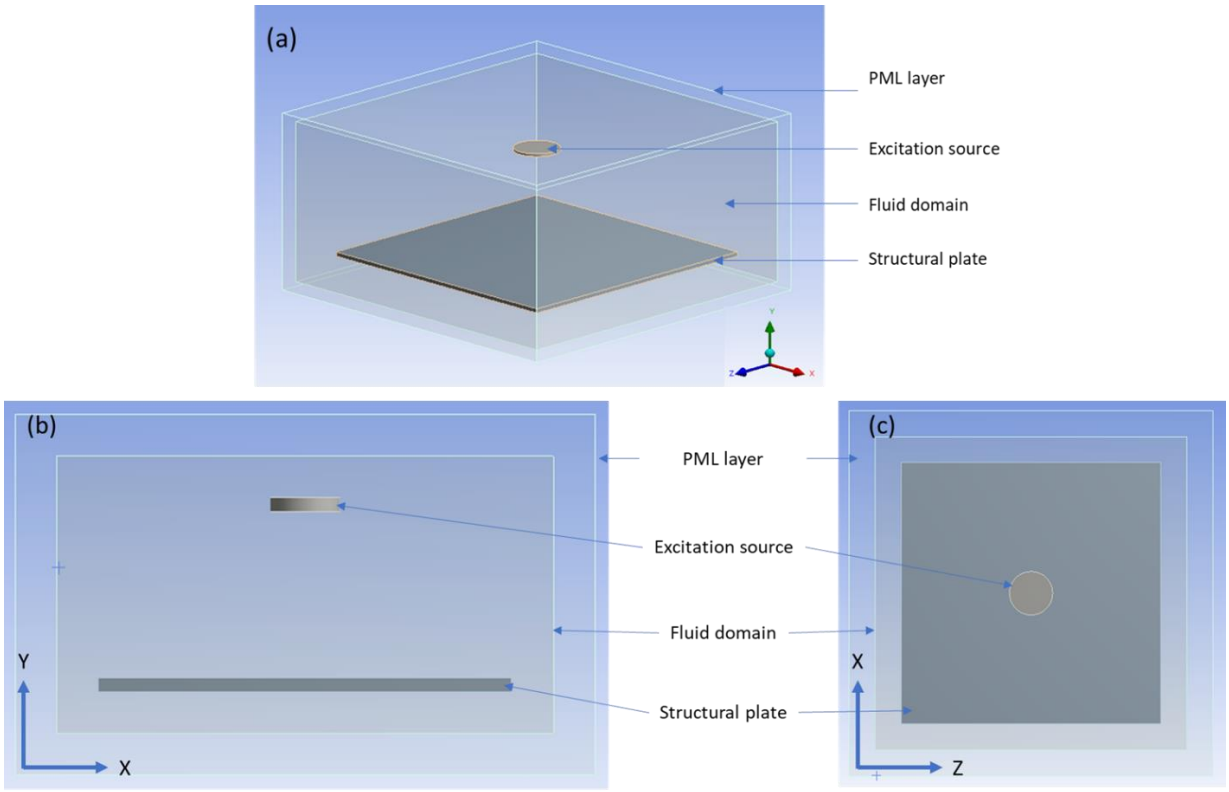

Figure 18 Configuration of full model

3.1.1 Excitation Source

The excitation source used is modelled based on a conventional piezoelectric transducer. This transducer is chosen because it is one of the most common and simplest transducer designs. By designing a simple model, modifications and changes can be made based on this model for further researches that requires more specific and complex model.

In Harmonic Acoustic, many types of excitation source can be applied such as acoustic and load source. In acoustic source, there are mass source, surface velocity, diffuse sound field, incident wave source and port in duct that can be applied to fluid domain. In load source, there are pressure, force and moment load that can be applied to structures. However, if these excitation sources are used, the piezoelectric properties of the transducer can't be implemented. Hence, the excitation source can't be modelled based on piezoelectric transducer.

As described in section 2.1.2, piezoelectricity works by applying voltage to a piezoelectric material and the electrical energy is converted to mechanical energy causing the material to vibrate thus producing sound. To model this behavior, a Piezo and MEMS extension is used. This extension is made for ANSYS Mechanical application and can be downloaded from (ANSYS, catalog.ansys.com, 2019). Using this extension, coupling between structural and electrical fields are established to enable the piezoelectric behavior. More info on this coupling and extension are available on ANSYS support [37] .

As mentioned previously, the conventional piezoelectric transducer consists of four main parts which are the active element, matching layer, backing material and casing. However, the transducer model seen in figure 18 consists of a thin cylinder only which represents the active element. The reasons behind this design are explained in the upcoming subsections.

Backing Material

As mentioned in Section 2.1.3, the purpose of backing material is to produce a damping effect on the vibration of the active element. However, since Harmonic Acoustic is used for this model, the effect of damping won't be observed. Hence, the backing material is disregarded from the transducer model. Because of this, the surface at the back of the active element need to be defined with some boundary condition to replace the backing material. The boundary condition used is described in the upcoming Section 3.4.1 of the Boundary Condition section.

Using Harmonic Acoustic instead of transient won't be a problem. The reason is in transient analysis, results processed are often based on the signal received at the beginning of the vibration, where the highest vibration amplitude is measured. In Harmonic Acoustic, no damping occurred, and the amplitude will remain the same equal to the measured highest amplitude in transient analysis which will yield the same result. Hence, the effect of damping is not necessary to be modelled. The only disadvantage is the incapability to observe the waves propagation in time domain.

Matching Layer

In this thesis, the coupling medium is air surrounding the transducer. The specific acoustic impedance of air is 0.0004Mrayls while other materials such as aluminium and steel are 17Mrayl and 45.4Mrayls respectively as shown in table 1. The significantly large value of acoustic impedance of solid material such as aluminium relative to air causes the wave vibration from the solid to air to be relatively easy. However, when a wave that travel through air incident on a solid, most of the waves are reflected due to the huge impedance mismatch. Thus, in an air-coupled ultrasonic transducer, matching layer plays a huge role for the receiver transducer to receive the wave vibration. Whereas for transmitter, the wave vibration can be transferred easily from the transducer surface to air. In this thesis, only acoustic waves produced by the transmitter is studied hence, eliminating the matching layer from the model won't affect the results much. Subsequently, the matching layer is not included in the model and the front surface of the active element is set as surface with free displacement.

Active Element and Casing

The thin cylinder labelled as the transducer is the active element. The diameter of the active element can be varied based on personal preferences. However, the thickness, t is determined according to the frequency of analysis based on equation 6:

Equation 6 Thickness of active element

$$t = \frac{w}{2} = \frac{v}{2f}$$

Where w = desired wavelength f = frequency of analysis and v = fluid medium speed. The reason for this is, the active element usually vibrates at a wavelength two times its thickness. Hence, the

thickness needs to be cut to half of the desired wavelength [15]. The casing is modelled as fixed support boundary condition since its purpose is only to fix the three components; active element, matching layer and backing material in place.

3.1.2 Solid Plate

A square plate is modelled using DesignModeler and the thickness and length of it can be varied freely. This plate is used to study the interaction between ultrasonic waves and a solid plate.

3.1.3 Fluid Domain

The fluid domain consists of the fluid surrounding the structure (computational domain) and PML layer. Enclosure tool in Design Modeler is used to create the model. The fluid surrounding the structure makes up the most part of the computational domain because in this zone, analysis is done to study the acoustic effect causes by the source excitation. Results such as acoustic pressure and potential energy are calculated in this domain. On the other hand, PML layer creates an unbounded system where acoustic wave can be propagated out of the computational domain as explained in Section 2.2.3 of Absorbing Boundary Condition section. Without the PML layer, the outer surface of the fluid surrounding the structure is modelled as rigid wall. This creates a close system where acoustic wave will be reflected at the boundary of the computational domain. Section 4.3.2 shows the difference between models with and without the far-field radiation zone. The reason PML layer are chosen is explained further in Section 3.4.3.

3.2 Material Properties

3.2.1 Transducer

Since piezoelectric material is used, some properties of the material need to be defined:

1. Permittivity Matrix
2. Piezoelectric Matrix
3. Elastic Coefficient Matrix
4. Sound speed and density of material

Permittivity matrix links the dielectric displacement of the material with the electric field using strain, $[\varepsilon^S]$ and stress, $[\varepsilon^T]$ matrix using equation 7.

Equation 7 Permittivity

$$[\varepsilon^S] = [\varepsilon^T] - [d]^t[s^E]^{-1}[d]$$

Where $[d]$ = piezoelectric strain matrix, s^E = Compliance matrix.

Piezoelectric matrix links the electric and stress/strain field. It consists of the stress, $[e]$ and strain matrix, $[d]$ related by compliance matrix, $[s^E]$ as in equation 8.

Equation 8 Piezoelectric properties

$$[e] = [s^E]^{-1}[d]$$

Elastic Coefficient matrix defines the material linear elastic properties where orthotropic elasticity is used for this material. For an orthotropic material, stiffness matrix is the inverse of the compliance matrix as shown in equation 9.

Equation 9 Elasticity properties

$$[c^E] = [s^E]^{-1}$$

Where c^E = stiffness matrix [37]

Figure 19 shows the input required for the active element material properties.

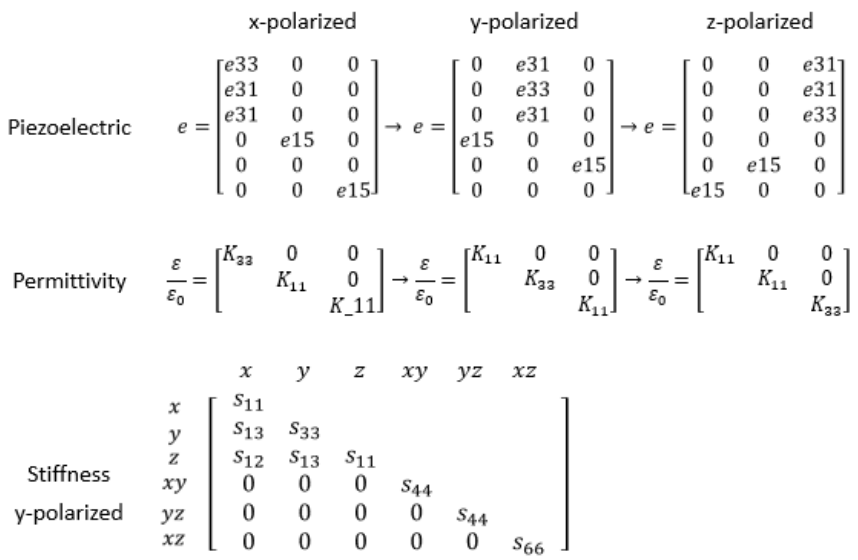

Figure 19 Coupling matrix for piezoelectric material

3.2.1 Solid Plate and Fluid Domain

Material for solid plate and fluid domain can be taken directly from 'Engineering Data' where properties for various materials has been defined by ANSYS. Other materials that are not in the database can also be used by manually defining the material. Material "air" is defined for fluid domain.

3.3 Mesh

This section describes the element type used for each components of the model; transducer, plate, fluid domain and PML layer and the reason for it. The element size used is also described and the resulting mesh are shown in Section 4.2.

3.3.1 Element Type

As discussed previously, the accuracy and efficiency of the simulation model is mainly based on the elements used. Hence, it is important that the right elements are chosen for the model. In simulation of fluid-structure interaction, high order interpolation polynomials are used to solve the model. Hence, it is important that the elements used to have a high order as well to produce accurate results. Based on table 4 in Section 2.2.2, the suitable elements for each component are listed as follows:

- Transducer – SOLID226 and SOLID227
- Fluid – FLUID220 and FLUID221
- Plate – SOLID186 and SOLID187

SOLID226, FLUID220 and SOLID186 are a 20 nodes element that can have various shape such as hexahedral, tetrahedral and pyramid. The other is a 10 nodes element and can have only tetrahedral shape. According to study by Langer et al [19] and book by Howard and Cazzolato [20] mentioned in Section 2.2.2 of Literature Review section, tetrahedral element is more suitable for modelling complex geometry where other shapes would have problem modelling. In this model, the geometry is rather simple hence the use of tetrahedral would be unnecessary and would only lead to extra computational cost. Thus, SOLID226, FLUID220 and SOLID186 are used since other shapes that are simpler to solve than tetrahedral such as hexahedral can be chosen. For validation of this element choice, simulation tests using the chosen elements and the 10 nodes tetrahedral elements were done to compare the results for both. This is shown in Section 4.1.2 in Validation Test section.

3.3.2 Element Size

As mentioned previously in Literature Review section, for the fluid elements there should be at least 6 elements per wavelength. Furthermore, for the structural body, at least 20 elements

per wavelength are required. From this, the element size required for both parts can be obtained using equation 11 and 12 where the sound speed of air = 343m/s.

Equation 10 Wavelength of propagating wave

$$wavelength, \lambda = \frac{sound\ speed, v}{sound\ frequency, f}$$

Equation 11 Element size for fluid body

$$Fluid\ element\ size, \Delta w_F = \frac{\lambda}{6}$$

Equation 12 Element size for structural body

$$Structural\ body\ element\ size, \Delta w_S = \frac{\lambda}{20}$$

These requirements will be studied further by performing a convergence test on the number of elements per wavelength required in Section 4.2.2. Since the structural body has different element size than the fluid domain, a few layers of fluid are added surrounding the structural body with element size in between the fluid and structural body required size so that the nodes between the elements can be connected and no drastic change between the element size of fluid and structural body occurred. Figure 20 shows the meshing of the model near a structural body.

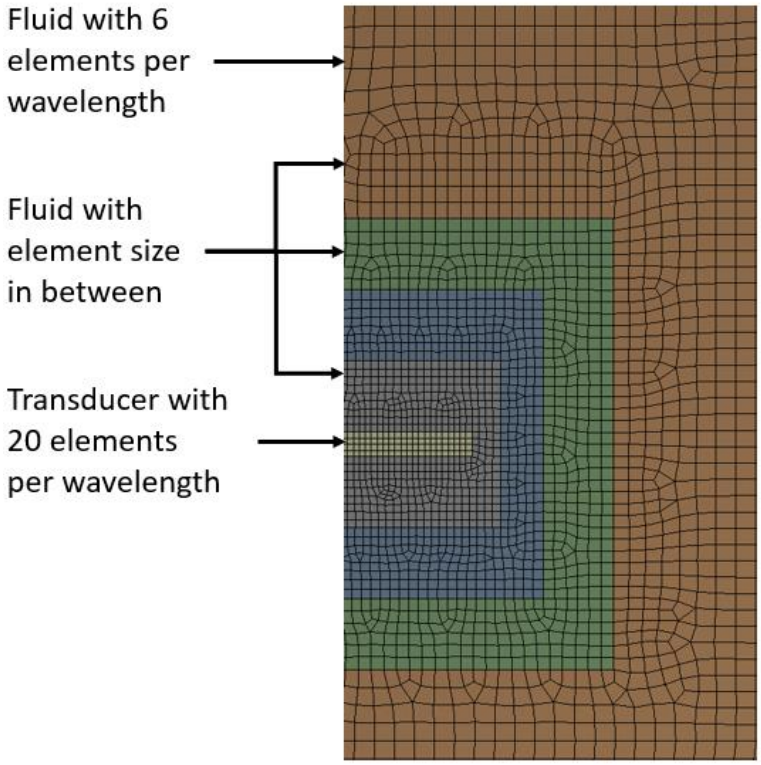

Figure 20 Mesh structure near structural body

3.4 Boundary Condition

3.4.1 Transducer

Fixed supports are applied at the side and back surface of the active element. Deformation due to piezoelectricity occurs only at the front surface. The fixed support at the side illustrate the attachment of the active element to the casing thus restricting its movement. The fixed support at the top surface represents the backing material described in section 3.1.1 under Backing Material section. In reality, the boundary condition at the active element surface attached with backing material is actually a free support. So, why is fixed support is used instead of free? The reason is discussed in Section 4 on the validation of boundary condition section. Comparison between the use of fixed support and free support at the back of the active element are made in the section. Figure 21(a) shows the illustration of the boundary condition and figure 21(b) shows the boundary condition applied in Workbench.

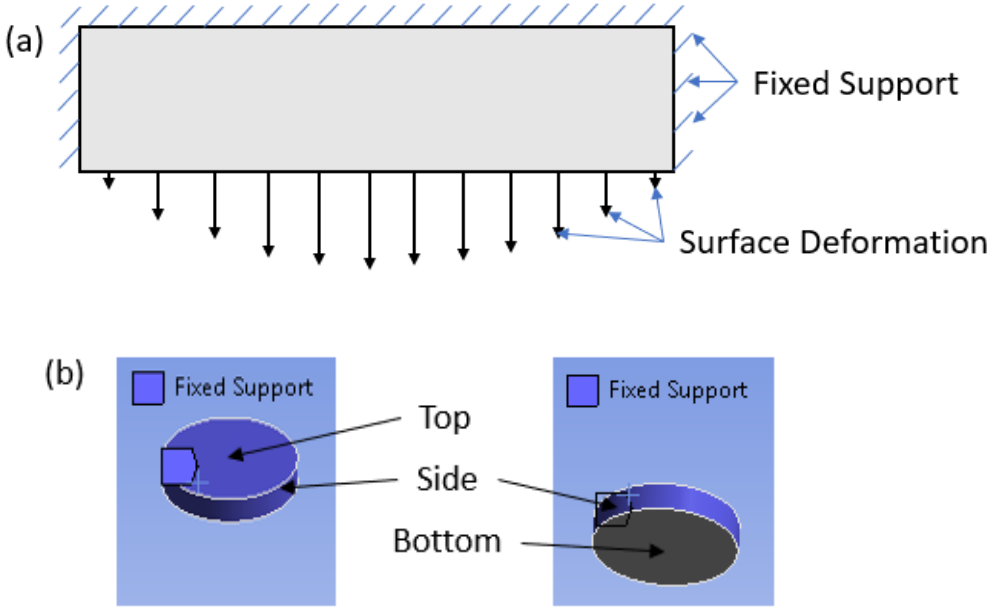

Figure 21 Boundary condition of active element

3.4.2 Solid Plate

Fixed supports are applied on the bottom surface at the two ends of the plate as shown in figure 22 to represents the holder of the plate in real life.

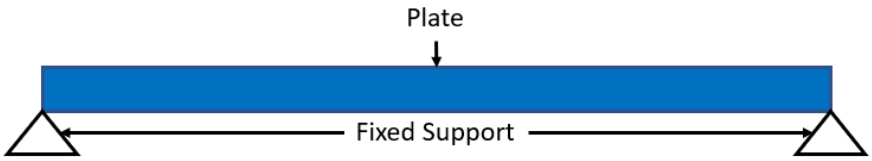

Figure 22 Boundary condition of solid plate

3.4.3 Fluid Domain

As mentioned previously, ANSYS has three types of ABC which are PML, RBC and infinite fluid element. Among these three, PML is used and with justifications from literature review regarding these ABCs, the reasons PML is used are:

1) Ultrasonic wave produced in this model is not planar hence, this will reduce the wave absorption at the boundary of the fluid domain if RBC is used
2) Wave reflected at solid plate will be at angle which will cause ineffective absorption by RBC
3) Using infinite fluid element would cause larger modelling size due to its requirement of having spherical shape whereas for this simulation it is more suitable to have cubic shape boundary to enclose the square shape of the solid plate.

Validation tests by comparing results obtained using RBC and PML are made in Section 4.3.2.

Based on the requirements of using PML in Section 2.2.3, the thickness of the PML is set to be more than three layers of element and thicker than a quarter of the acoustic wavelength. The thickness of the buffer zone is also set to be more than three layers of element. Convergence test is done in Section 4.3.2 by varying the PML thickness to determine the validity of these requirements.

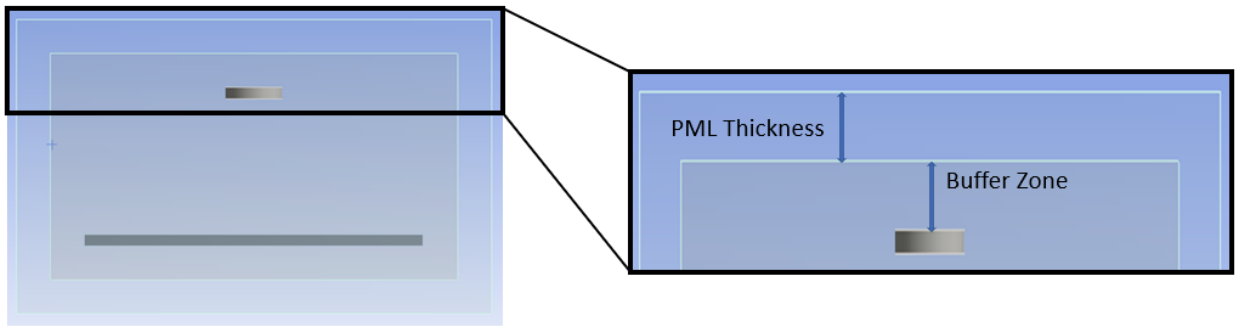

Figure 23 PML dimensions

3.4.4 Fluid-Structure Interaction (FSI)

Symmetric matrix solver is used for the FSI boundary condition since it is more efficient than unsymmetric matrix solver. To use this, all the components need to be set as one body in DesignModeler as shown in figure 24 (a). Then the FSI are defined at all surfaces of structural body that are in contact with fluid element. Figure 24 (b) shows an example of surfaces (highlighted blue) that have been defined as in contact with fluid element.

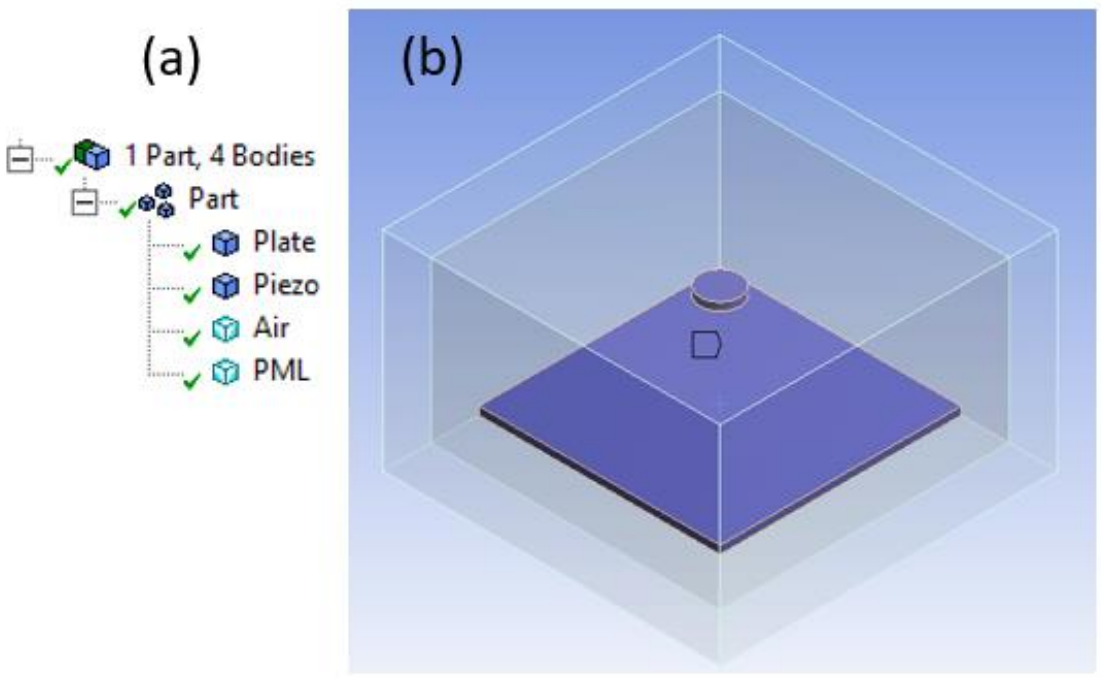

Figure 24 FSI boundary condition

3.4.5 Symmetry

Since the model is axisymmetric, symmetry boundary condition is applied on the XY plane at Z = 0 and on YZ plane at X = 0. Using this boundary condition, only a quarter of the model is needed to be solved. This will reduce the total computational cost and simulation time. Figure 25 shows the model with symmetry boundary condition applied. First on (a) XY plane only producing half model and next on both (b) XY and YZ plane producing quarter model. Comparison between results simulation using models with symmetry and no symmetry are made in Section 4.3.3.

(a) Half Model,
Symmetry on XY Plane

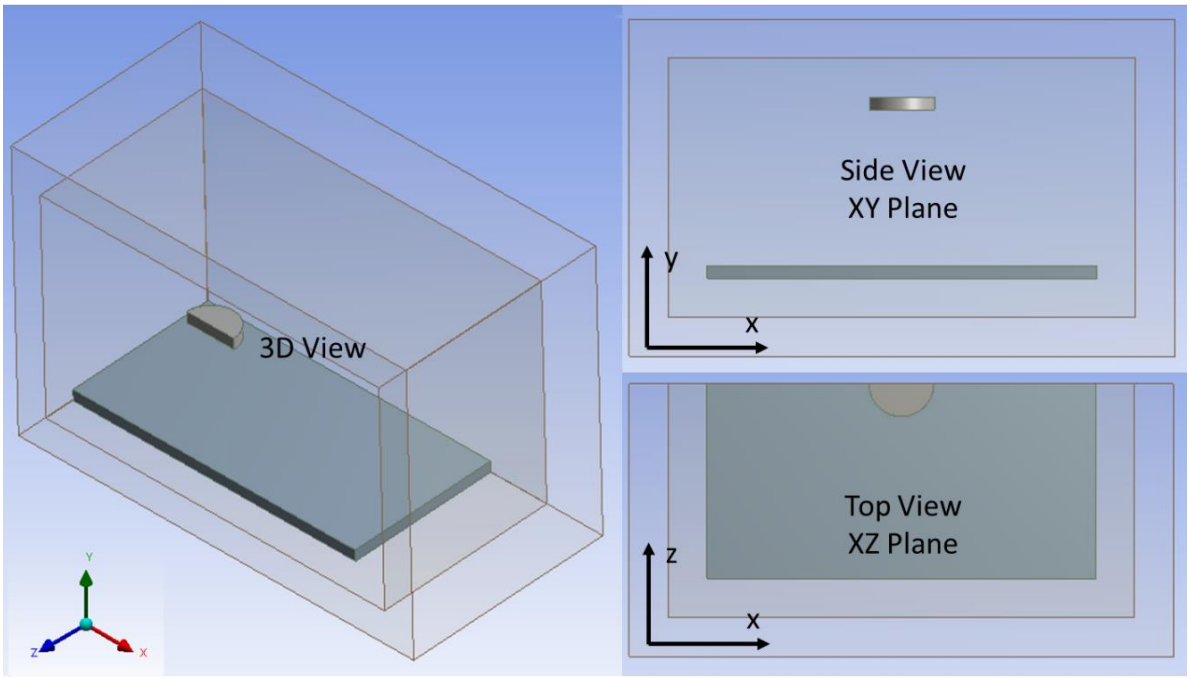

(b) Quarter Model,
Symmetry on XY and YZ Plane

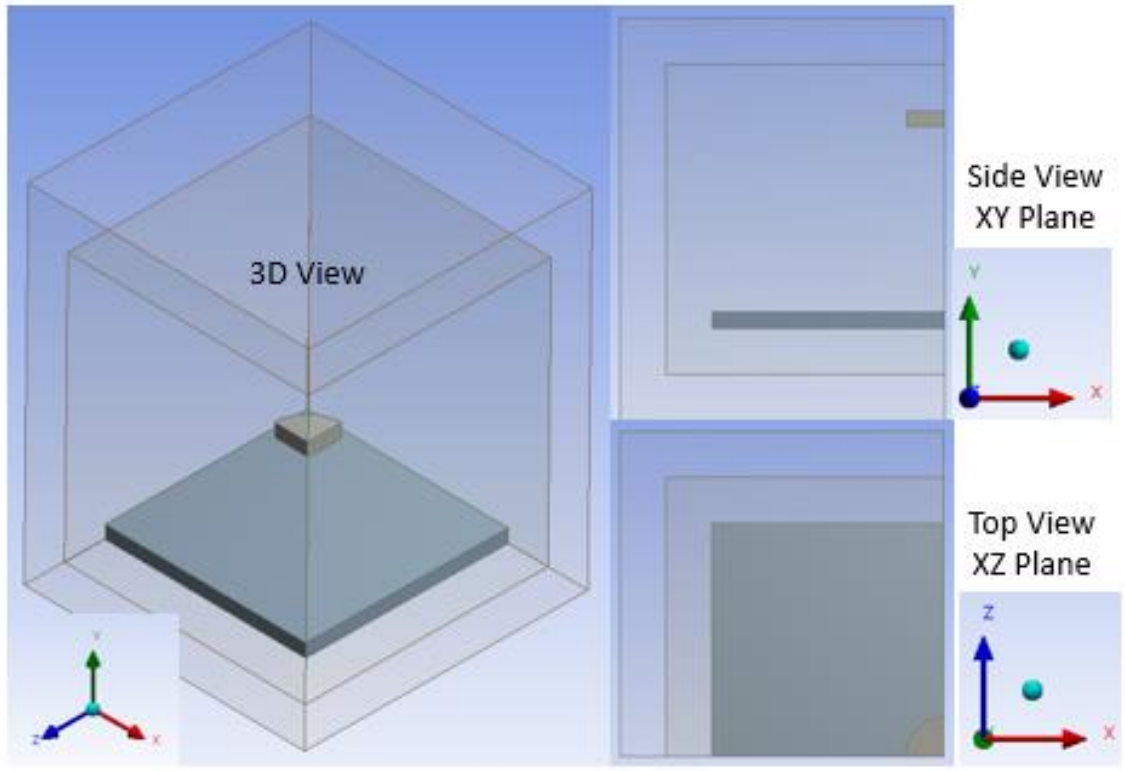

Figure 25 Symmetrical model

3.5 Excitation Load

Excitation load in this model comes from the voltage input into the active element. Two different voltage amplitudes are applied at top and bottom of the transducer surfaces to produce a potential difference across the active element. Due to piezoelectricity, the active element vibrates, and the alternating current causes it to vibrate sinusoidally thus producing sound wave. In this model, the transducer is polarized in y-direction. This is defined by using y-polarized matrix shown in figure 19 in Section 3.2.1. The transducer will emit ultrasonic wave in negative y-direction towards the solid plate as seen in figure 26.

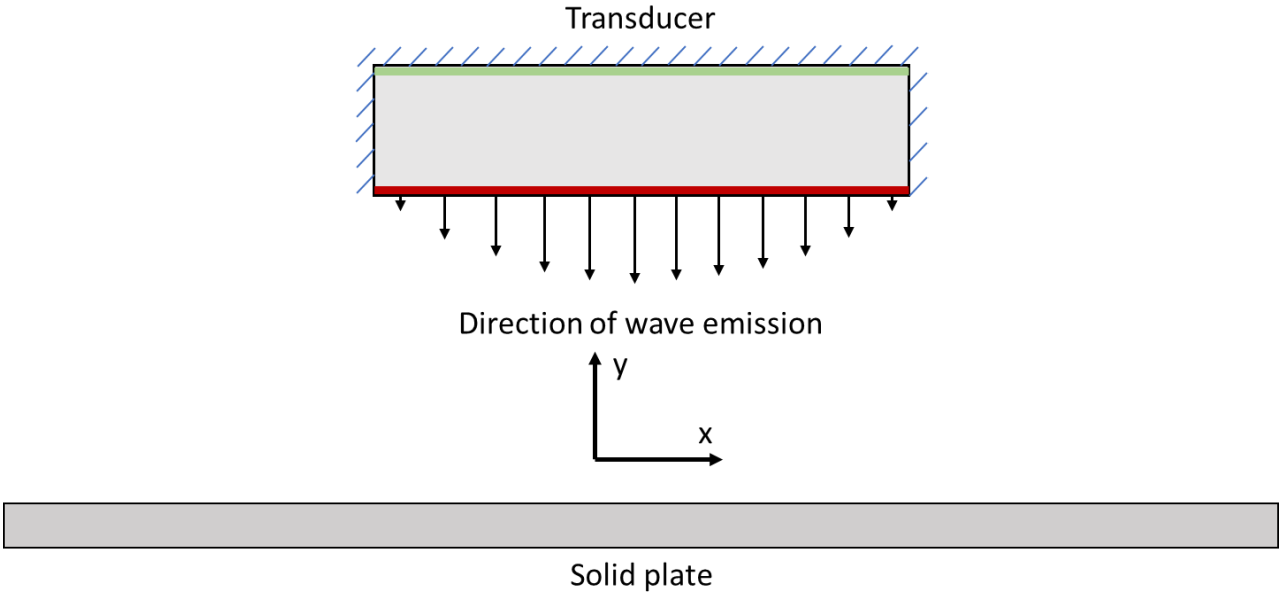

Figure 26 Wave emission direction

3.6 2.5D Model

The main aim of developing a 2D model is to reduce the total computational cost and simulation time required in 3D model. Since in 2D model less elements are used, its simulation time is typically much lower than a 3D model, it serves as a great tool for validation studies. This will complement the 3D model by producing preliminary results that can be studied before proceeding with 3D model.

For a 2D model, FLUID29 and FLUID129 are required as the element of the fluid domain. However, in V19.1, Workbench doesn't support these elements. Hence, a fully 2D model can't be developed. To overcome this problem, a 2.5D model is developed. The basis of this model such as the material, mesh, excitation source and boundary conditions are similar to the 3D model. The only difference between these models are on the symmetry boundary condition. Figure 27 shows the 2.5D model.

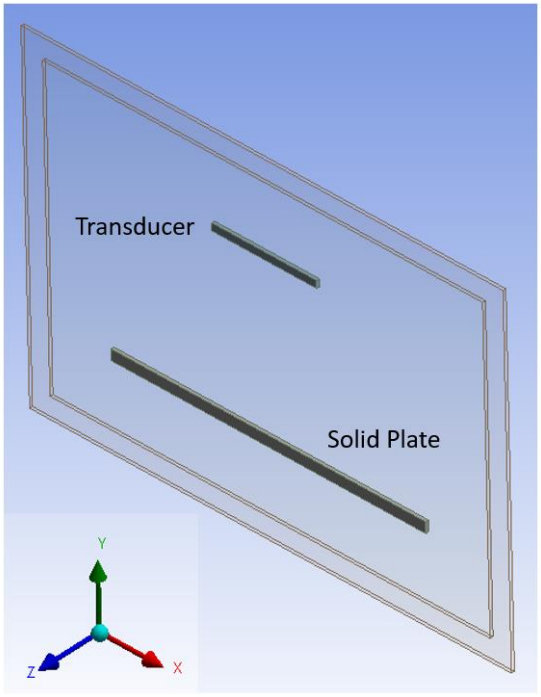

Figure 27 2.5D model

In 3D model, symmetry boundary conditions are applied on XY and YZ plane at Z and X = 0 respectively. However, in 2.5D, an additional symmetry is applied on the XY plane. This means two symmetry boundary condition are applied at XY plane at a certain distance. This distance between the symmetry BC on XY plane determines the model thickness. Applying two symmetry BC on a same plane causes the model to have an infinite length in Z-direction. This causes the transducer to have a rectangular shape instead of circular. To minimize the model size, the thickness of the 2.5D model in Z-axis is set equal to the max mesh element size. This is done to minimize the total computational cost to solve the model. Changing the model thickness gives no effect on simulation results due to the symmetry boundary condition causing all value to be equal along the Z-axis. The validity of this model is studied in Section 4.1.

Chapter 4: Validation Test

This chapter aims to provide confidence on the validity of the simulation model described. Three validation methods are used:

1. Using literature sources to compare with the obtained results
2. In-ANSYS iteration test using different parameters
3. Convergence test

The validation tests are done on three main parts which are:

1. Comparison of 3D and 2.5D and whole model validation
2. Meshing
3. Boundary condition

Descriptions for each test are described and results and discussions of the validation tests are presented in their respective sections. In these validation tests, solid plate is excluded from the model. This is to focus on the validation of other parts of the model first before proceeding with the study of ultrasonic wave interaction with solid plate. All boundary conditions, element types and sizes and other parameters used in the validation tests are based on the model described in the previous chapter unless stated otherwise. Any parameters that is not mentioned such as voltage difference applied, frequency of analysis, transducer's material and dimension will be described beforehand. The model used for the test are in symmetry boundary condition explained in Section 3.4.5 hence, for most of the results, only a part of the whole model is visible. All tests are done using 6 cores i5-7600 CPU @3.50GHz with 8 GB of installed memory (RAM) and 64-bit Operating System. This information is to provide context on the test's simulation time relative to the CPU capability as different CPU specifications will result in different simulation time.

4.1 3D and 2.5D

This section provides comparison of results between 3D and 2.5D model. This is to validate that the 2.5D model is reliable to be used for validation purpose. Furthermore, the results are also compared to a work by Chen et al [38] titled "Experimental mapping of acoustic field generated by ultrasonic transducer". For simplicity, in this section, the model used in the work by Chen et al is addressed as "referred model". Transducer used in the referred model is a non-contact ultrasonic transducer, Ultran NCG50-D50 with an active diameter of 50mm and nominal operating frequency of 50kHz. 30 Vrms of sinusoidal voltage is applied on the transducer as an excitation voltage. Frequency range between 0 – 80kHz is studied.

For comparison, the transducer diameter and voltage applied for the 3D and 2.5D models are set to the same value as in the referred model. However, there are limitations as to how far the 3D and 2.5D models can be validated using the referred model. The limitations are shown in table 6.

Limitations	Description
Inability to create a model with identical properties and parameters equivalent to the referred model	Information such as the material, elastic coefficient and thickness of the active element of the transducer is not provided in the referred model. Consequently, the properties used in 2.5D and 3D models are different to the referred model resulting in different vibration response.
For 3D model, the range of frequency that can be measured is limited up to 20kHz	This is due to the huge number of nodes and elements required for higher frequency range. Error faced when analyzing more than 20kHz is shown in Section 4.1.3.
For 2.5D model, limitation on the shape of the transducer	The model is infinitely long in the z-direction with rectangular shape. Hence, it is impossible to model a cylindrical transducer identical to the one used in the reference model.

Table 6 Limitation on the comparison between 2.5D and 3D model with referred model

These are the specifications of the transducer used for 2.5D and 3D models in all upcoming tests:

1) Material: PZT4
2) Thickness of active element: 3.43mm
3) Diameter: 50mm
4) Voltage difference: 30Vrms

Using this specification, the transducer's vibration and pressure field produced are analysed.

4.1.1 Surface deformation and velocity

To determine the accuracy of the models, it is important to study the vibrational behavior of the transducer as the excitation source first. In this study, surface deformation and velocity at the center of transducer in y-direction are measured. The measurements are taken between 0-20kHz frequency range. The measurement point is shown in figure 28 marked with 'X'. Figure 29 shows the results obtained.

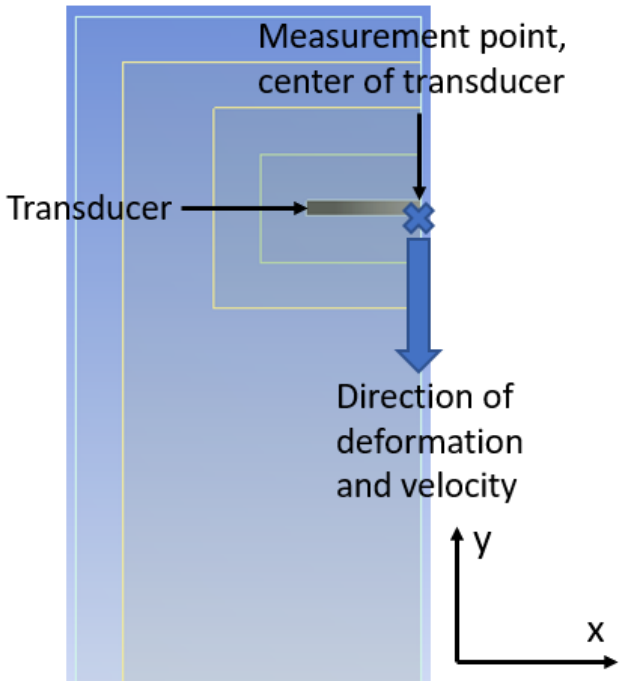

Figure 28 Measurement point for surface deformation and velocity

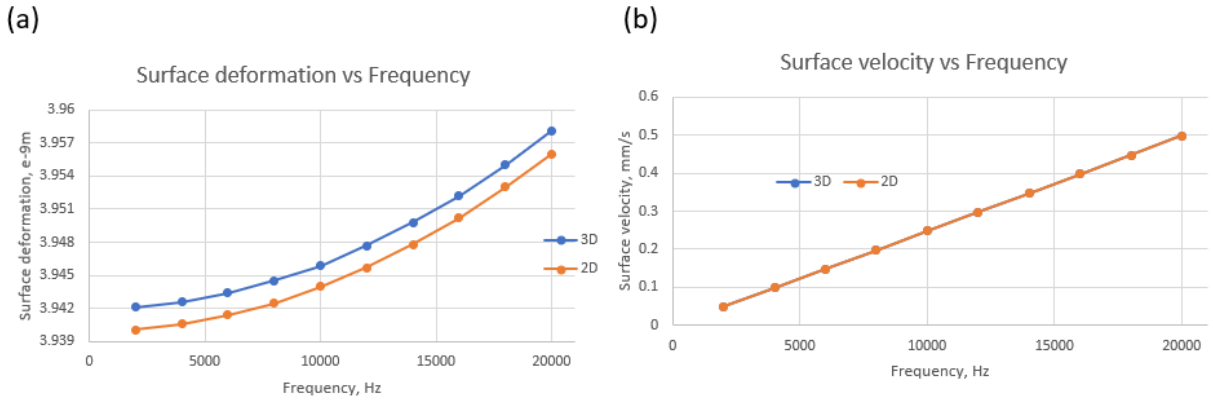

Figure 29 Comparison of surface (a) deformation and (b) velocity for 3D and 2.5D model

The graphs show that the 3D and 2.5D model has similar amplitudes of surface deformation and velocity throughout the frequency. The plot for surface velocity overlaps each other whereas

for surface deformation plot, the difference between 3D and 2.5D are only around 0.002e-9 meter throughout the whole frequency. To study the reliability of 2.5D model to replace 3D model, percentage errors of 2.5D model are calculated based on 3D model using equation 13. The results are plotted in figure 30.

Equation 13 Surface velocity and deformation percentage error of 2.5D model

$$2.5D\ \%\ error = \frac{Deformation_{3D} - Deformation_{2.5D}}{Deformation_{3D}}, = \frac{Velocity_{3D} - Velocity_{2.5D}}{Velocity_{3D}}$$

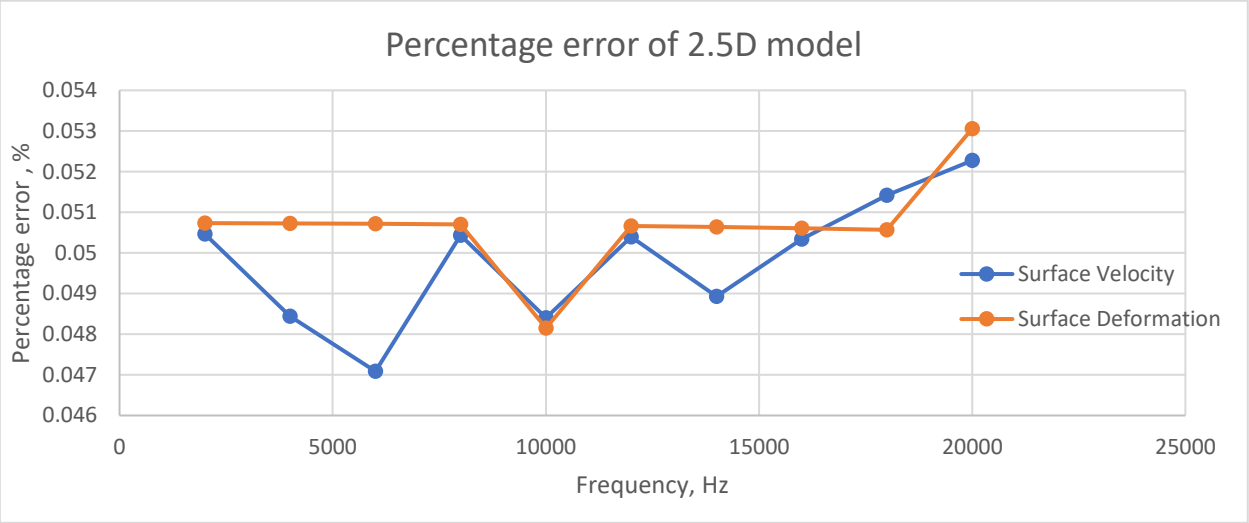

Figure 30 Percentage error of surface deformation and velocity in 2.5D model

2.5D model have unexpectedly low percentage error with an average of 0.05% for both plots. This shows that the vibrational behavior of the 2.5D model are similar to the 3D model despite the difference in transducer shape. For further validation of the vibrational behavior, the results are compared with referred model. Since 3D model isn't capable to be simulated at more than 20kHz frequency, only 2.5D model is compared to the referred model. Figure 31 shows the comparison of surface velocity of (a)2.5D model with the (b)referred model at the center of the transducer's surface at 0-80kHz frequency range.

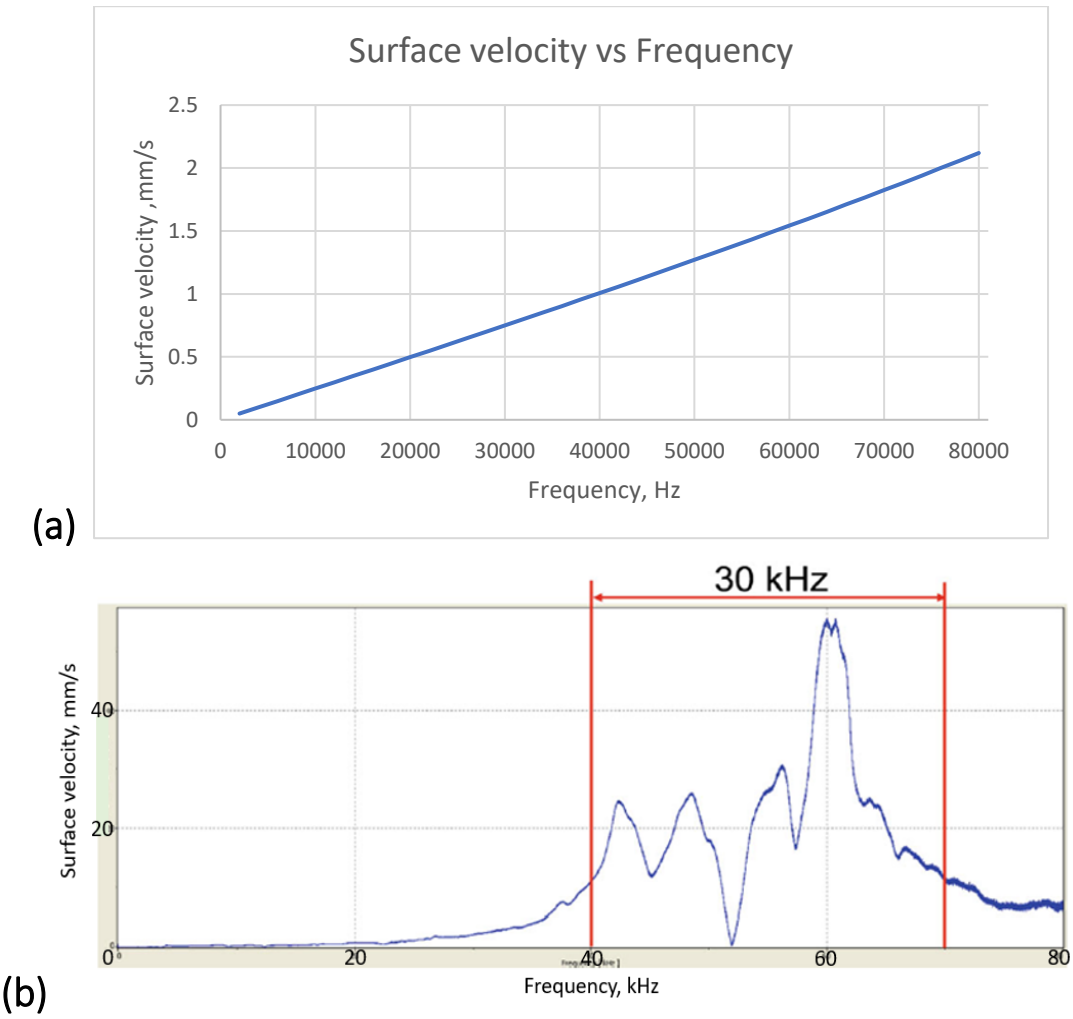

Figure 31 Surface velocity of (a) 2.5D and (b) referred model

The result shows that there's no similarity in the trend of the surface velocity plot between these models. In the referred model, amplitudes for both measurements fluctuate throughout the frequency where the peak amplitude is at around 55-60kHz. The result agrees with the specification of the transducer where the optimum operating frequency are at 50kHz. For 2.5D model, the surface velocity increases linearly throughout the frequencies with no fluctuation. The reason for this difference is, it is assumed that for the 2.5D model, the optimum operating frequency could be higher than the maximum frequency range analysed (80kHz). Hence, the results couldn't show the peak amplitude where the optimum operating frequency is. This assumption can't be validated due to the limitation of computational resources available. Simulation at high frequency is required to identify the optimum operating frequency of the transducer and with the current available computational resources, only simulation up to 100kHz can be done in 2.5D.

An example of transducer with high optimum operating frequency is a curved ultrasonic transducer used in [39] by Chen et al. Figure 32(a) shows the pressure FRF plot of the curved transducer. Highest vibration response is observed at 362.5 kHz indicating its optimum operating frequency. Figure 32 (b) shows the FRF plot of phase vs frequency of the transducer. Based on the plot, the phase remains steady between 0 – 200kHz indicating no sudden increment in the velocity similar to the 2.5D model where no sudden increase in velocity amplitude is observed between 0 – 80kHz. Drastic changes in phase occur at 200kHz and 360kHz where the later phase shift results in the highest vibration response for the transducer.

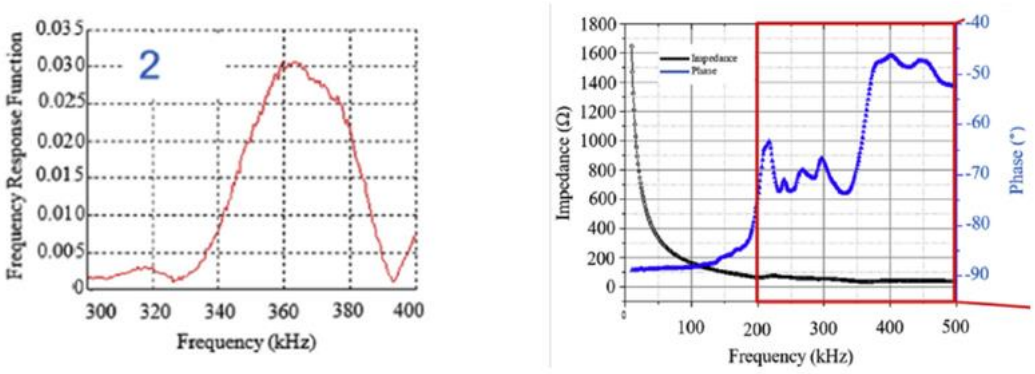

(a) FRF plot of pressure vs frequency of a curved transducer

(b) FRF plot of phase, Impedance vs frequency

Figure 32 FRF plot of curved ultrasonic transducer in [38]

4.1.2 Pressure Field

In this section, pressure field produced by transducer in 3D and 2.5D models at 16 and 20kHz frequency are compared. Figure 33(a) and (b) show the comparisons between (i)3D and (ii)2.5D at 16 and 20kHz respectively. The result shows that the type of pressure fields produced by 3D and 2.5D are similar at both 16 and 20kHz. However, the amplitudes are observed to be different based on the color of the pressure field contour. The values at the side of the pressure field figure represents the amplitude for each color of the contour where red is the maximum and blue is minimum acoustic pressure amplitude. Furthermore, pressure fields of 2.5D model at 50 and 60kHz are also plotted as shown in figure 34.

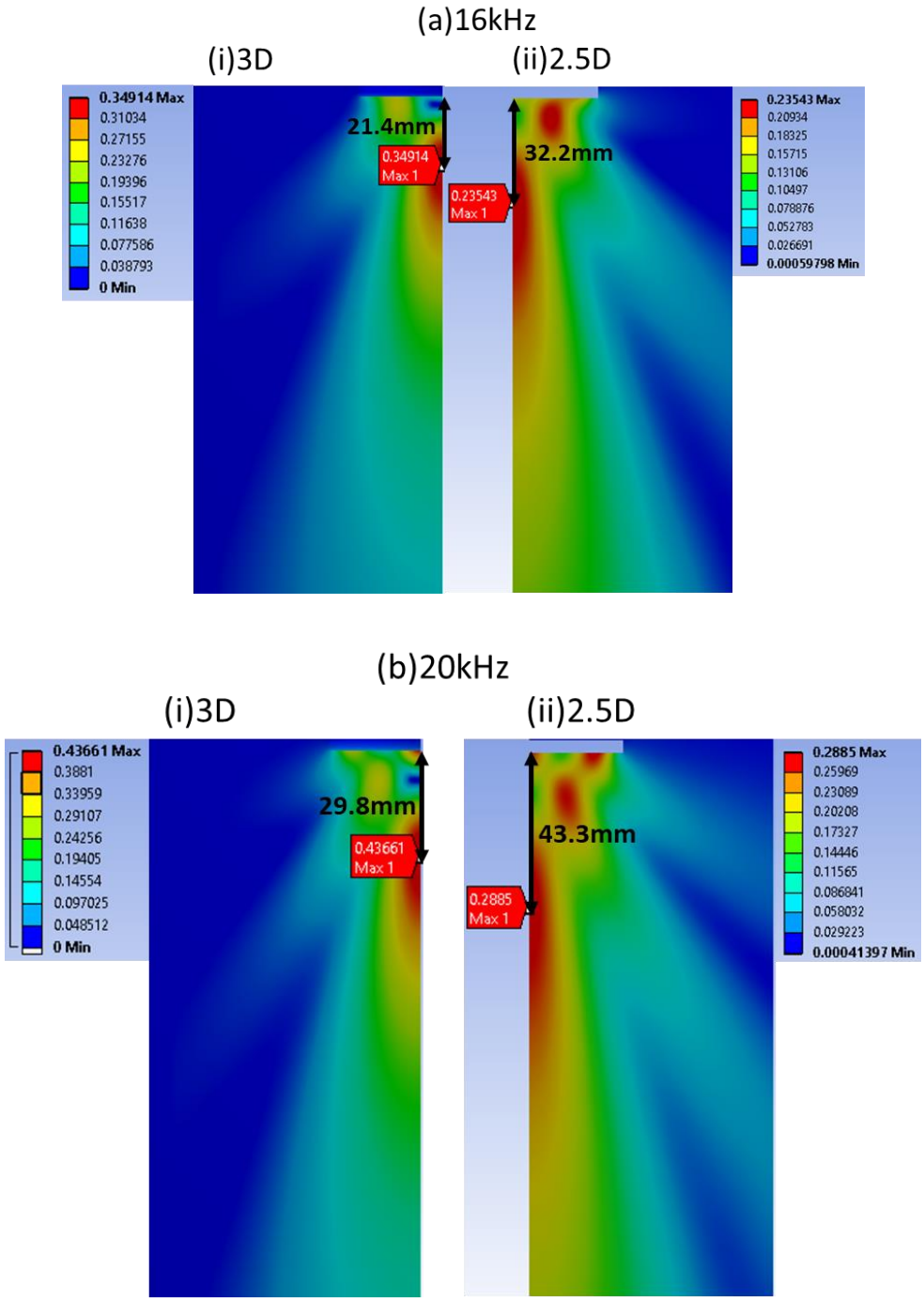

Figure 33 Comparison of pressure field of (i)3D and (ii)2.5D at (a)16 and (b)20kHz

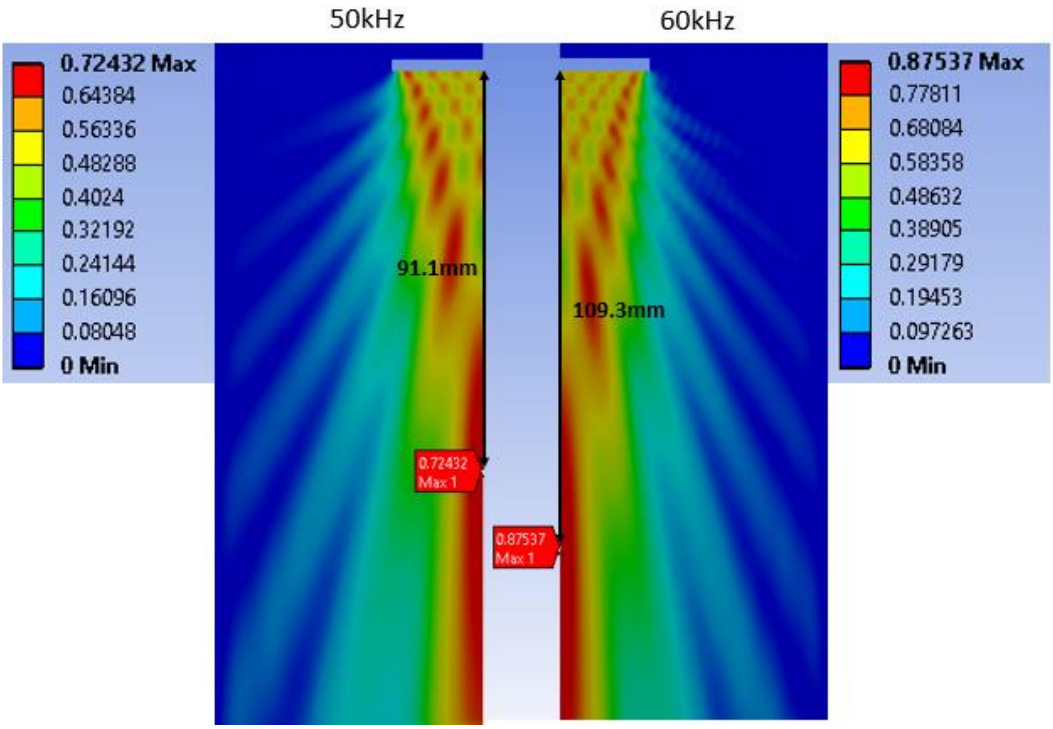

Figure 34 Pressure field of 2.5D model at 50 and 60kHz

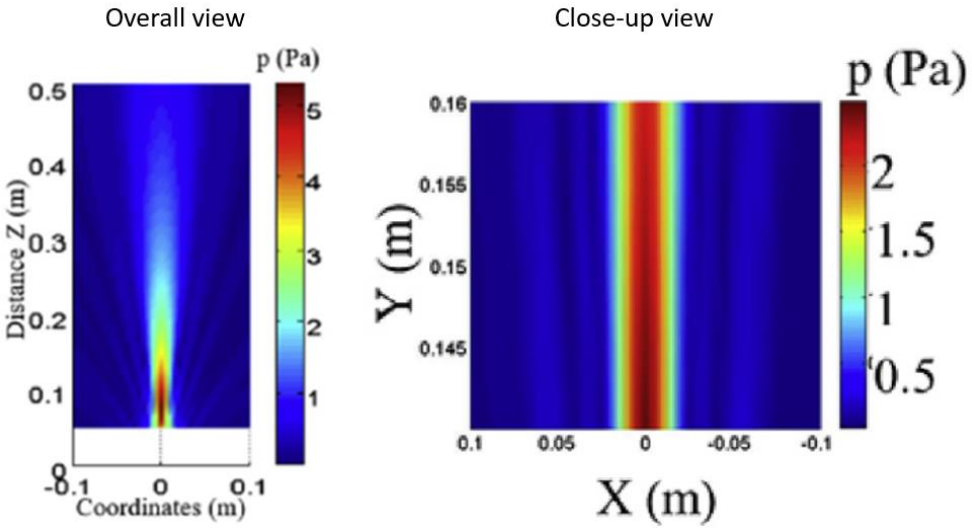

Figure 35 Pressure field of referred model at 60kHz

Comparing the pressure field of 2.5D at 20 and 60kHz, it is evident that at higher frequency, more sound pressures are produced. Furthermore, similarities can be seen between the pressure fields produced by the 3D and 2.5D models with the pressure field produced by referred model shown in figure 35. Pressure field produced has high pressure concentrated at the center of the transducer along the y-axis indicated by the red contour. Further from the center, the pressure

decreases. This agrees with the literature review regarding the wave radiation in Section 2.1.4 stating that the pressure beam uniformly spreads out from the center as it moves further from the transducer's surface

Near to far field transitional point

The near to far-field transition point described in Section 2.1.4 (Literature review) can be seen in figure 33 and 34 where there are fluctuations of pressure near the transducer's surface. The pressure field started to stabilize only at a certain distance from the transducer. The labels indicate the measured maximum acoustic pressure and its distance from transducer. These results are compared with theoretical calculations of transition distance using equation 4 in Literature Review section. Percentage difference of the transitional point distance from the theoretical value for both 3D and 2.5D models are calculated using equation 14 and the results are recorded in table 7. The maximum pressure measured for both models are also included in table 7.

Equation 14 Near to far-field percentage difference

$$Percentage\ difference, \% = \frac{Distance_{theory} - Distance_{3D/2D}}{Distance_{theory}}$$

Frequency, kHz	Maximum pressure, Pa		Transitional point distance from transducer, mm			Distance percentage difference	
	3D	2.5D	3D	2.5D	Theoretical	3D	2.5D
16	0.349	0.235	21.4	32.2	29.2	26.7%	10.3%
20	0.437	0.289	29.8	43.3	36.4	18.1%	19.0%
50	-	0.724	-	111.8	91.1	-	22.7%
60	-	0.875	-	133.8	109.3	-	22.4%

Table 7 Results of near to far-field transitional point for 3D and 2.5D compared with theory

The result shows that the maximum pressure measured in 2.5D model is smaller than 3D model despite the same value of surface velocity and surface deformation. These differences in values might be due to the shape difference of the transducer modelled in 2.5D where it is infinitely long in z-direction. Comparing the transitional point from near to far-field, both models have different value of transitional point distance at all frequencies measured. The value difference between the models and theoretical value is relatively large with about 26.7% difference for test using 3D model at 16kHz and 10.3% using 2.5D model at 16kHz. It was expected for 2.5D model to have such large difference since the theoretical equation used (equation 4) is only for circular transducer but for 3D model, it is quite unexpected.

To gain more understanding on near and far-field zone, acoustic pressure is measured at various points in the zones at 0-20kHz frequency range for both 3D and 2.5D models. In the near-field, acoustic pressures at 10 and 20mm away from the center of the transducer's surface in y-direction are measured. In the far-field, measurement at 110, 130 and 150 mm away from the center of the transducer's surface in y-direction is taken. The measurement points are shown in figure 36.

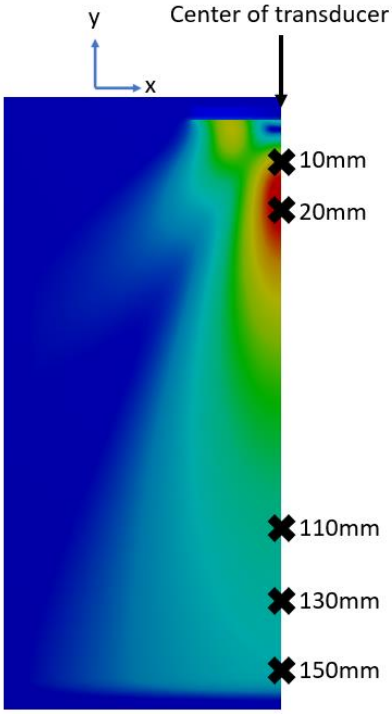

Figure 36 Measurement points of acoustic pressure

Results of acoustic pressure are compared between the measurement points and are plotted in figure 37 where(a) is for 3D and (b) is for 2.5D. Graph of acoustic pressure comparison between 3D and 2.5D for measurement points in far-field are also plotted in figure 38.

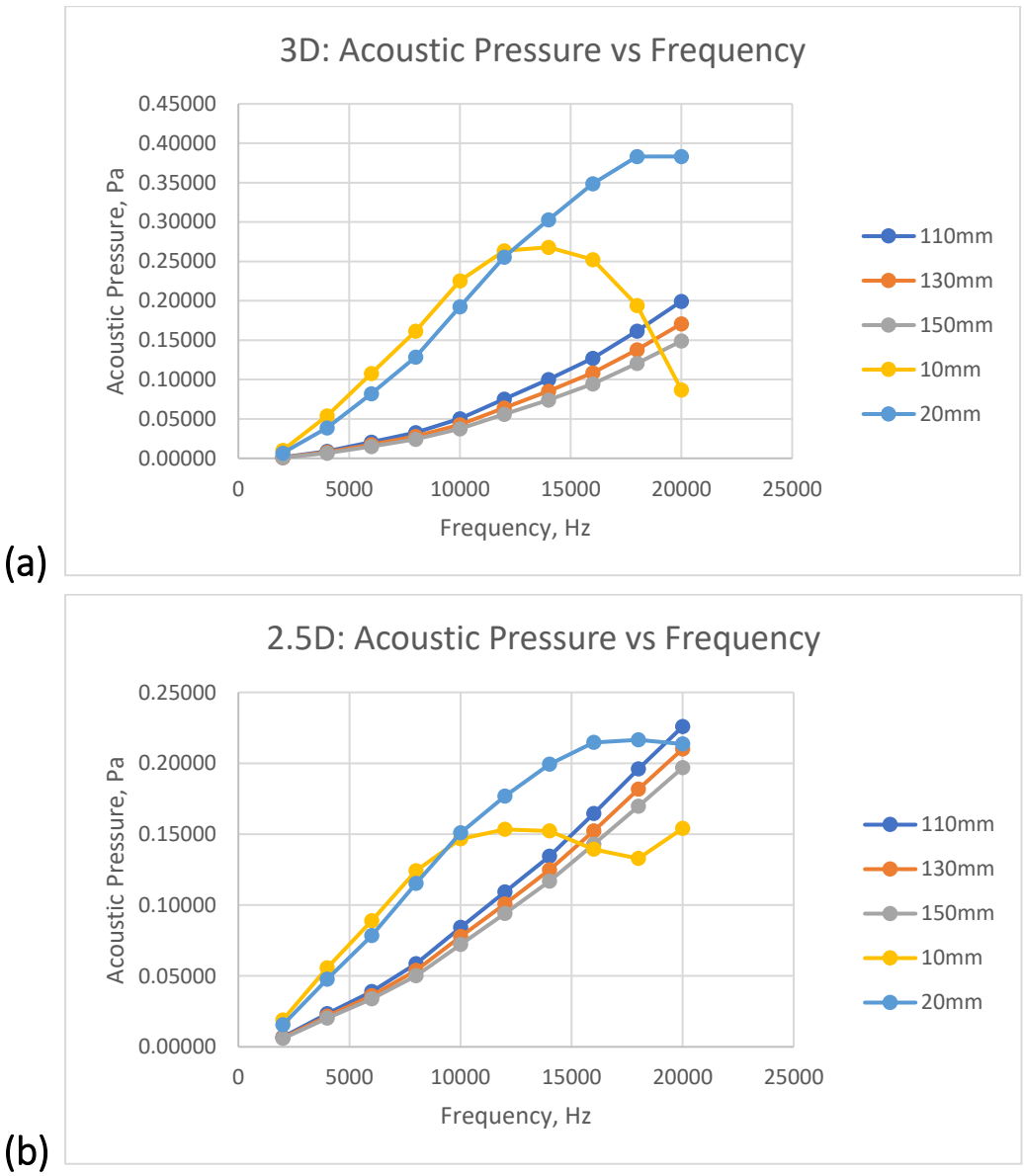

Figure 37 Plot of acoustic pressure vs frequency for (a)3D and (b)2.5D in near and far-field zone

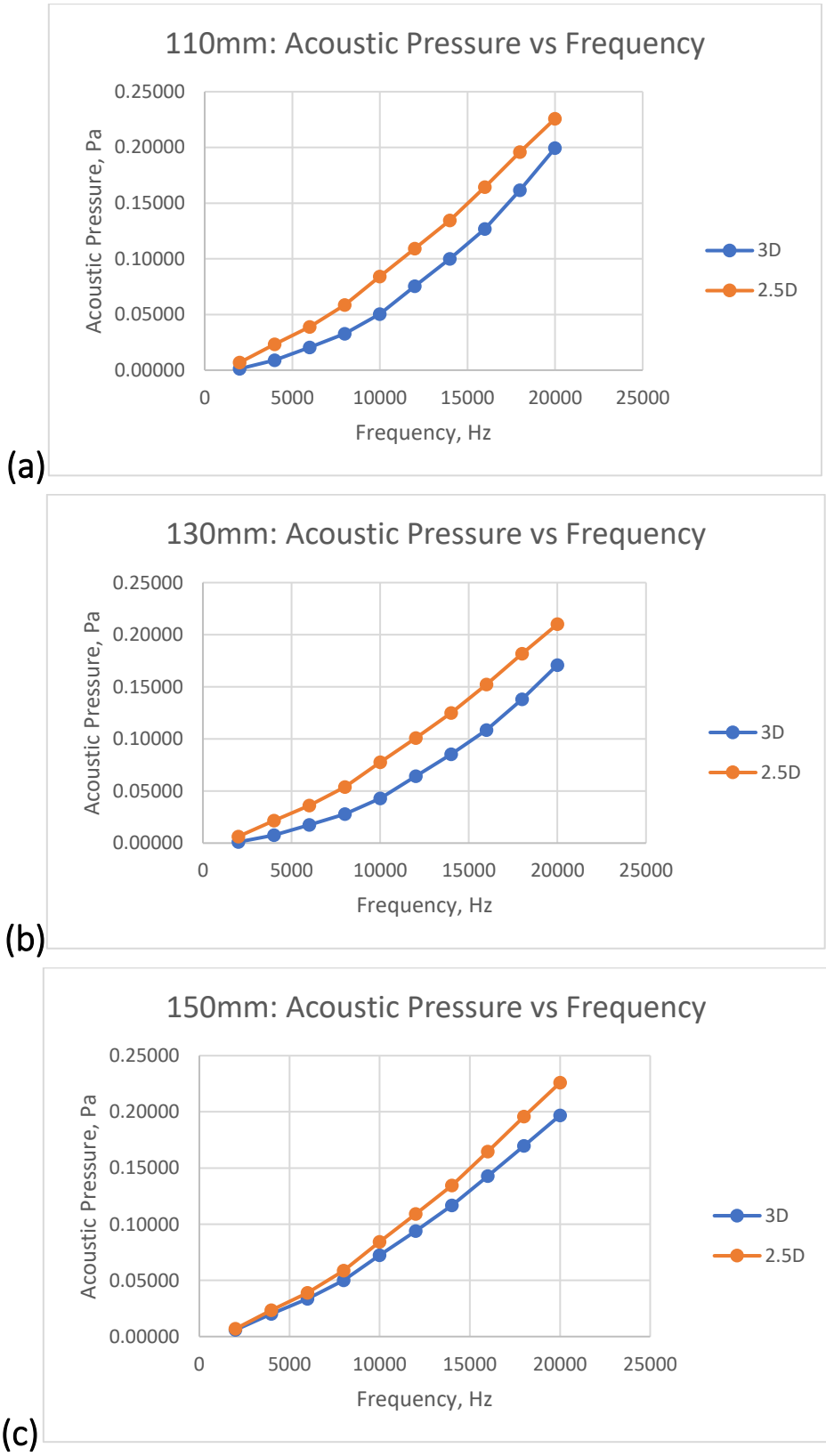

Figure 38 Acoustic pressure comparison between 3D and 2.5D

The results are also compared with the referred model. Table 8 shows the maximum pressure measured in referred model in planes at 140, 160 and 180mm away from transducer surface in y-direction at 56, 57 and 58kHz. Figure 39 shows the acoustic pressure measured at plane 140mm from the transducer surface between 40-70kHz.

Frequency, kHz	Maximum pressure in measurement plane, Pa		
	140mm	160mm	180mm
56	33.4	32	30.3
57	38.1	36.5	34.6
58	35.7	34.4	32.7

Table 8 Acoustic pressure in far-field of referred model

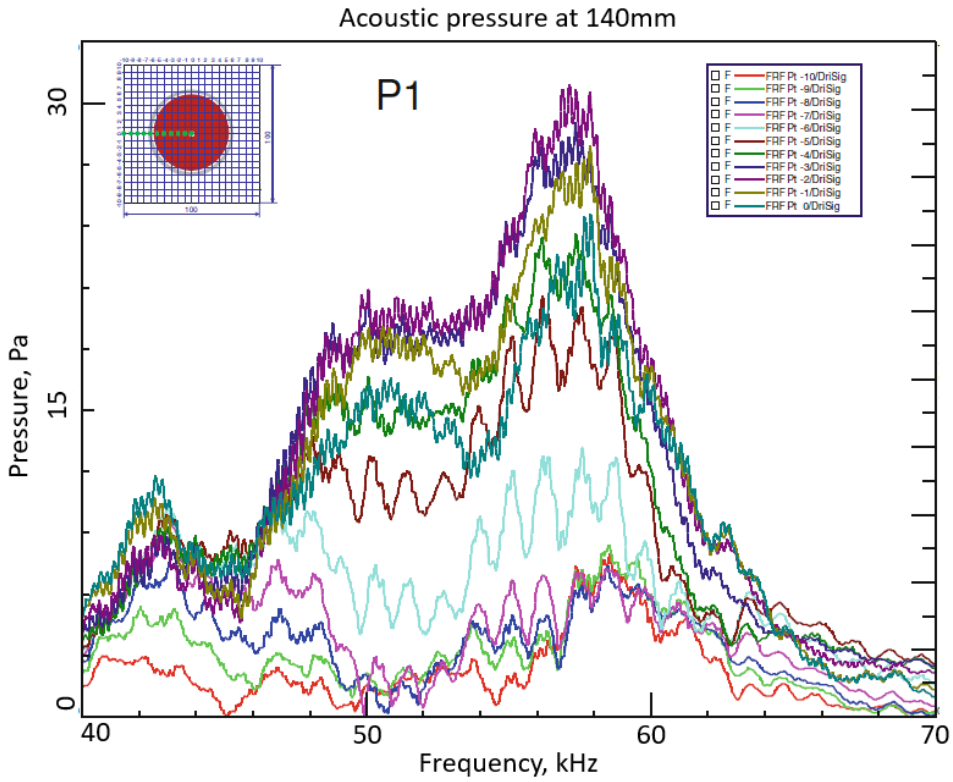

Figure 39 Acoustic pressure of referred model at 140mm

Based on figure 37, all the acoustic pressure measured in the far-field zone has similar trend for both 3D and 2.5D. The acoustic pressure increases as the frequency increase throughout the whole frequencies. This corresponds to the surface velocity of the transducer measured in figure 29 where the velocity also increases as the frequency increase. This agrees with the result of

referred model where the acoustic pressure of the referred model in figure 39 also corresponds to the surface velocity plot in figure 31 where it peaks at around 55-60kHz.

Furthermore, analyzing the relation between acoustic pressure and distance from transducer, plot of pressure at 150mm is measured to be the lowest throughout the whole frequency. This is followed by 130 and 110mm. This shows that the further the measurement points are from the transducer, the lower the acoustic pressure are. This is expected since the maximum acoustic pressure occurs at the transitional point. From this point onwards, the acoustic pressure starts to decrease as it gets further from the transducer's surface. The results by referred model in table 8 also agrees with this observation. Pressures at 180mm are the lowest at all three frequencies followed by 160 and 140mm.

In the near-field however, there are fluctuations in the acoustic pressure throughout the frequencies for both 3D and 2.5D model. Based on figure 37, at 12.5kHz, the acoustic pressure at 10mm measurement point starts to decrease. At 20mm, the acoustic starts to become constant as the frequency increases at 17500kHz. This is due to the fluctuations of pressure field in the near-field zone explained previously in Section 2.1.4 making this zone unreliable to be used for analysis due to its uncertainty.

Comparing the results of 3D and 2.5D model in figure 38, there are differences in amplitude where the acoustic pressure of 2.5D model is always higher than the 3D model for all the measurement points in far field zone. To investigate these differences, percentage errors of the acoustic pressure for the 2.5D model in relative to 3D model are calculated using equation 15. Results are plotted in figure 40.

Equation 15 Acoustic pressure percentage error of 2.5D model

$$Percentage\ error_{2.5D} = \frac{Pressure_{3D} - Pressure_{2.5D}}{Pressure_{3D}}$$

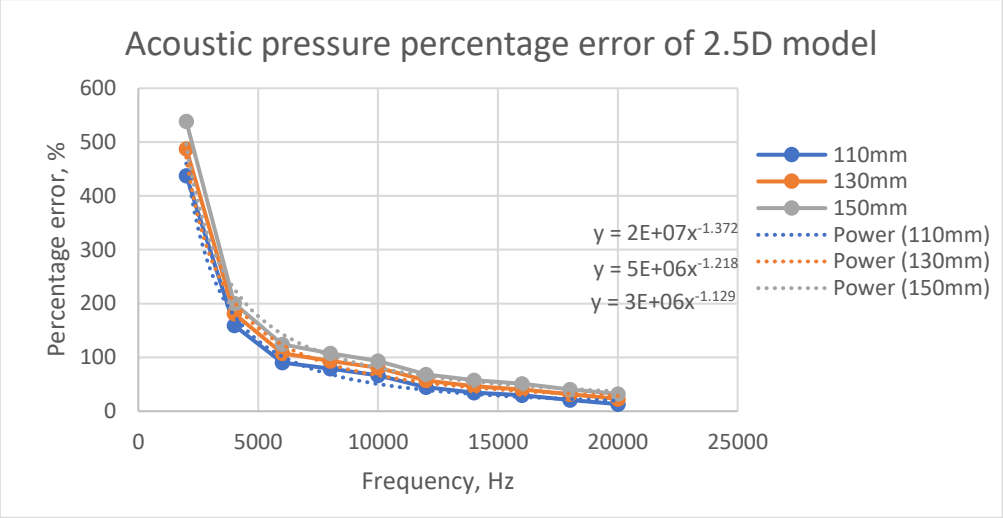

Figure 40 Acoustic pressure percentage error of 2.5D model

Despite the small percentage errors in the surface deformation and velocity of the 2.5D model, the acoustic pressure has unexpectedly high percentage errors with about 450% at 2kHz. However, the error shows a decline in trend where as the frequency increases, the percentage error decreases. At 20kHz, about 23% of errors are measured at 130mm measurement point. Even though this is still high, it is a significant decrease from the 450% error at 2kHz. Based on the results, equations of the trendlines for all measurement points are obtained as shown in table 9 where x is the frequency of analysis and y is the percentage error. Using these equations, errors at higher frequency can be predicted as shown in table 10.

Measurement point	Trendline equation
110mm	$y = 2e07 \times x^{-1.372}$
130mm	$y = 5e06 \times x^{-1.218}$
150mm	$y = 3e06 \times x^{-1.129}$

Table 9 Trendline equation of acoustic pressure percentage error

Frequency, kHz	Acoustic pressure percentage error prediction, %		
	110mm	130mm	150mm
20	25.12	28.86	41.81
50	7.15	9.45	14.86
100	2.76	4.06	6.79
150	1.58	2.48	4.30
200	1.07	1.75	3.11
250	0.785	1.33	2.41

Table 10 Prediction of percentage error of acoustic pressure at high frequency using trendline

From the trendline prediction of the acoustic pressure, it shows that at higher frequency, acoustic pressure percentage errors associated with the 2.5D model are considerably smaller for frequency above 150kHz. If based on this trendline prediction alone, the 2.5D model can be considered reliable for use at high frequency. However, there are limitations on using the trendlines for prediction as it only uses measurements of frequency only up to 20kHz. Using measurements only up to 20kHz to represent results at frequency more than 200kHz which is 10 times larger is unreasonable.

One of the reasons is at higher frequency, the transition of near to far-field zone of the acoustic field is further from the transducer's surface. For example, at 200kHz, using equation 4, for a 50mm diameter transducer, the transition point for this frequency is at 364.4mm away from the transducer's surface. This means that the measurement points used to predict the percentage errors is in the near-field zone for this frequency. Whereas the studies are done at far-field zone further from the near to far-field transitional point which is 36.4mm for a 20kHz frequency. Hence, using measurement points at 110, 130 and 150mm away from the transducer surface for up to 20kHz can't represent the percentage error predictions for higher frequency where the near to far-field transitional point is much further than the measurement points used.

Furthermore, observing the acoustic pressure percentage errors for the three measurement points in figure 40, measurement point at 150mm has the highest percentage error throughout the whole frequency range followed by 130mm and 110mm. This means that the further the measurement points are from the transducer's surface, the higher the error of the measured acoustic pressure in 2.5D model. Hence, it is not suitable to be used for high frequency. This is because at high frequency, the near to far-field transitional point is further from the transducer's surface as shown in table 7.

Based on the result, two conclusions are made:

1) The accuracy of 2.5D in relative to 3D increases as the frequency increases
2) At further distance from transducer, higher errors are obtained for the 2.5D model

4.1.3 Computational Cost

This section shows the comparison of computational cost between 3D and 2.5D model. This includes the memory usage, file size and simulation time required to complete one simulation at various frequencies. At each frequency, the models are meshed using maximum element size allowed calculated using equation 11 and 12 and element type described in Section 3.3.1. Table 11 shows the no of nodes and elements using said mesh for frequency between 10-22.5kHz for (a)3D model and 20-80kHz for (b)2.5D model.

(a) 3D model				
Frequency, kHz	Element size, mm	nodes	elements	nodes/elements
10	5.716	71663	47390	1.512
12.5	4.573	139608	93997	1.485
15	3.811	236513	160039	1.478
17.5	3.266	372339	255326	1.458
20	2.858	541469	373181	1.451
22.5	2.540	756426	525693	1.439
(b) 2.5D model				
Frequency, kHz	Element size, mm	nodes	elements	nodes/elements
20	2.858	14494	1998	7.254
30	1.905	31268	4360	7.172
40	1.429	54036	7579	7.130
50	1.143	84393	11880	7.104
60	0.952	120926	17064	7.087
70	0.816	164011	23184	7.074
80	0.714	215669	30528	7.065
90	0.635	271272	38437	7.058

Table 11 No of nodes and elements based on element size

Computational costs at different frequencies are also recorded as shown in table 12. For 3D model, only results between 10 to 20kHz are simulated. At higher frequency, error occurred due to high computational resource required to solve the model. Error associated with this are discussed in the upcoming section. For 2.5D model, results between 20 to 90kHz are simulated.

(a) 3D model			
Frequency, kHz	Simulation time, s	Memory usage, GB	File size, MB
10	10	1.323	53.06
12.5	104	2.376	104.13
15	200	2.116	176.50
17.5	421	3.060	280.06
20	675	4.656	408.13
22.5	-	-	-
(b) 2.5D model			
Frequency, kHz	Simulation time, s	Memory usage, GB	File size, MB
20	9	0.612	59.31
30	15	0.644	130.13
40	25	0.613	224.19
50	43	0.796	349.56
60	70	1.147	500.19
70	109	1.566	678
80	196	2.061	890.88
90	475	2.652	1094

Table 12 Computational cost of 3D and 2.5D models

As expected, the computational cost increases as the frequency increases due to the increase in number of elements. Comparing 3D and 2.5D models, at 20kHz frequency, simulation time for 3D is 675s while for 2.5D, it only took 9s. This means that the 2.5D model are able to solve the simulation 75 faster than 3D model while using the same element type and size. Furthermore, solving for 90kHz in 2.5D still take less time to simulate than 3D at 20kHz. This makes 2.5D model much more efficient than 3D model.

Since the results for 3D are only limited up to 20kHz, it is interesting to investigate how long it will take for it to complete simulations at higher frequency. Using results obtained, prediction of the 3D model simulation time can be made. This can be done by finding a relation between the no of nodes and elements with the simulation time. To do this, it is better to understand first the relationship between the number of nodes and elements. Using results in table 11, ratio of no of nodes/elements vs frequency for 3D model are plotted in figure 41.

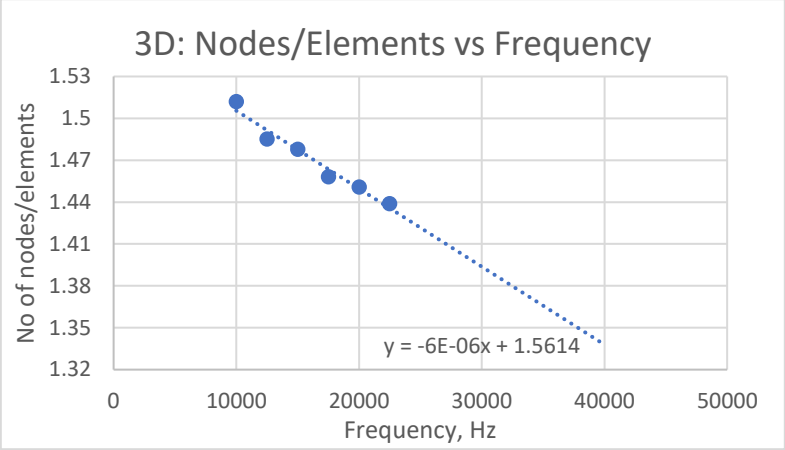

Figure 41 Nodes/elements vs frequency of 3D model

The plot shows that the ratio of nodes/elements decrease linearly as the frequency increase. Next, the data of no of elements vs frequency is plotted as shown in figure 42. The no of elements increases quadratically with frequency. From this, trendline equation for no of elements at any given frequency can be obtained. The trendline equation obtained is:

$$n = 0.0021f^2 - 30.422f + 142722$$

Where n = no of elements and f = frequency. Since, the ratio of nodes/ elements is linear, the graph for node is not plotted as it will just show similar trend.

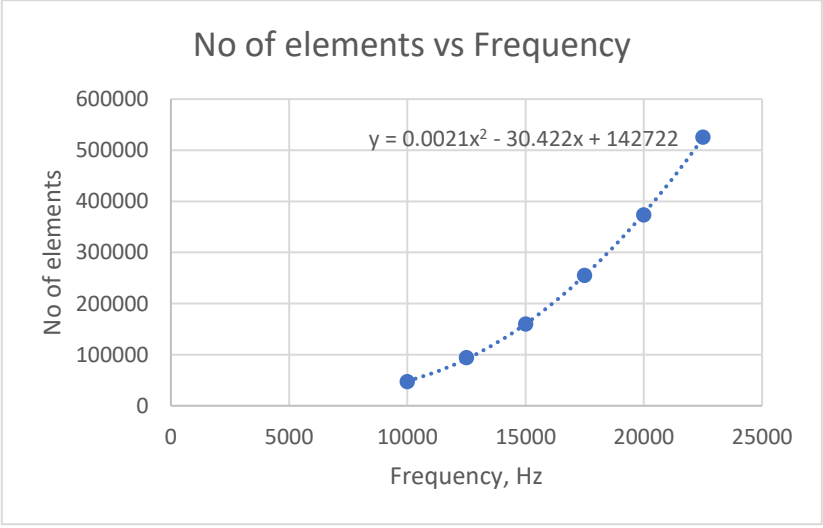

Figure 42 Plot of no of elements vs frequency

Using the trendline equation from figure 42, no of elements at higher frequency can be predicted. Next, plot of simulation time against no of elements is obtained as shown in figure 43.

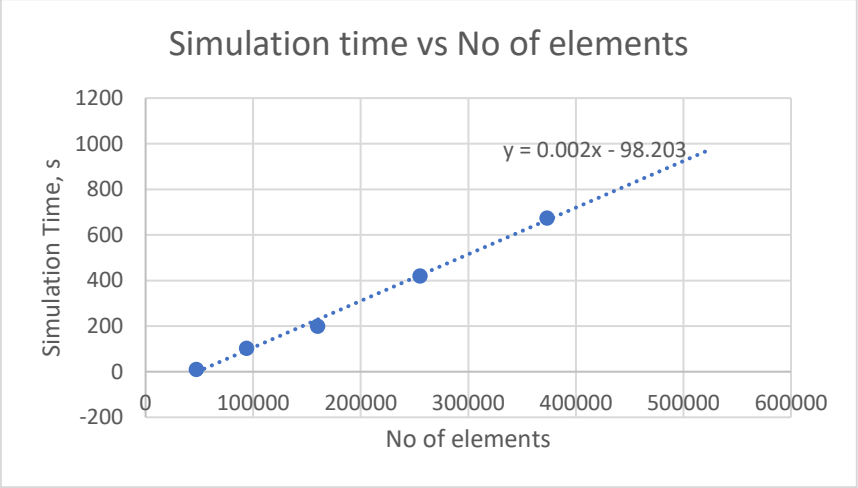

Figure 43 Plot of simulation time vs no of elements

The trendline equation obtained are:

$$t = 0.002n - 98.203$$

Where t = simulation time and n = no of elements. Using these equations, simulation time at higher frequency can be predicted. Table 13 shows the results of the predictions.

Frequency, kHz	No of elements	Simulation time, s	Simulation time, hours
70	8303182	16508	4.586
80	11148962	22199	6.167
90	14414742	28731	7.981
250	123787222	247476	68.743

Table 13 Simulation time prediction for 3D

Frequency, kHz	Simulation time in 3D, s	Simulation time in 2.5D, s	Ratio
70	16508	109	151.45
80	22199	196	113.26
90	28731	475	60.48

Table 14 3D and 2.5D simulation time comparison

The prediction result shows that at 90kHz, the 3D model will take 60 times longer than 2.5D model to complete one simulation. This is a huge difference in computational efficiency between 3D and 2.5D model. However, results may vary based on computer specification and meshing method. These results are only to provide an estimate on the total simulation time for 3D model at higher frequencies for comparison with 2.5D model used in this section. This section shows the huge advantage of using the 2.5D model to replace the 3D model.

Computational cost error

Error faced due to high computational cost are often associated with the physical memory available (RAM) in the computer. Figure 44 shows some of the errors occurred when solving the model.

```
*** FATAL ***                          CP =    1105.969   TIME= 01:27:47
This model requires more scratch space than available.  The program has
currently allocated 12352 MB and was not able to allocate enough
additional memory in order to proceed.  Please increase the virtual
memory on your system and/or increase the work space memory and rerun
the program.  Problem terminated.

*** ERROR ***                          CP =     146.078   TIME= 11:45:19
There is not enough memory for the Distributed Sparse Matrix Solver to
proceed using the out-of-core memory mode.  The total memory required
by all processes = 18105 MB.  The total physical memory that is
available on the system = 7723 MB.  Please decrease the model size, or
run this model on another system with more physical memory.
```

Figure 44 Error due to lack of physical memory

Besides, lack of RAM could also cause the elapsed simulation time to exceed the actual CPU simulation time required. Figure 45 shows the warning that the elapsed time exceeded the CPU time by 40%. Figure 46 shows the difference between elapsed time and CPU time. In figure 46, CPU time is 218s while the elapsed time is 362s which makes it 66% longer.

```
*** WARNING ***                        CP =     476.906   TIME= 12:54:34
During this session the elapsed time exceeds the CPU time by 40%.
Often this indicates either a lack of physical memory (RAM) required
to efficiently handle this simulation or it indicates a particularly
slow hard drive configuration.  This simulation can be expected to run
faster on identical hardware if additional RAM or a faster hard drive
configuration is made available.  For more details, please see the
ANSYS Performance Guide which is part of the ANSYS Help system.
```

Figure 45 Elapsed time exceeded CPU time warning

```
CP Time      (sec) =       218.406       Time   =  23:00:28
Elapsed Time (sec) =       362.000       Date   =  05/10/2019
```

Figure 46 Example of difference in elapsed and CPU time

The error can be avoided by:

1) Using simpler model to reduce the problem size such as using 2.5D model
2) Increasing the physical memory of the computer.

4.1.5 Validity of the model

Overall, there are resemblances between the 3D and 2.5D model and the referred model. The pressure fields produced are similar and the direct relationship between surface velocity and acoustic pressure is observed. This provide a verification on the validity of this model to be used for the study of interaction of ultrasonic wave and solid plate in Chapter 5. The study in Chapter 5 are more focused on the type of interaction occurred rather than the amplitude of pressure produced. Accordingly, the amplitude of acoustic pressure produced by the transducer are irrelevant. Hence, this is the reason 2.5D model is used for the study rather than 3D model. The difference in the 2.5D and 3D models are only on the amplitude of the acoustic pressure. The pattern of pressure field produced and relationship between surface velocity and acoustic pressure are discovered to be similar. Hence, it is valid to use 2.5D model. Furthermore, using 2.5D model also proves to be beneficial due to the lesser computational cost required to solve the model and it's ability so simulate for higher frequency than 3D model.

4.2 Mesh

Validation on the choice of element type and size described in Section 3.3 are made here. Different element types are tested to show that the chosen element is the best choice. Convergence tests are also done to show that the element size used are able to produce accurate results. 3D model is used for the tests in this section. Other test parameters such as transducer material, voltage applied etc. are similar to the one used in previous section. The only difference is the meshing.

4.2.1 Element type

This section shows the performance comparison between quadratic hexahedral (FLUID220, SOLID226, SOLID186) and tetrahedral (FLUID221, SOLID227, SOLID187) elements. To compare the performance, two model are meshed separately using the hexahedral and tetrahedral elements and solved at 20kHz frequency. Figure 47 shows the meshing for both models. Table 15 shows the no of nodes, elements and computational time taken to solve the model for each element type.

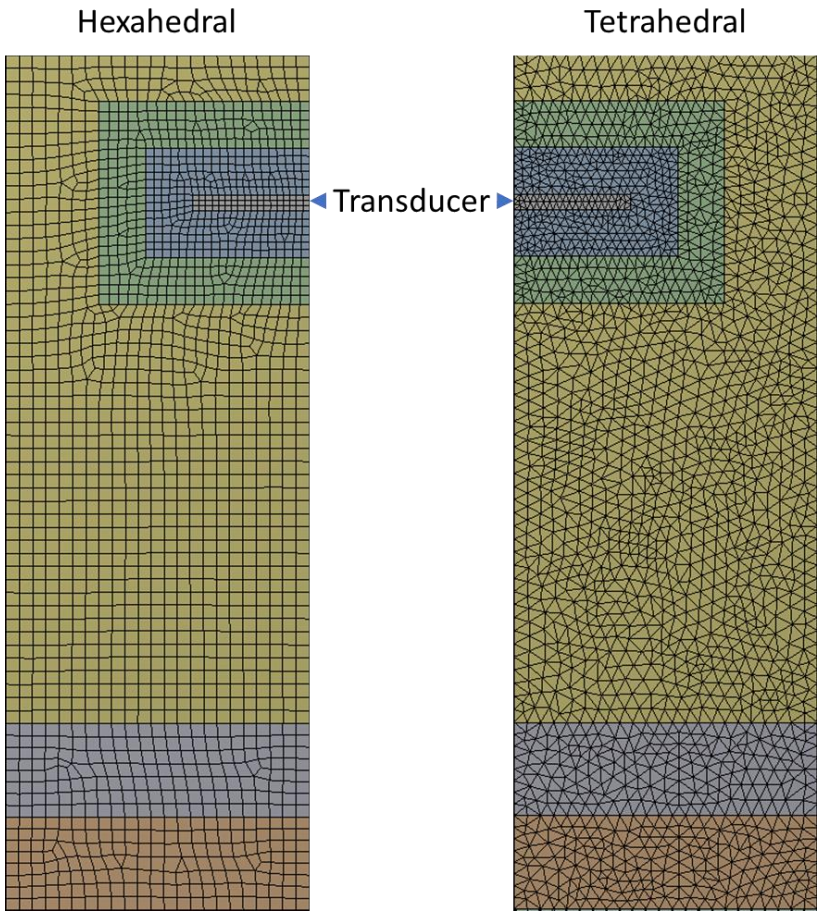

Figure 47 Mesh structure of hexahedral and tetrahedral element

Hexahedral: FLUID220, SOLID226, SOLID186				Tetrahedral: FLUID221, SOLID227, SOLID187			
Nodes	Elements	Nodes/ Elements	Time, minute	Nodes	Elements	Nodes/ Elements	Time, minute
417618	191779	2.177	94	698995	508380	1.374	186

Table 15 Hexahedral and Tetrahedral comparison

Model with tetrahedral have higher number of elements, nodes and simulation time compared to hexahedral. This shows the efficiency of using the hexahedral elements for modelling simple geometry. As seen in figure 47, model with hexahedral elements have more uniform mesh compared to tetrahedral. This uniformity causes less elements required to create the model. Since hexahedral have less elements compared to tetrahedral, the simulation time is also less. Comparing the nodes/elements ratio, the ratio of tetrahedral model is lower than hexahedral. This is expected since tetrahedral only has 10 nodes per elements while the hexahedral has 20 nodes as shown in table 4 in Section 2.2.2 (Literature Review).

To compare the accuracy between the two elements, acoustic pressure at 140m from the center of transducer's surface are measured at frequency between 0 to 20000kHz. The result is shown in figure 48. The plotline for tetrahedral is not visible because it is overlaid by hexahedral plotline. This shows that similar results are produced using the two elements type. This means that the extra computational time when using tetrahedral is unnecessary since model with hexahedral elements already has good result accuracy. Hence, the hexahedral element (FLUID220, SOLID226, SOLID186) is the better choice for this model.

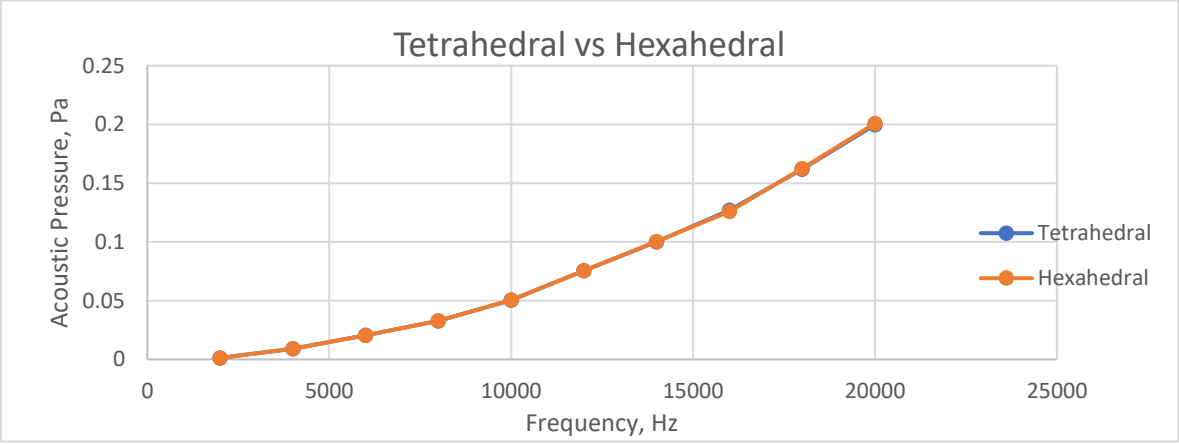

Figure 48 Acoustic pressure comparison between Hexahedral and Tetrahedral element

4.2.2 Element size

This section validates the requirement of element size to obtain accurate results mentioned in Section 3.3.2. This is done using a convergence test by varying the element size of the model. Hexahedral element is used for this study. The studies are done at 20 and 40kHz using 2.5D model. As described in Section 3.3.2 (Model Description), the maximum allowable element size is different for structural and fluid element hence, different element size is used for the two parts as shown in figure 20. For the two frequencies, based on equation 11 and 12, the maximum allowable element size is as follow:

Part	20kHz	40kHz
Fluid (6 elements/λ)	2.858mm	1.429mm
Structural body (20 elements/λ)	0.857mm	0.428mm

Table 16 Max mesh size allowed at 20 and 40kHz

To validate the element size equations, two convergence tests are done for the fluid and structural body:

1) For the convergence test on fluid, the fluid element size is varied between 2 to 9 elements per wavelength for both frequencies. The no of element per wavelength for structural body is constant at 20 elements
2) For the convergence test on structural body, the structural body element size is varied between 10 to 20 elements per wavelength for both frequencies. The element size for fluid is constant at 6 elements per wavelength.

Fluid Domain

Using the mentioned setup for fluid domain, acoustic pressure at 140mm away from the center of the transducer's surface are measured. Figure 49 shows the results of convergence test for fluid's element size.

(a) 20kHz

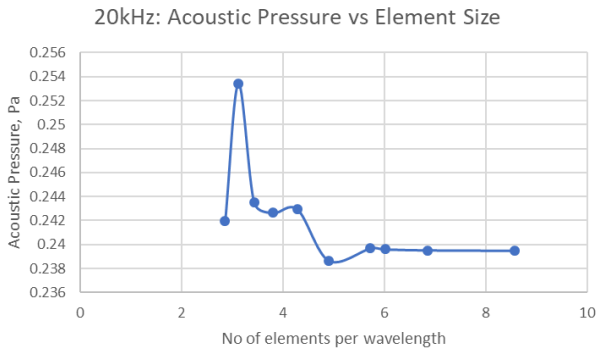

(b) 40kHz

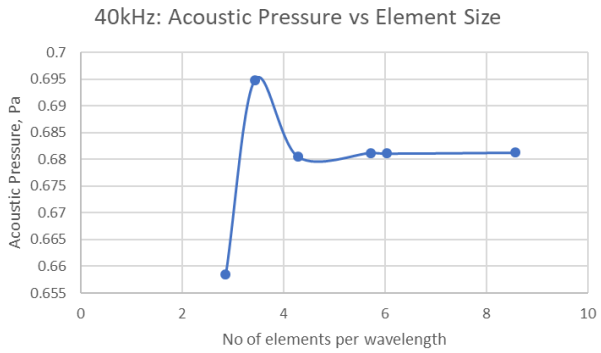

Figure 49 Convergence test for fluid domain element size

Based on the convergence test result, it is seen that the acoustic pressure measured is not converged when the no of elements per wavelength used are less than six. For the case of 20kHz, the element size converged at acoustic pressure of 0.239Pa and for 40kHz, it converged at acoustic pressure of 0.681Pa both at six elements per wavelength. Observing the results before it converged, at 20kHz, a maximum pressure of 0.253Pa is measured when 3 elements per wavelength are used. This results in percentage error of 5.82%. For 40kHz, an acoustic pressure of 0.658Pa is measured also when three elements per wavelength are used which results in a percentage error of 3.91%. These shows that the results before the acoustic pressure has converged is not accurate. Hence, it is important that the recommended no of element per wavelength is used.

The findings that the acoustic pressure converged at six elements per wavelength is similar to the finding by Langer et al [19]. This validate the use of equation 11 to find the required element size to model the fluid. This means that for future work, convergence test to determine the required element size is not necessary anymore. Instead, equation 11 can be used directly to determine it which could save a lot of time. In addition, using smaller element size than the maximum allowed provides no benefit as the value of the acoustic pressure remains the same after it has converged. Instead, it will only increase the total simulation time which is not desired.

Figure 50 shows a pressure field produced at 40kHz when the element size requirement is not met. Figure 50 (a) is meshed with six elements per wavelength which meets the requirement and (b) three elements per wavelength. The contour of the pressure field in (b) is not as smooth as in (a). This is because element size used is not small enough to model the wavelength of the sound wave hence, the inaccurate result. It is concluded that for the fluid domain, the element size used will be determined using equation 11 as it will provide an accurate result whilst minimizing the simulation time required to obtain it.

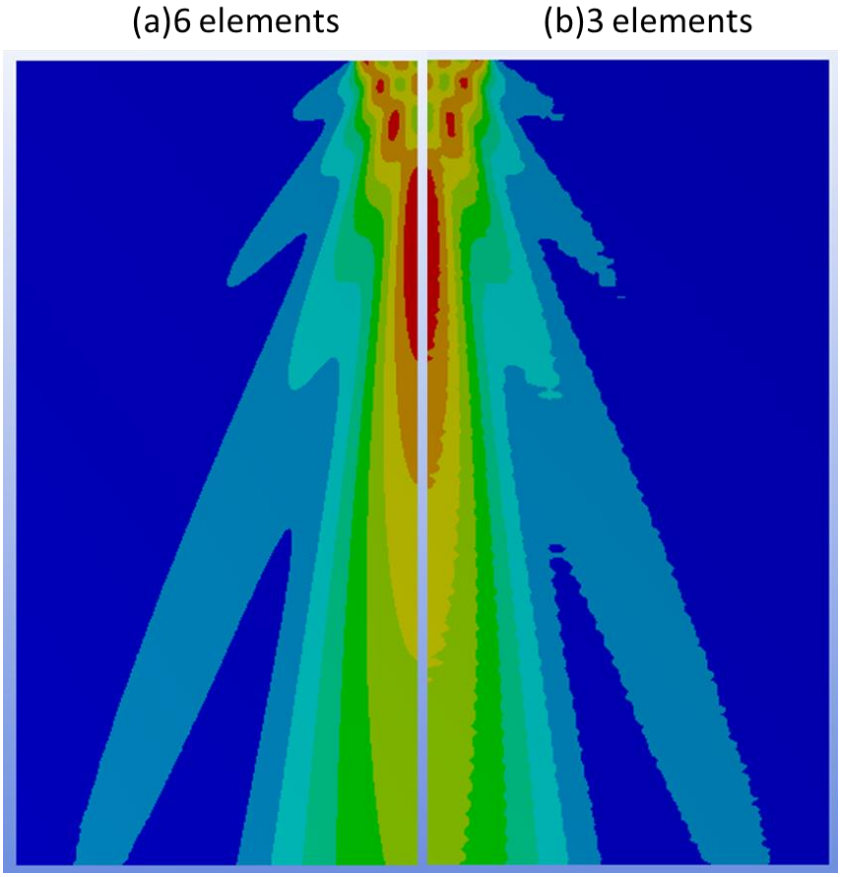

Figure 50 Pressure field when not enough elements per wavelength are used

Structural Body

Figure 51 shows the convergence test result for structural body

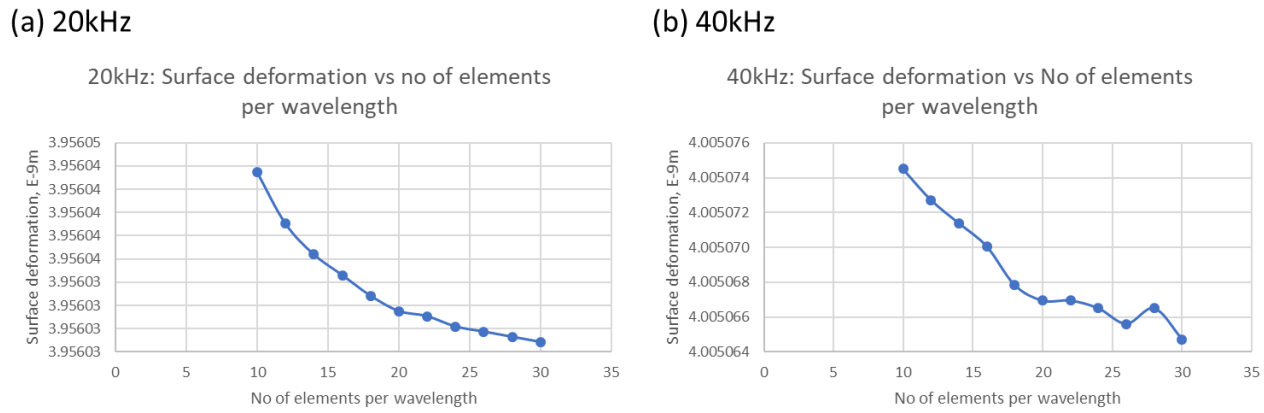

Figure 51 Convergence test for structural body element size

Based on figure 51, the plot trend does not show any convergence. However, when observing the difference of surface deformation between using 20 elements per wavelength and elements less than that, only a small difference in surface deformation is observed with about 0.00001E-9m. This shows that result has already converged. Similar behavior is also noted for 40kHz plot. Hence, this shows that the equation 12 defined in Section 3.3.2 is reliable for the modelling of structural body's element size.

4.3 Boundary Condition

Validation tests on the boundary conditions used for transducer, symmetry and absorbing boundary condition described in Section 3.4 are presented in this section. Similar to previous tests, parameters used in this section is similar to the parameters in Section 4.1 unless otherwise stated.

4.3.1 Transducer

This section shows the validation tests on the use of fixed support to represents the backing material instead of free support. Comparison between fixed and free support boundary condition are made to show the validity of using fixed support rather than free support. In the end, reasonings for this choice are given. In the free support model, no support is defined at the back of the active element hence, the surface is free to move.

Surface deformation

For each case of support, surface deformation in y-direction of the center of the transducer at frequency range between 0 to 40kHz are measured and the results are plotted as shown in figure 52. (a) is for fixed support, (b) for free support and (c) shows the results for both.

(a)

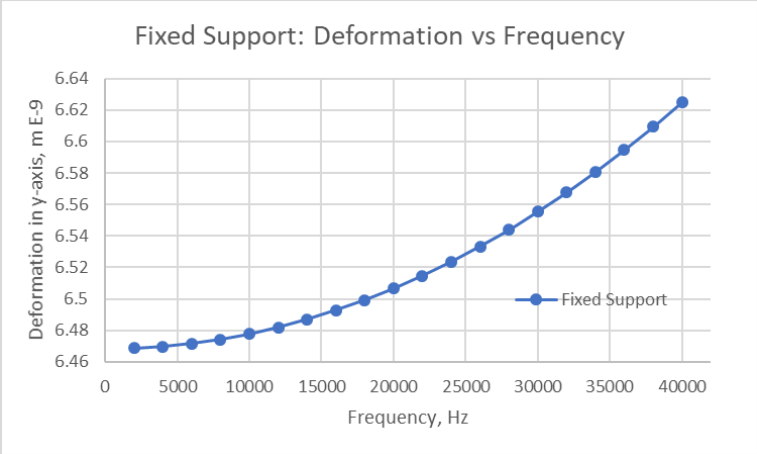

(b)

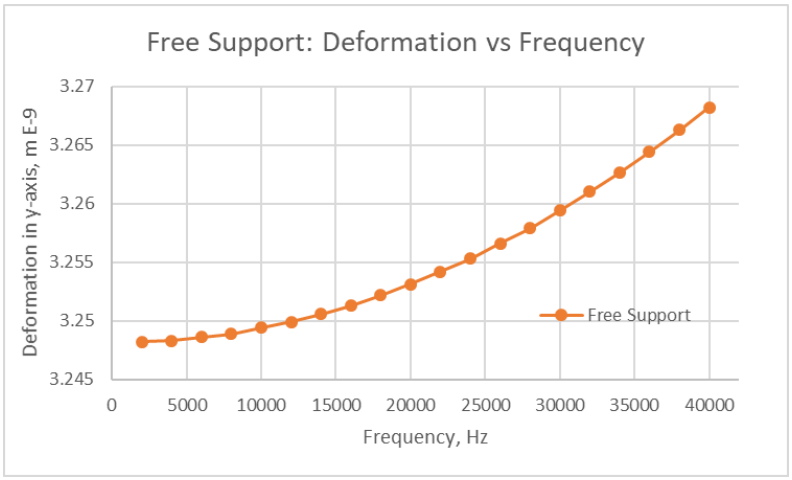

(c)

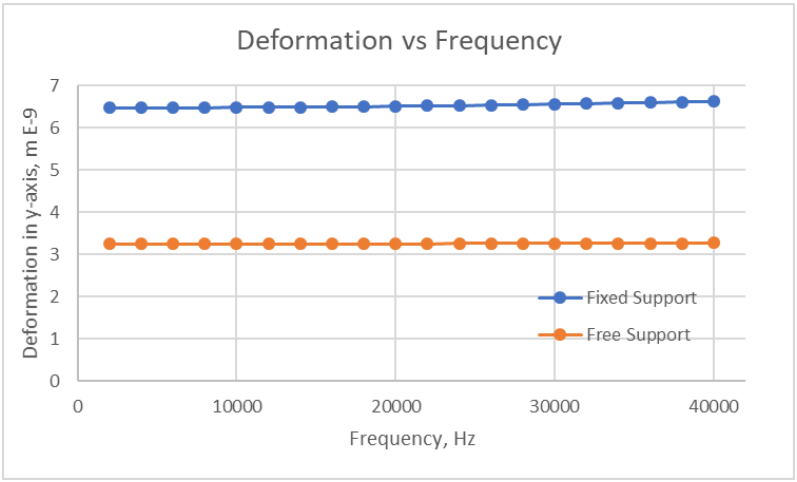

Figure 52 Graph of transducer's surface deformation in y-axis for (a) fixed support, (b) free support, (c) both support

Figure 52 (a) & (b) shows that the deformation amplitude for both type of supports increase in a same trend throughout the frequency. When compared in a same figure, 52 (c), it shows that the amplitude of deformation using fixed support is about two times larger than the surface deformation using free support.

Acoustic pressure produced

To further study the effect of using each support, pressure fields produced by each case at 20 and 40kHz of frequency are plotted as shown in figure 53 where (a) is for 20kHz and (b) is for 40kHz and (i) is for fixed and (ii) is for free support.

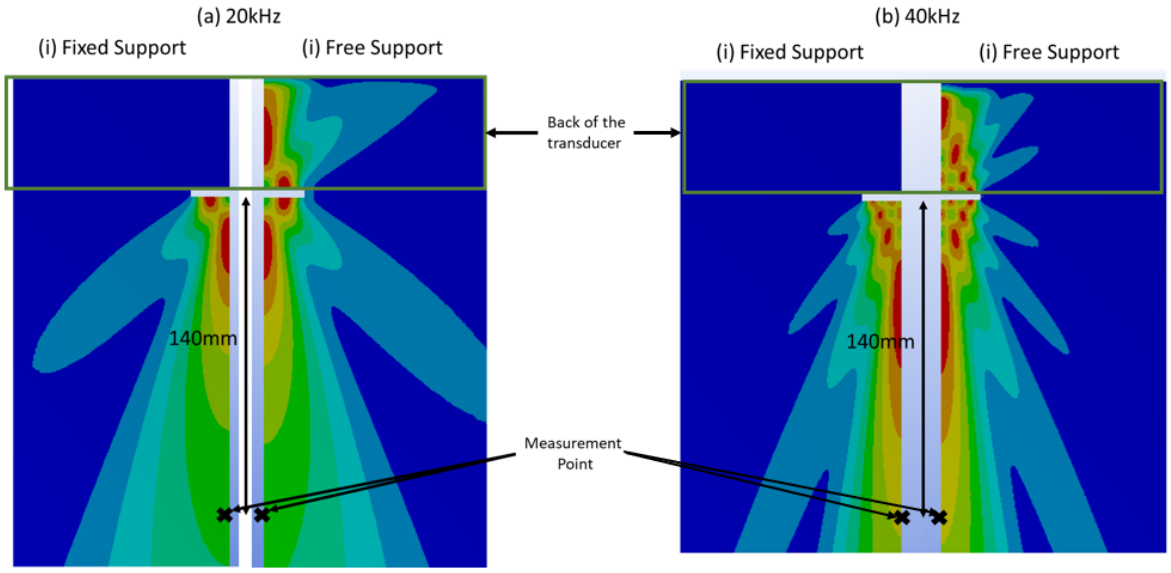

Figure 53 Comparison of pressure field at 20 and 40kHz for both (a) fixed and (b) free support

Figure 53 shows that similar pressure fields are produced by the front surface of the transducer at both frequencies using both supports. However, for free support, acoustic pressure is also produced at the back of the transducer marked by the box in figure 53 (ii). This is the reason why transducer with fixed support produced pressure two times larger than transducer with free support. For both model, same voltage is applied and for fixed supported transducer, deformation is only on one side of the active element but for free supported transducer, deformation on both sides of the active element occurred hence reducing the acoustic pressure produced at the front of the free supported transducer by half.

Next, acoustic pressure at 140 millimeters away from the center of the transducer's surface marked X in figure 53 is measured for both cases at frequency between 0-40kHz. The results are plotted in figure 54.

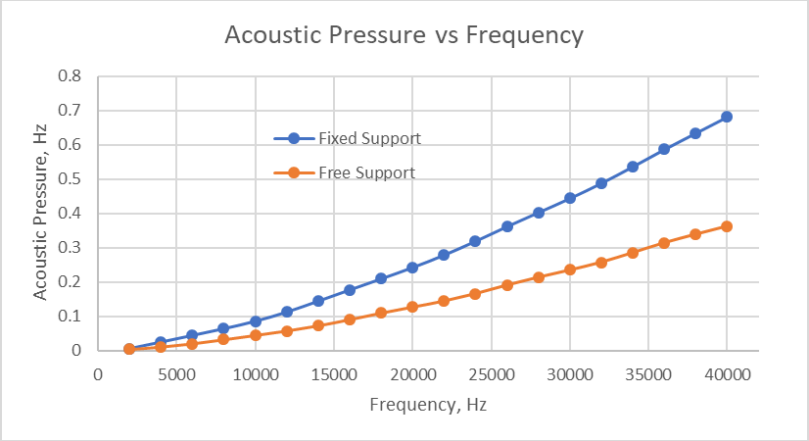

Figure 54 Comparison of acoustic pressure at measurement point marked X

To study the relation between the surface deformation and acoustic pressure produced by the transducer, a plot of acoustic pressure/surface deformation vs frequency is made as shown in figure 55. A quadratic trendline of the graph are plotted and its quadratic equations are shown in the figure.

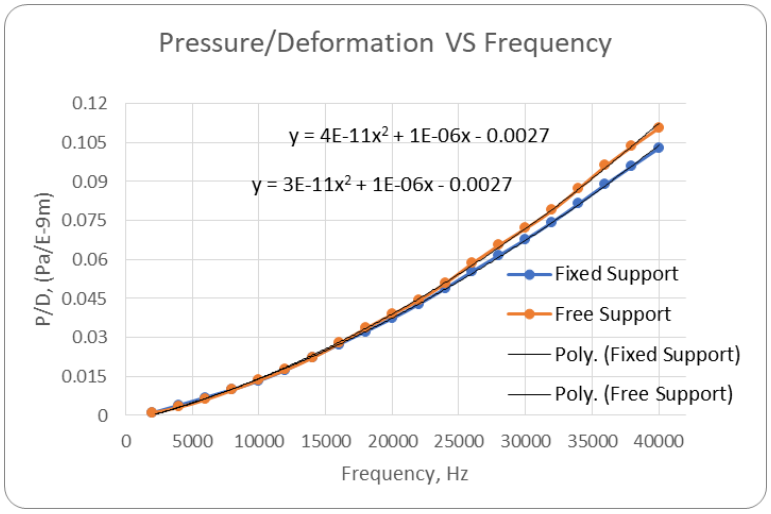

Figure 55 Acoustic pressure/surface deformation vs frequency

Reasoning of using fixed support

Results of the fixed and free support comparison shows that the deformation amplitudes for both models are different. However, the trend of amplitude increase across the frequencies is the same. The same results are also observed for the acoustic pressure measured in figure 54 where the pressure increase as the frequency increase. For validation purpose, amplitude of transducer deformation or acoustic pressure produced is not of concerned. Instead, it is the type

of pressure field produced by the deformation that needs to be considered. From figure 55, the trendline quadratic equation for both type of supports is obtained. Fixed support has a trendline of $y = 3e^{-11}x^2 + 1e^{-6} - 0.0027$ while free support has a trendline of $y = 4e^{-11}x^2 + 1e^{-6} - 0.0027$. The only difference between these two equations is the coefficient of the x^2 where free support has larger amplitude. This shows that both type of supports has similar correlation between the acoustic pressure and the transducer's surface deformation. The difference is only on the amplitude of pressure produced.

This correlation means that both type of supports can be used as the backing material boundary condition since they will produce similar results. However, the reason fixed support is chosen as the boundary condition is because, using this boundary condition deformation doesn't occur at the back of the transducer. Using free support, the deformation at the back of the transducer produced unnecessary pressure field that could affect the results upfront of the transducer. This is not desired especially during the study of interaction between ultrasonic wave and solid plate as it will mislead the determination of location of maximum or minimum acoustic pressure within the air domain. Hence, the reasons why fixed support is chosen as the boundary condition at the bottom surface of the transducer. This is acceptable because the damping material is not included in this model since this analysis is in frequency domain. However, in future work, for analysis in time domain, the damping material will be required to introduce the damping effect. Hence, the surface at the back of active element must be set to free surface.

4.3.2 Fluid Domain

This section shows the results of validation tests for absorbing boundary condition used in the model described in Chapter 3. A comparison of pressure field produced by the transducer at 40kHz between Radiation, PML and no absorbing boundary condition is shown in figure 56. For simplicity, the boundary of the air domain where the ABC is applied is called far-field surface.

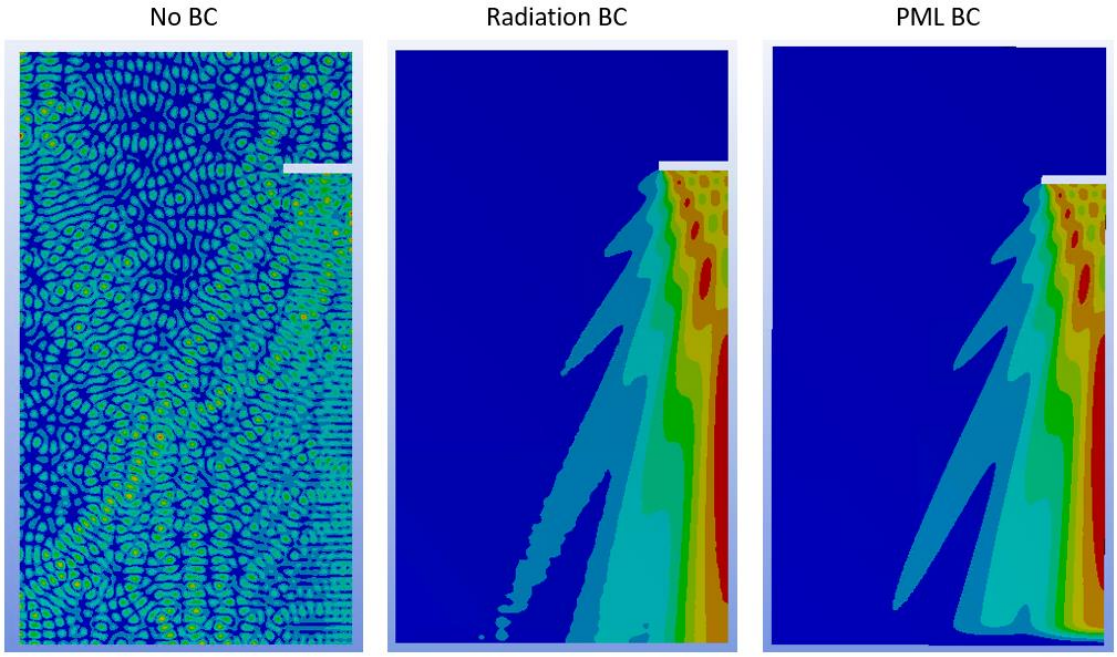

Figure 56 Pressure field using different ABC

Purpose of Far-Field Boundary Condition

Pressure field of model with no BC is observed to be completely different than the pressure field of models with Radiation and PML BC. It has an oscillating pattern of high and low pressure across the fluid domain. This pattern is due to constructive and destructive interference of waves caused by the reflection of pressure waves within the fluid domain. Since no boundary condition is defined, the fluid domain is modelled as closed system allowing no waves propagation out of the domain. This demonstrates the importance of having absorbing boundary condition defined at the boundary of the air domain to allow wave propagation outward into infinity.

Radiation VS PML Boundary Condition

Models with Radiation and PML BC almost have similar pressure fields. However, when carefully examined, there are disturbances in the pressure field produced by model with Radiation BC. Figure 57 shows a close-up comparison of pressure field between the two boundary conditions.

Figure 57(a) is for PML and figure 57(b) is for Radiation boundary condition. Pressure field in the highlighted red box of figure 57(b) appear to be disturbed compared to figure 57(a) which has a smooth contour. The disturbance observed is due to some of the waves reflected back into the fluid domain at its boundary. Hence, causing result inaccuracy for model with RBC.

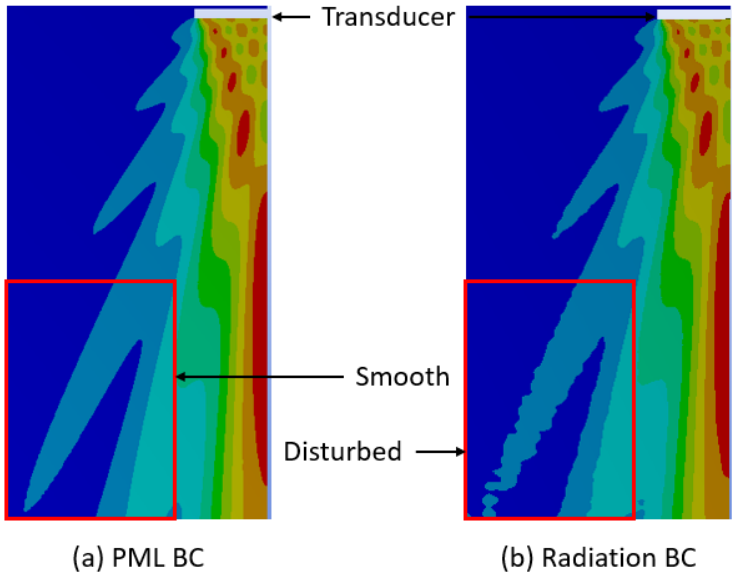

Figure 57 Comparison of pressure field between (a)PML and (b)Radiation BC

Errors of Radiation BC

To further investigate the difference between these two boundary conditions, acoustic pressure at certain points in the acoustic field are measured. Figure 58 shows the points in which the acoustic pressures are measured. Y is the distance between the measurement point and far-field surface in y-direction. X is the distance between the measurement point and y-axis in x-direction. Since PML BC has better accuracy than Radiation BC, percentage errors of acoustic pressure using Radiation BC in relative to PML are calculated using equation 16. Figure 59 shows the plot of percentage error of Radiation BC at the measurement points shown in figure 58.

Equation 16 Percentage error of RBC

$$Percentage\ error_{RBC} = \frac{Pressure_{PML} - Pressure_{PML}}{Pressure_{RBC}}$$

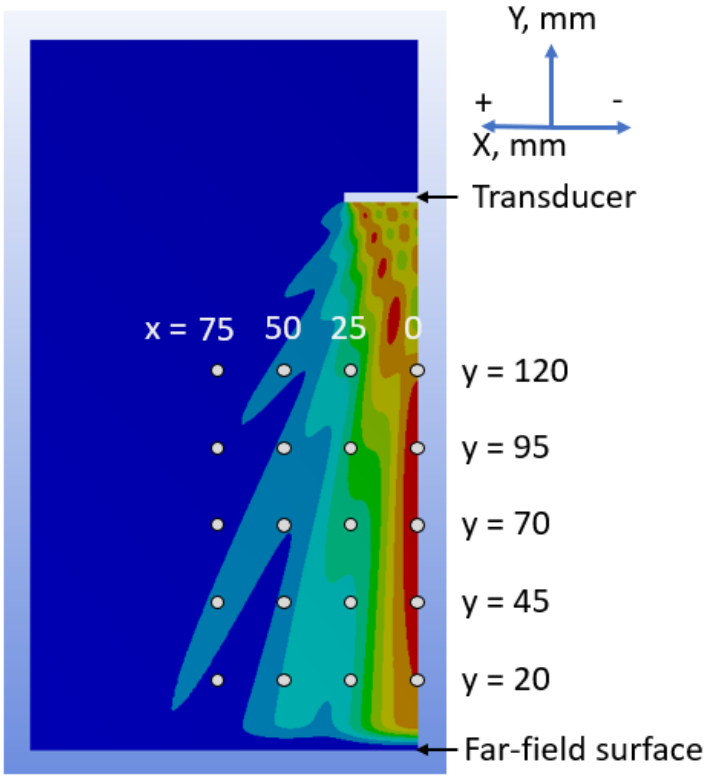

Figure 58 Measurement points for pressure to compare RBC and PML

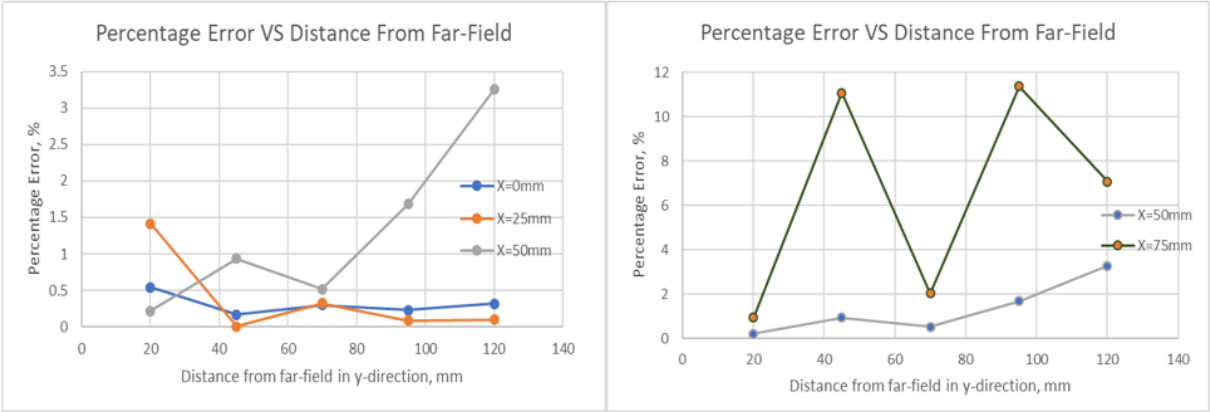

Figure 59 Percentage error of RBC in relative to PML

Initially, it was assumed that the further the measurement points are from the far-field surface, the less error using Radiation BC will be measured. The reason is that, most waves that lead to result inaccuracy are reflected at the far-field surface hence the higher measurement of error near the surface. However, this isn't entirely true. Based on the results, this assumption holds true only for pressure at points between $0 < X < 25$mm.

The percentage error for measurement at X = 0 and 25mm is higher than 0.5% only at measurement distance of Y = 20 mm from the far-field surface. At Y > 40 mm, the percentage error is below 0.5%. Whereas, at area far from y-axis (X = 50, 75mm), the percentage errors increased as the distance from the far-field surface increased. At X = 50mm, the percentage error is higher than 0.5% at Y > 45mm. At X = 75mm, the percentage errors reach up to 11%. The reason is at low pressure area (X > 50mm) indicated by blue contour in figure 58, slight change in pressure caused by the reflection of waves on the far-field surface will cause huge deviation from the actual pressure hence the high percentage error. This shows the importance of having all the outgoing waves to be fully absorbed by the far-field boundary condition. Errors caused by the reflected wave doesn't only affect results near the far-field boundary but also throughout the whole air domain.

As mentioned in Section 3.4.3, Radiation BC are most effective only at absorbing planar waves and waves that incident normal to the far-field boundary. In this simulation model, pressure waves produced by the transducer is not planar hence the error associated with it. This proves that the statements made by Howard & Cazzolato [20] regarding the requirements of using Radiation BC are true. Hence, for accuracy of results, PML boundary condition is the better choice. However, if minimizing simulation time is the priority, using Radiation boundary condition would be the better option since Radiation boundary condition doesn't requires extra nodes and elements to model the far-field boundary condition. However, this will be at a cost of result accuracy.

Computational cost

Table 17 shows the comparison of computational cost for the two boundary conditions. As expected, PML boundary condition has higher computational cost than Radiation boundary condition due to the increase no of element in the model as explained in Section 2.2.3 (Literature Review).

Boundary condition	Simulation time, s	Memory usage, MB	File size, MB
Radiation	49	941	367.63
PML	60	1060	437.38

Table 17 Computational cost of different far-field boundary conditions

PML Thickness Convergence Test

As mentioned in Section 3.4.3, the PML thickness needs to follow certain requirements for accurate results. This section aims to validate these requirements by performing a convergence test on varying PML thickness. Acoustic pressure at three measurement points, x = 0, 25, 50mm along the boundary of air domain are measured as shown in figure 60 where x = 0mm is the center of the transducer in x-axis. The tests are done at 40kHz using element size calculated using equation 11 and 12. The PML thickness is varied between 0.5-7 element size. Results are shown in figure 61(a), (b) and (c).

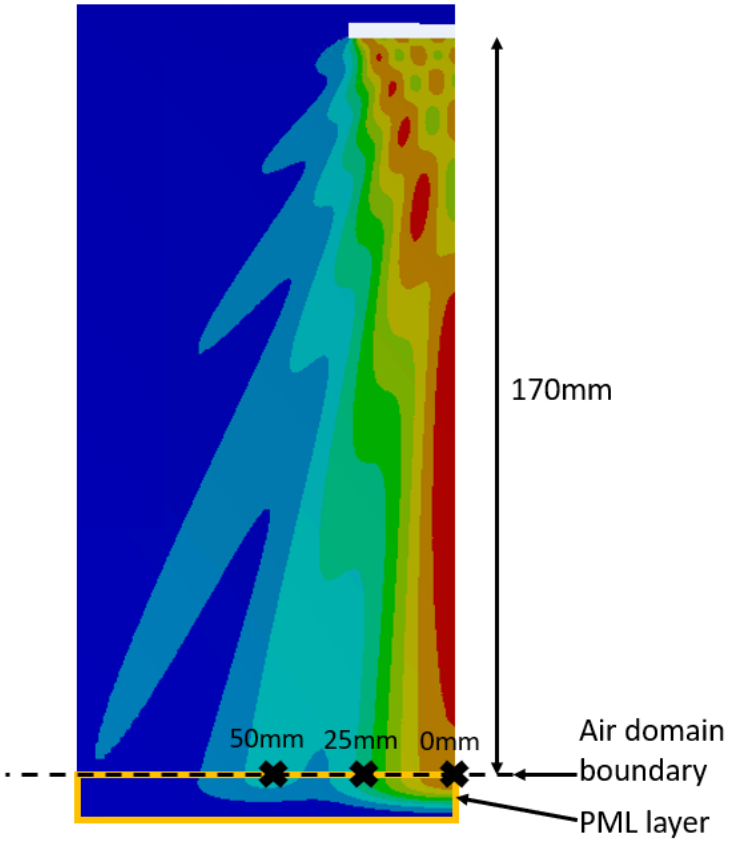

Figure 60 PML thickness convergence test measurement points

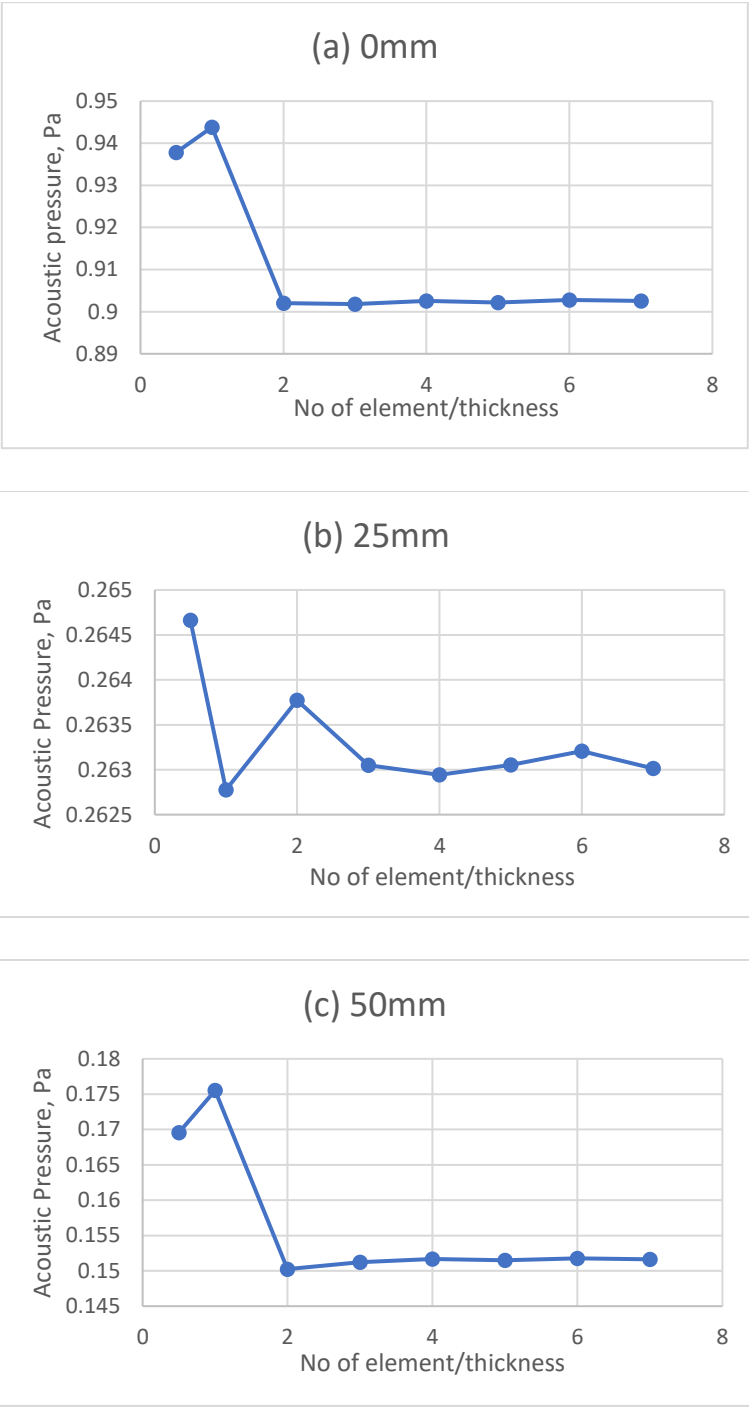

Figure 61 PML thickness convergence test

First, notice in the highlighted zone of PML layer in figure 60, the contour drastically changes colour from high pressure colour to low pressure. At the end of the PML layer, the contour has blue colour which indicates there are zero pressure in the field. This shows that the acoustic waves are fully absorbed and radiated to far-field within this layer. Hence, it is important that the PML layer is thick enough to allow full waves absorption to far-field. Figure 61 shows that the result

converged at around three to four element/thickness. Less than this, the measured acoustic pressure is not converged yet. This validates the requirement mentioned by Howard and Cazzolato [20]. Hence, it is important that the conditions are followed for accurate results.

Furthermore, it is also important that the no of element/PML thickness used does not exceed the required amount excessively as this can lead to increase in computational cost. This is particularly crucial for a 3D model where a small increase in thickness will significantly increase the no of elements and nodes of the model. Four or five no. of element/PML thickness is recommended. Nevertheless, at high frequency such as 200kHz, it is easier to satisfy the requirement since smaller element size is used. Hence, satisfying the requirement for PML thickness should be relatively easy at high frequency than low frequency.

ABC section summary

The results demonstrate the importance of having far-field boundary condition defined at the boundary of the air domain. Without this boundary condition, the model is essentially a close system where no wave can propagate out of the air domain. Analyzing the pressure fields of Radiation and PML boundary condition, PML is proved to have higher accuracy. However, simulation time for PML is also higher than RBC. Since result accuracy is the main priority, PML is chosen as the ABC for this model. Furthermore, to use the PML certain requirements need to be fulfilled to get the best accuracy and efficient computational cost.

4.3.3 Symmetry

This section shows the effect of using symmetry boundary condition explained in Section 3.4.5 to reduce the size of the model. Results of full model, half and quarter model are compared. Pressure field produced by the transducer at 10kHz for each symmetry condition are plotted in figure 62. The models are meshed using meshing method explained in Section 3.3 (Model Description).

(a) Full model

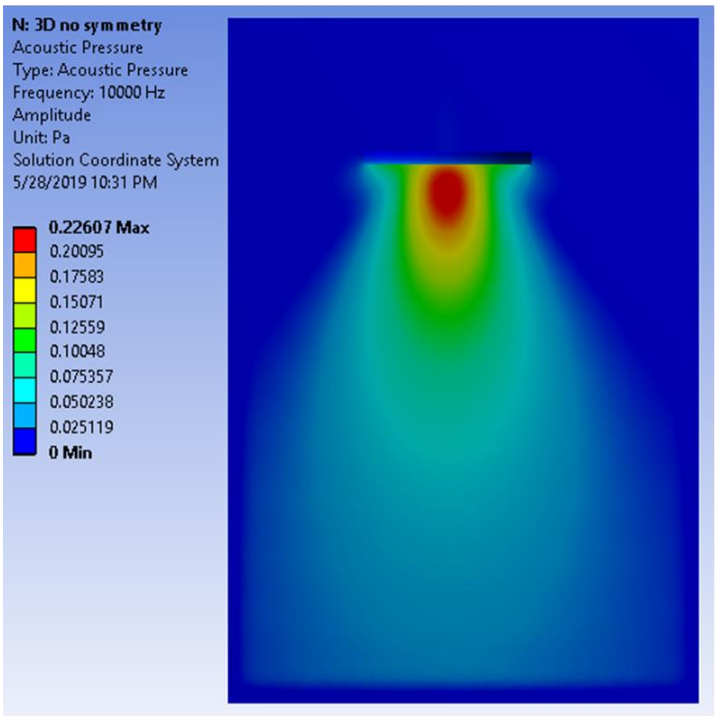

(c) Quarter model

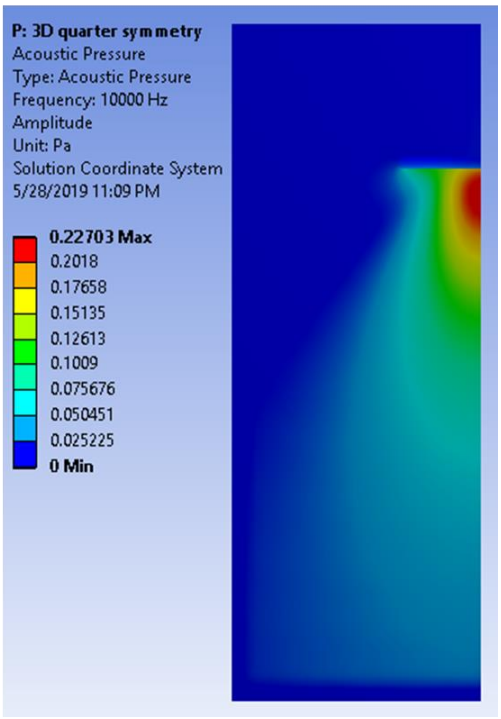

(b) Half model

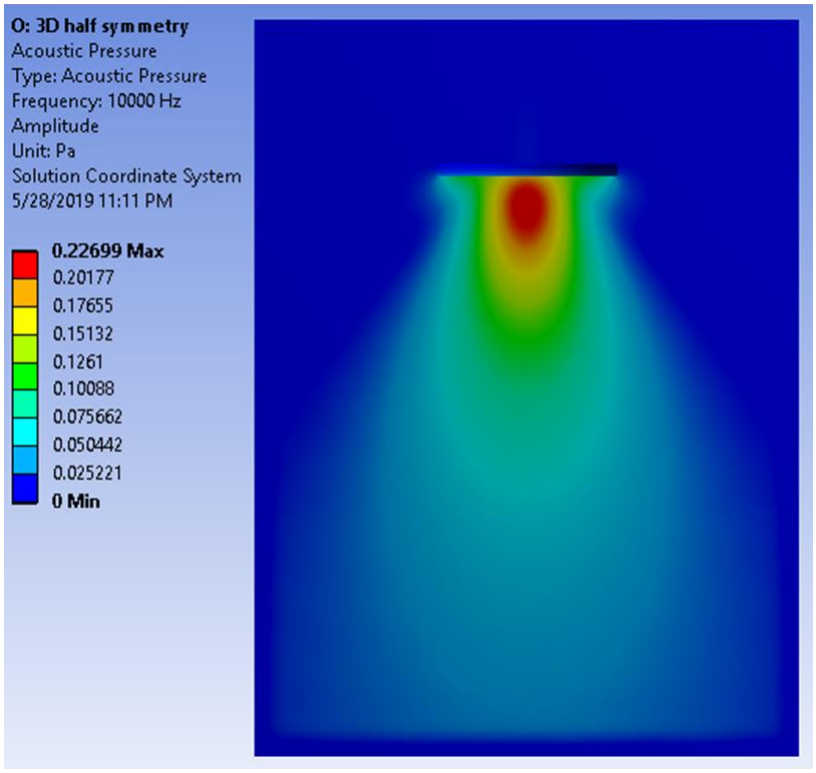

Figure 62 Pressure field using of (a) full model, (b) half model, (c) quarter model

Similar contour is observed for all three models. All the colors of the contour also have almost the same magnitude seen at the left side of each model. This shows that using symmetry boundary condition is reliable as similar results are obtained. The computational time to solve each model is calculated as shown in table 18.

Full Model	Half Model	Quarter Model
442s	135s	13s

Table 18 Computational time of model with different symmetry BC

As expected quarter model has the lowest total computational time of about 13s which is 34 times lower than the computational time for full model. This shows the importance of using symmetry model whenever the model is axisymmetric to reduce the total computational cost without reducing accuracy of the result.

Chapter 5: Interaction between Ultrasonic Wave and Solid Plate

This chapter aims to study the interaction between ultrasonic wave and solid plate. Interaction such as impedance mismatch, reflection and propagation of wave at the air-plate interface are studied. Furthermore, this chapter also aims to demonstrate the capability of the simulation tool to easily implements different simulation setup. These are done by varying variables such as frequency, wave angle of incident and plate material to investigate its effect on the air-plate wave interaction. Model described in Chapter 3 is used for this study. All tests are done using 2.5D model.

5.1 Flexible vs Rigid plate

Effect of wave propagation can be observed by analyzing the wave interaction with flexible and rigid plate. Since no vibration can occur in rigid body, it is expected that no waves are propagated through it. Whereas, some waves will be propagated through the flexible body. This is the aim of the study in this section, to demonstrate the wave propagation from air to plate. Table 19 shows the parameters used in this study. Figure 63 shows the test setup. This setup is used for studies in the upcoming sections as well. To model the rigid plate, fixed support is applied to all surface of the plate hence, no deformation can occur. For flexible plate, boundary condition described in Section 3.4.1 is used where fixed support is applied only at the edge of the plate.

Parameters	Description
Angle of incident, Θ	45^o
Plate material	Aluminium
Plate thickness, t_p	5mm
Plate length, L_p	150mm
Transducer material	Pzt4
Transducer thickness	3.43mm
Transducer length	50
Voltage difference	30V

Table 19 Parameter used for flexible vs rigid plate study

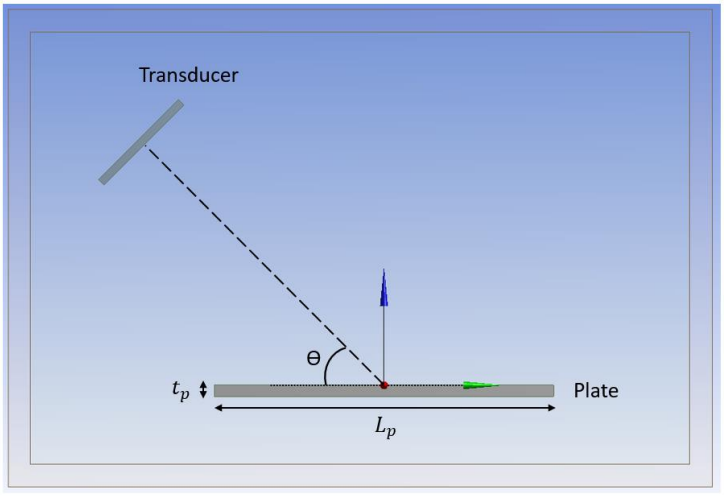

Figure 63 Setup for plate study

To ensure that rigid and flexible plate are modelled correctly, deformation on both plates due to waves emitted from transducer are computed as shown in figure 64. The values on the left side of the figure represents the amplitude of deformation in meter for each colour of the contour. The magnitude of deformation shown is scaled to around 1e+10 to demonstrate the deformation mode clearly. Deformation can be seen on the flexible plate, whereas for rigid plate, no deformation is observed. This proves that the rigid and flexible plate are modelled correctly.

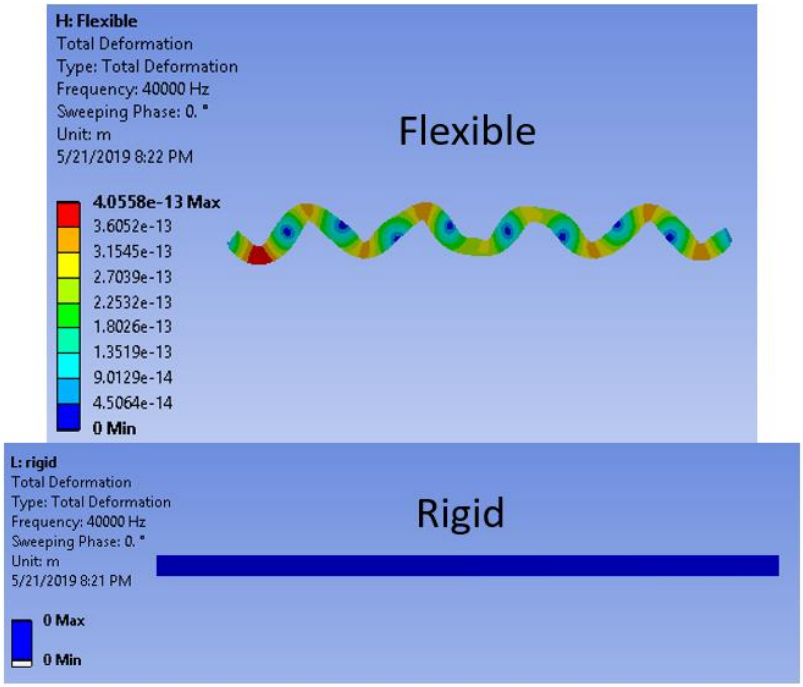

Figure 64 Deformation of flexible and rigid body

Next pressure field produced above the plate is examined. Figure 65 shows the comparison of pressure field between studies on flexible and rigid plate. The pressure field produced in both tests is unexpectedly identical. Maximum pressure occurred near the center of the plate's top surface. At this point, sound waves are compressed due to the reflection of wave at the plate's top surface resulting in the maximum acoustic pressure. To further study the difference in results between flexible and rigid plate, acoustic pressure in the air domain near the center of transducer marked 'X' in figure 65 is measured. Measurement are taken between 20 – 40kHz. The results are plotted in figure 66.

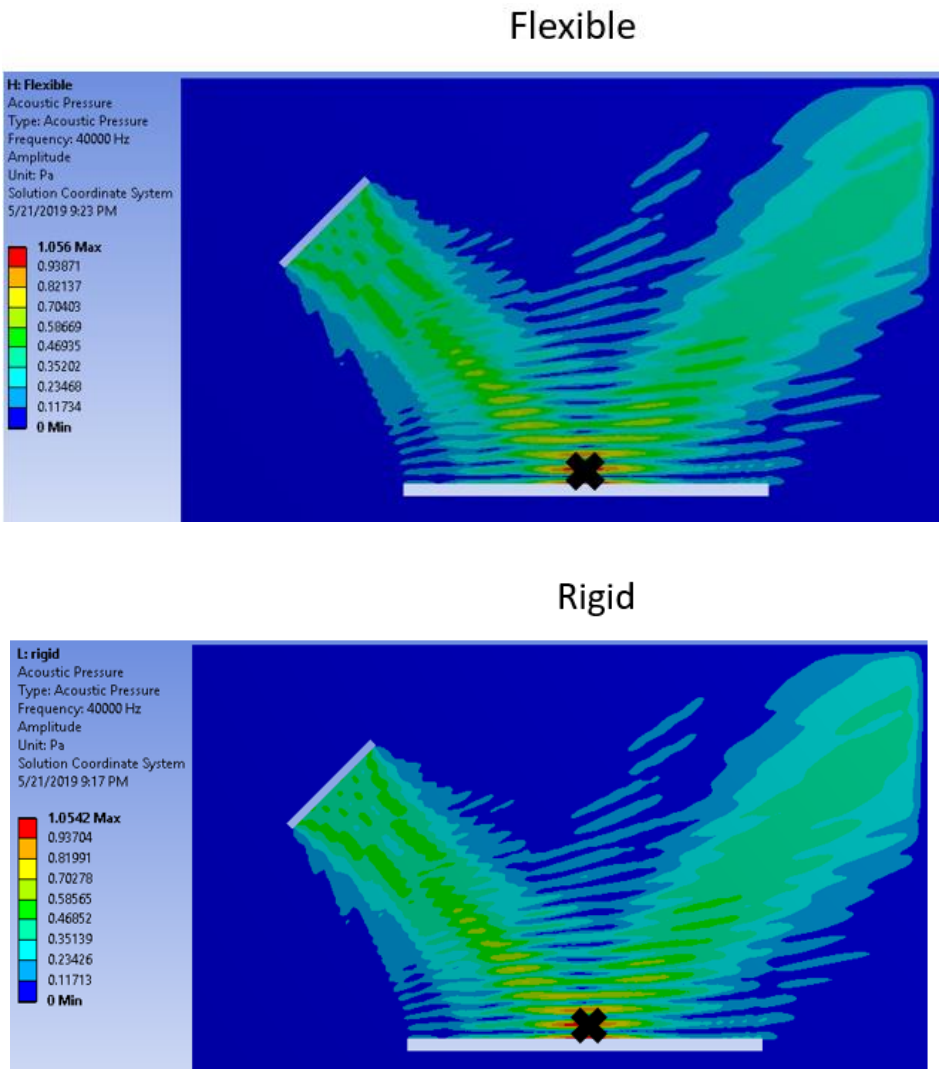

Figure 65 Pressure field on flexible and rigid plate at 40kHz

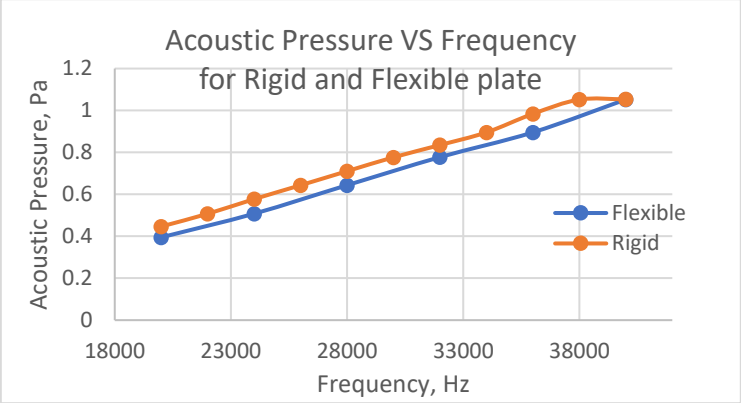

Figure 66 acoustic pressure at the center of flexible and rigid plate's surface

Acoustic pressure measured for rigid plate is higher than flexible plate throughout the whole frequency. The reason is, when acoustic waves incident on the surface of the rigid plate, all the waves are reflected, and none propagates through the plate. In contrast, at the surface of the flexible plate, some of the waves propagate through the plate. This cause a reduce in acoustic pressure in the air domain when compared to the rigid plate where all waves are reflected. Hence, the reason acoustic pressure measured at 'X' for rigid plate is higher than for flexible plate throughout the whole frequency range.

5.2 Effect of frequency on plate deformation

Next, effect of frequency on the plate deformation are studied. In this section and upcoming sections, flexible plate is used. In addition, similar parameters as in table 19 are also used. Average plate deformation due to ultrasonic wave emitted by transducer for frequency between 0-80kHz is studied. Figure 67 shows the amplitude of average plate deformation vs frequency.

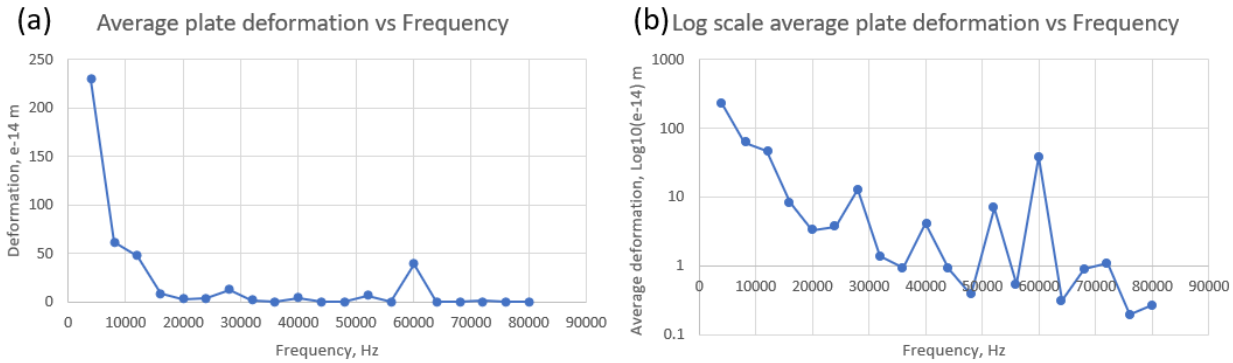

Figure 67 Average plate deformation vs frequency

Observing figure 67(a), deformation at low frequency (<10kHz) is significantly higher than frequency more than 20kHz making the results at high frequency hard to be analysed. Hence, the average deformation is scaled with $\log_{10}$ as shown in figure 67(b). Analyzing figure 67(b), even though there are fluctuations in the deformation amplitude across the frequency range, the trend generally shows a decrease in average plate deformation as the frequency increase. This is because at high frequency, the wavelength is smaller. At smaller wavelength, the waves get reflected easier as mentioned in Section 2.1.2. Hence, less waves propagate through the plate causing less plate deformation. Furthermore, the plate deformation mode and pressure field produced at different frequencies are plotted. Figure 68 shows the plate deformation at 40, 60 and 80kHz and Figure 69 shows the pressure field produced at 40, 60 and 80kHz.

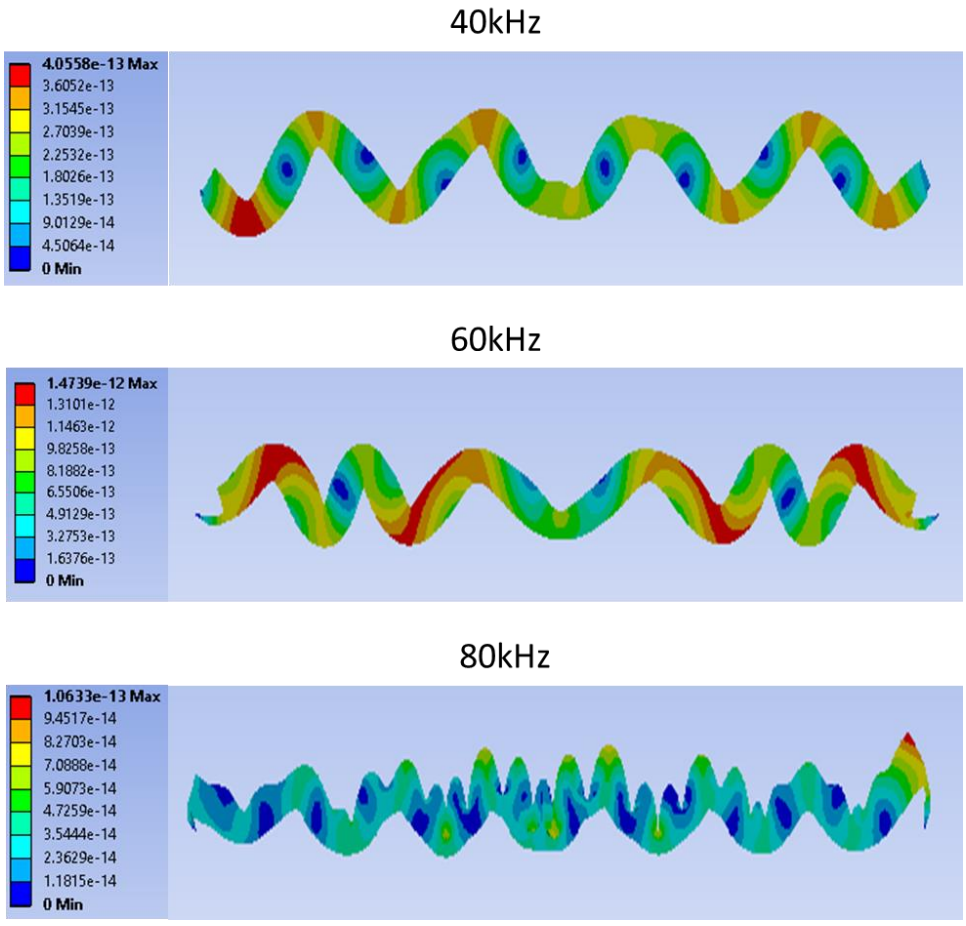

Figure 68 Plate deformation at 40, 60 and 80kHz

40kHz

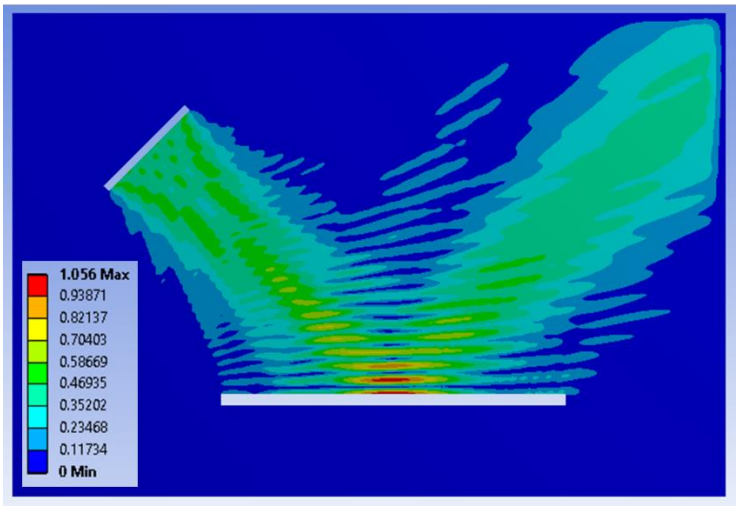

60kHz

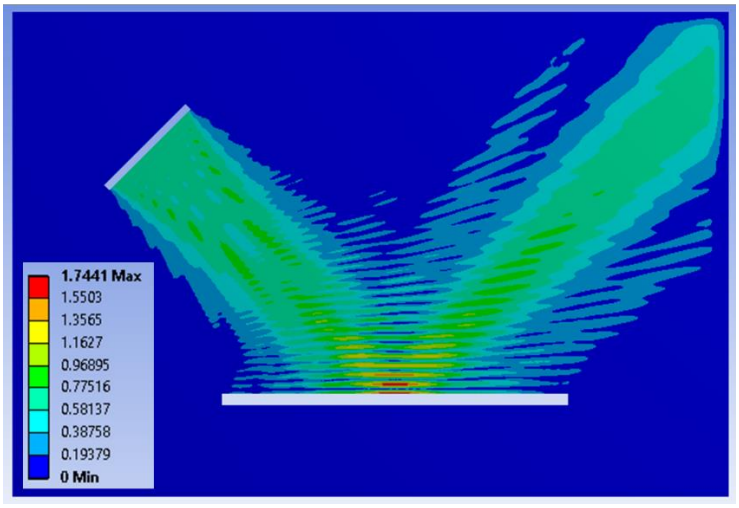

80kHz

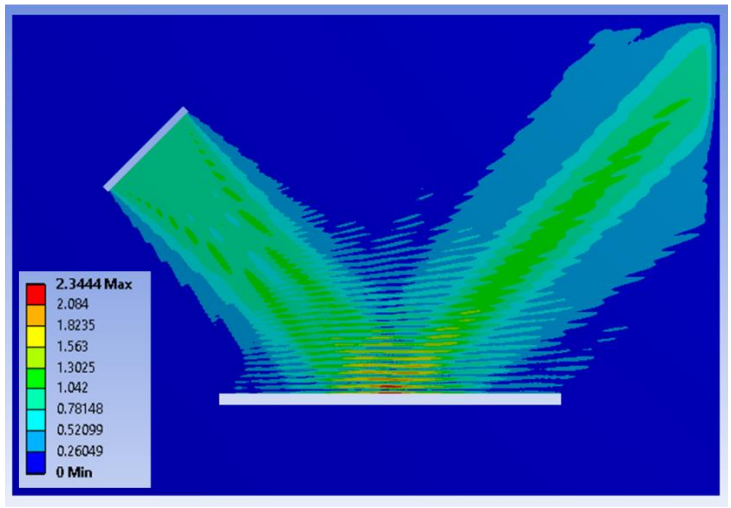

Figure 69 pressure field at 40, 60 and 80kHz

Figure 68 shows that at 80kHz the plate deformation mode has the smallest wavelength followed by 60 and 40kHz corresponding to the ultrasonic wave frequency. Similar result can be seen in figure 69 where the pressure field at 80kHz has higher oscillation of high and low pressure compared to 40 and 60kHz.

5.3 Effect of incident angle on plate deformation

In this section, the effect of varying the ultrasonic wave incident angle on the average amplitude of plate deformation is studied. Ultrasonic waves are emitted from transducer towards the test plate. The tests are done at 40kHz with other parameters remain constant as in table 19. The only parameter changed are the incident angle varied between 15^0 and 90^0. The average plate deformation for these incident angles are measured.

Figure 70 shows the relationship between wave incident angle and plate deformation. Between 15 and 75°, the average plate deformation increases as the wave incident angle increases. This agrees with the theory of wave reflection where the larger the incident angle, less waves are reflected at the air-plate interface, and more waves are propagated through the plate. This causes the plate deformation to increase as the angle increase. However, at larger than 75°, the average plate deformation starts to decrease. This is because at this angle, destructive interference occurred between the reflected waves from air-plate interface and emitted waves from transducer which are propagating in opposite direction. Because of this destructive interference, the waves amplitude is smaller thus, decreasing the average plate deformation.

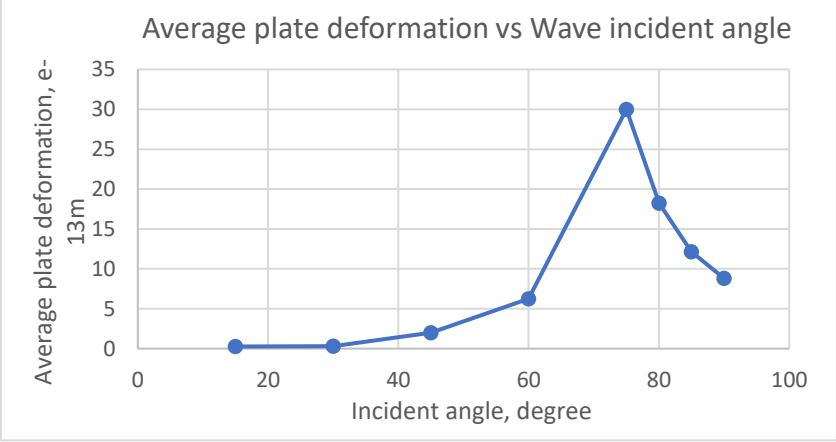

Figure 70 Incident angle vs plate deformation

Furthermore, the pressure field produced at different incident angles, 30^0, 60^0 and 90^0 is also investigated. Figure 71 shows the pressure field produced by the transducer at these incident angles at 40kHz.

30 degree

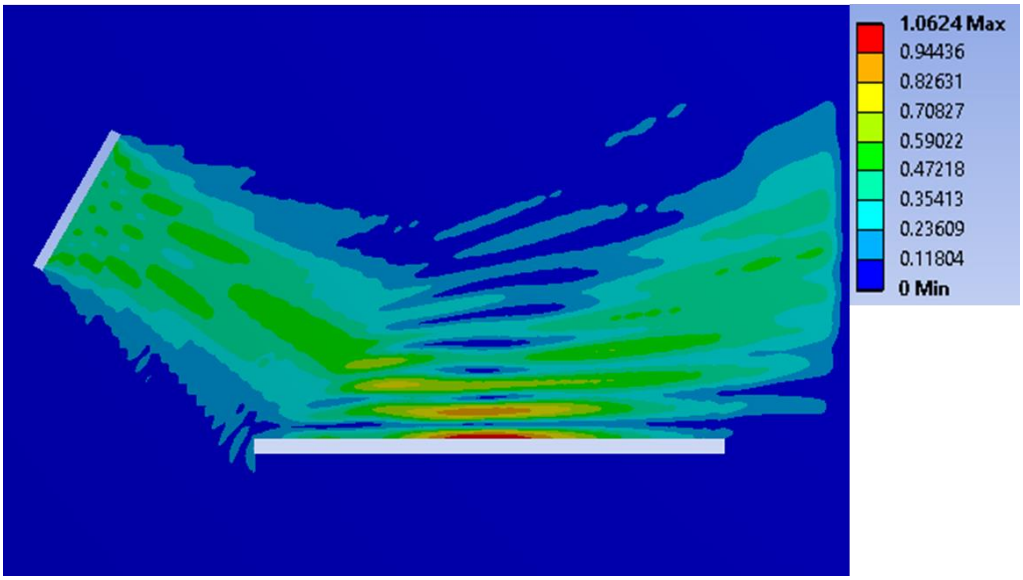

60 degree

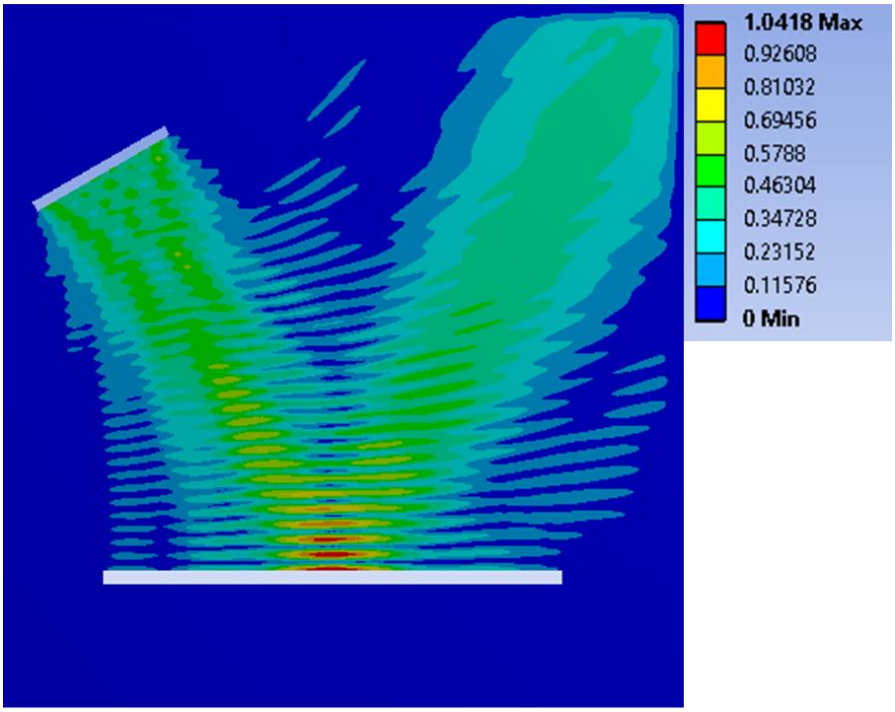

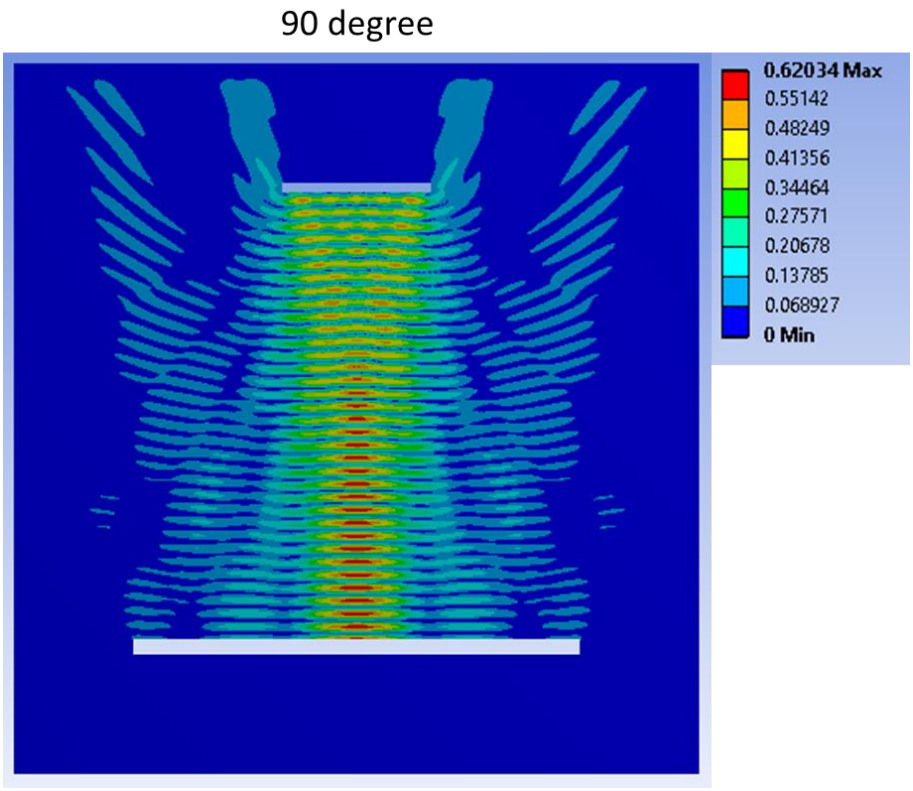

Figure 71 Pressure field produced at 30^0, 60^0 and 90^0 incident angle

Observing figure 71, the waves are reflected at angle equal to the incident angle for 30^0 and 60^0 incident angles. This agrees with Snell's Law where it stated that the angle of reflected wave is the same with angle of incident. Furthermore, observing incident angle at 90^0, the emitted wave by transducer and wave reflected by plate is propagating in opposite direction. This causes the destructive interference mentioned previously. Analyzing the pressure, the maximum pressure at 90^0 indicated by the red contour only has amplitude of 0.6203Pa which is lower than 1.0624 and 1.0418Pa for 30^0 and 60^0 respectively. This causes less deformation on the plate for 90^0 incident angle.

5.4 Effect of material change on plate deformation

This section studies the effect of changing material plate on the plate deformation. Three different plate materials are tested which are stainless steel, aluminium and magnesium alloy. Ultrasonic waves are emitted towards the plate using parameters shown in table 19. The tests are done at 40kHz. Each material has different specific acoustic impedance as discussed in Introduction and Literature Review section. The acoustic impedance for stainless steel, aluminium and magnesium alloy are 45.45, 17 and 10.98MRayls respectively. This means that stainless steel has the highest impedance mismatch with air medium while magnesium has the lowest. Relation between acoustic impedance and average plate deformation are plotted in figure 72.

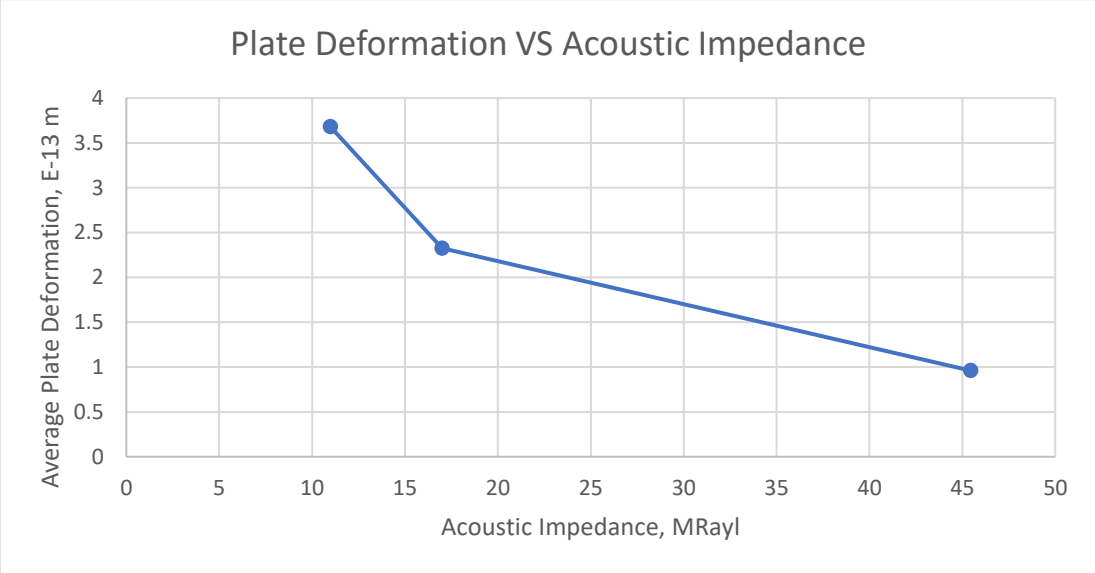

Figure 72 Average plate deformation vs acoustic impedance

The result shows that as the acoustic impedance increases, average plate deformation decreases. This agrees with the theory that as the impedance mismatch between two medium gets larger, more waves will be reflected at the interface. As stated before, the more waves reflected, the lower the average plate deformation. In the result, stainless steel has the lowest average plate deformation since it has the highest impedance mismatch with air followed by aluminium and magnesium.

5.5 Chapter Summary

The test on the flexible and rigid body shows the effect of wave propagation on the deformation of plate. When wave propagates through the plate, deformation occurs. This observation can be related to other studies done on different frequency, angle of incidence and plate material as well. As observed, the deformation of plate is lower when:

1) Higher frequency of analysis is used
2) Wave angle of incidence decreases
3) Material with higher acoustic impedance is used

As the frequency of analysis increases, wavelength of the sound waves gets smaller. Smaller wavelength makes the sound waves get reflected easier at the boundary of two different medium such as the air and plate. Since more waves are reflected at high frequency, less waves are transferred through the plate causing less deformation. This is one of the weakness of air-coupled transducer, the effective frequency for this type of transducer coupling are much lower compared to other transducer such as water and contact transducer. Since, higher frequency means smaller defect can be detected by the ultrasonic wave, air-coupled transducer is only limited to analysis of defect with larger size compared to fluid and contact transducer.

Same observation can be made on the effect of wave angle of incidence. As mentioned previously, as wave incident angle gets smaller, sound waves get reflected easier. This causes less wave propagation through the plate thus less plate deformation is observed. Finally, in the test of different material, Magnesium has the lowest specific acoustic impedance followed by aluminium and stainless steel. This means that magnesium plate has the lowest acoustic impedance mismatch at the interface between air and plate's surface. Thus, among the three materials, most waves are propagated through the air-magnesium plate interface causing it to have the highest average surface deformation. This shows the effect of acoustic impedance mismatch on the reflection and propagation of sound wave as described in Section 2.1.3.

Chapter 6: Conclusion and Recommendation

6.1 Conclusion

The aim of this thesis is to develop a finite element tool capable of studying the interaction of air-coupled ultrasonic wave and solid plate with great accuracy and computational efficiency. This has been a success and the reliability of the developed simulation tool has been validated. This is done through series of tests on various aspects of the modelling such as the element type, size and boundary conditions. For the element aspects, computational efficiency and result accuracy are achieved through the use of quadratic hexahedral element with 6 and 20 elements per wavelength for fluid and structural body respectively. For absorbing boundary condition, PML is proven to provide better accuracy than RBC with only slight increase in computational cost through optimizing the PML layer thickness.

More computational efficiency has been achieved by applying symmetry boundary condition and 2.5D model. The application of symmetry boundary condition has no impact on result accuracy whatsoever whilst considerably reducing the computational cost. 2.5D model on the other hand, might have some differences in the amplitude of acoustic pressure produced in relative to 3D model, however, the overall behavior of wave produced is similar to the 3D model thus validating the use of 2.5D model in place of 3D model for validation test. The 2.5D model has not only helped minimizing the computational cost but it has also overcome the limitation of 3D model where it is only capable for simulation of up to 20kHz. On the other hand, 2.5D model is capable of simulating up to 100kHz using the same computer specification which opens up the opportunity for studies at high frequency. The only limitation of 2.5D is in its infinitely long rectangular shape hence it can't be used for modelling of real-life transducer.

Furthermore, the studies done on interaction between air-coupled ultrasonic wave and solid plate have shown the effect of using different test parameters on the wave-plate interaction. In the study of rigid vs flexible plate, the effect of wave propagation from air medium to solid plate is demonstrated. For change in frequency, it is shown that at higher frequency, more waves are reflected. This is also the case for change in incident angle and plate material. At smaller incident angle and for material with high impedance mismatch with air, more waves are reflected at the

air-plate interface. The tests done on various parameters have also shown the practicality of using this simulation tool for various test setups which would otherwise be time-consuming and expensive through experimental work. Overall, the model developed is proved to be reliable and could become the foundation for future study regarding the use of finite element model to study the interaction between air-coupled ultrasonic waves and solid plate.

6.2 Recommendations for Future Work

The following are recommendations for future work regarding finite element modelling of ultrasonic testing:

1) Finite element modelling in the time domain using transient analysis instead of harmonic. Transient analysis is more appropriate for modelling the transducer vibrational behavior where the vibration amplitude damps out over time due to the backing material. Using transient analysis, more accurate model can be tested, and model based on a real-life transducer can be developed. If real-life transducer can be developed, this opens up opportunity for testing on different transducer characteristic such as the type of matching layer backing material used.
2) Developing an appropriate 2D model using Mechanical APDL in ANSYS. 2.5 model developed in this thesis has limitation on the shape of the transducer hence it's not capable to model real-life transducer. However, if an appropriate 2D model is developed, this will be hugely beneficial in terms of computational cost.
3) Simulation on different types of wave propagation through the plate such as bulk wave and lamb wave.
4) Modelling of receiver transducer and conversion of ultrasonic wave to electrical signal. This way, effect of impedance mismatch can be studied in more details.

References

[1] P. C. R. F. G. H. M. Castaings, "Single Sided Inspection of Composite Materials Using Air Coupled Ultrasound," *Journal of Nondestructive Evaluation,* pp. 37-45, 1998.

[2] I. N. M. E. L. L. M. C. Bhardwaj, "Contact-Free Ultrasound: The Final Frontier in Non-Destructive Materials Characterization," in *24th Annual Conference on Composites, Advanced Ceramics, Materials, and Structures: A: Ceramic Engineering and Science Proceedings, Volume 21*, The American Ceramic Society, 2008, pp. 163-172.

[3] R. J. Kazys, R. Sliteris and J. Sestoke, "Air-Coupled Ultrasonic Receivers with High Electromechanical Coupling PMN-32%PT Strip-Like Piezoelectric Elements," *MDPI,* pp. 1-18, 2017.

[4] M. Toda, "New Type of Matching Layer for Air-Coupled Ultrasonic Transducers," *IEEE Transactions on Ultrasonics, Ferroelectrics and Frequency Control,* vol. 49, no. 7, pp. 972-979, 2002.

[5] R. Singh, "Ultrasonic Testing," in *Applied Welding Engineering: Processes, Codes, and Standards*, Elsevier Science, 2015, pp. 293-294.

[6] "Ultrasonic testing," [Online]. Available: https://commons.wikimedia.org/w/index.php?curid=997839.

[7] H. K. Josef Krautkramer, "Chapter 7 Piezo-electric Methods of Generation and Reception of," in *Ultrasonic Testing of Materials 4th edition*, Springer-Verlag Berlin Heidelberg GmbH 1990 , 2002, pp. 117-125.

[8] P. C. M. Castaings, "AIR-COUPLED ULTRASONIC TRANSDUCERS FOR THE DETECTION OF DEFECTS IN PLATES," *Review of Progress in Quantitative Nondestructive Evaluation, Vol. 15 ,* pp. 1083-1090, 1996.

[9] J. L. San Emeterio and A. Ramos, "Models for Piezoelectric Transducers Used in Broadband Ultrasonic Applications," in *Piezoelectric Transducers and Applications*, Berlin, Heidelberg, Springer, 2008, p. 97.

[10] Z. Wang, J. Miao and C. W. Tan, "Acoustic transducers with a perforated damping backplate based on PZT/silicon wafer bonding technique," *Sensors and Actuators A: Physical,* vol. 149, no. 2, pp. 277-283, 2009.

[11] I. L.Ver, "Interaction of Sound Waves with Solid Structures," in *Noise and Vibration Control Engineering*, Hoboken, New Jersey, John Wiley & Sons Inc., 2006, pp. 403-406.

[12] S. Thiagarajan, R. W. Martin, A. Proctor, I. Jayawadena and F. Silverstein, "Dual Layer Matching (20) MHz) Piezoelectric Transducers with Glass and Perylene," *IEEE Transactions on Ultrasonics, Ferroelectrics and Frequency Control,* vol. 44, no. 5, pp. 1172-1174, 1997.

[13] T. L. Szabo, "Chapter 5: Transducer," in *Diagnostic Ultrasound Imaging: Inside Out*, Boston, USA, Elsevier Inc., 2014, p. 142.

[14] N. Fletcher and S. Thwaites, "Multi-horn matching plate for ultrasonic transducers," *Ultrasonics,* vol. 30, pp. 67-75, 1992.

[15] N. Bowler, J. Clasen and R. Ernst, "NDT Resource Center," [Online]. Available: https://www.nde-ed.org/EducationResources/CommunityCollege/Ultrasonics/EquipmentTrans/radiatedfields.htm. [Accessed 5 March 2019].

[16] D. G. Pavlou, "An Overview of the Finite Element Method," in *Essentials of the Finite Element Method*, Norway, Academic Press, 2015, p. 1.

[17] J. T. Bennett, "Development of a finite element modelling system for piezocomposite transducers," Glasgow, United Kingdom, 1995.

[18] L. Deepsoft, "fea-cae-engineering," Deepsoft, LLC, [Online]. Available: http://fea-cae-engineering.com/fea-cae-engineering/element_types.htm. [Accessed 24 May 2019].

[19] P. Langer, M. Maeder, C. Guist, M. Krause and S. Marburg, "More Than Six Elements Per Wavelength: The Practical Use of Structural Finite Element Models and Their Accuracy in Comparison with Experimental Results," *Journal of Computational Acoustics,* p. 23, 2017.

[20] C. Q. Howard and B. S. Cazzolato, Acoustic Analyses Using MATLAB and ANSYS, Florida: CRC Press, 2017.

[21] "ANSYShelp: Element Reference," ANSYS, [Online]. Available: https://ansyshelp.ansys.com/account/secured?returnurl=/Views/Secured/corp/v193/ans_elem/Hlp_E_LIBRARY.html. [Accessed 27 May 2019].

[22] H. Gan, P. L. Levin and R. Ludwig, "Finite element formulation of acoustic scattering phenomena with absorbing boundary condition in the frequency domain," *Acoustical Society of America,* pp. 1651-1662, 1993.

[23] L. Jianguo and L. Q. Huo, "A novel Radiation boundary condition for Finite Element Method," *Microwave and Optical Technology Letters,* pp. 1995-2002, 2007.

[24] J. Bielak, L. F. Kallivokas and R. C. MacCamy, "Symmetric Local Absorbing Boundaries in Time and Space," *Engineering Mechanics,* pp. 2027-2048, 1992.

[25] J. Lysmer and R. Kulemeyer, "Finite dynamic model for infinite media," *Engineering Mechanics Division,* pp. 859-878, 1969.

[26] R. Clayton and B. Engquist, "Absorbing boundary conditions for acoustic and elastic wave," *Bulletin of the Seismological Society of America,* pp. 1529-1540, 1977.

[27] J.-P. Berenger, "A perfectly matched layer for the absorption of electromagnetic waves," *Computational Physics,* pp. 185-200, 1994.

[28] A. R. Dalkhani, A. Javaherian and H. M. Basir, "Frequency domain finite-element and spectral-element acoustic wave modeling using absorbing boundaries and perfectly matched layer," *Waves in Random and Complex Media,* pp. 367-388, 2018.

[29] Y. Liu and S.-Q. C. Xiang-Yang LI, "Application of the double absorbing boundary condition in seismic modelling," *Applied Geophysics,* vol. 12, no. 1, pp. 111-119, 2015.

[30] M. Andre, K.-U. Bletzinger and R. Wuchner, "A complementary study of analytical and computational fluid-structure interaction," *Computational Mechanics,* vol. 55, no. 2, pp. 345-357, 2015.

[31] C. S. Peskin, "The immersed boundary method," *Acta Numerica,* vol. 11, pp. 479-517, 2002.

[32] R. Glowinski, T.-W. Pan and J. Periaux, "A lagrange multiplier/fictitious domain method for the numerical simulation of incompressible viscous flow around moving rigid bodies: (I) case where the rigid body motions are know priori," *Comptes Rendus de l'Academie des Sciences Series I Mathematics,* vol. 324, no. 3, pp. 361-369, 1997.

[33] B. Despres, Numerical methods for Eulerian and Lagrangian conservation laws Bruno Despres, Paris: Cham: Birkhauser, 2017.

[34] L. Zhang, A. Gerstenberger, X. Wang and W. K. Liu, "Immersed finite element method," *Computer Methods in Applied Mechanics and Engineering,* vol. 193, no. 21-22, pp. 2051-2067, 2004.

[35] R. v. Loon, P. Anderson, F. v. d. Vosse and S. Sherwin, "Comparison of various fluid-structure interaction methods for deformable bodies," *Computers and Structures,* vol. 85, no. 11, pp. 833-843, 2007.

[36] ANSYS, "Acoustic Analysis Guide," 2019. [Online]. Available: https://ansyshelp.ansys.com/account/secured?returnurl=/Views/Secured/corp/v193/ans_acous/acous_intro_geneq.html.

[37] ANSYS Inc., "Theory reference Chapter 10: Coupling," ANSYS, [Online]. Available: https://ansyshelp.ansys.com/account/secured?returnurl=/Views/Secured/corp/v193/ans_thry/thy_coup2.html?q=piezoelectric. [Accessed 1 April 2019].

[38] S. Chen, C. Niezrecki and P. Avitabile, "Experimental Mapping of the Acoustic Field Generated," in *Conference Proceedings of the Society for Experimental Mechanics Series*, 2016.

[39] S. Chen, A. Sabato, C. Niezrecki, P. Avitabile and T. Huber, "Characterization and modeling of the acoustic field generated Characterization and modeling of the acoustic field generated excitation," *Journal of Sound and Vibration,* vol. 432, pp. 33-49, 2018.

[40] F. D. Hastings, J. B. Schneider and S. L. Broschat, "Application of the perfectly matched layer (PML) absorbing boundary condition to elastic wave propagation," *Acoustical Society of America,* pp. 3061-3069, 1995.